NASA/TM–20210025992

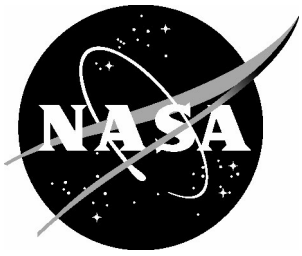

# Application of a Developmental Composite Material Model to Predict the Crush Response of Two Energy Absorbers

*Karen E. Jackson*
*National Institute of Aerospace, Hampton, Virginia*

*Robert K. Goldberg and Trenton M. Ricks*
*Glenn Research Center, Cleveland, Ohio*

*Rudy T. Haluza*
*Penn State University, State College, Pennsylvania*

*Javier Buenrostro*
*University of California at San Diego, California*

December 2021

# NASA STI Program Report Series

Since its founding, NASA has been dedicated to the advancement of aeronautics and space science. The NASA scientific and technical information (STI) program plays a key part in helping NASA maintain this important role.

The NASA STI program operates under the auspices of the Agency Chief Information Officer. It collects, organizes, provides for archiving, and disseminates NASA's STI. The NASA STI program provides access to the NTRS Registered and its public interface, the NASA Technical Reports Server, thus providing one of the largest collections of aeronautical and space science STI in the world. Results are published in both non-NASA channels and by NASA in the NASA STI Report Series, which includes the following report types:

- TECHNICAL PUBLICATION. Reports of completed research or a major significant phase of research that present the results of NASA Programs and include extensive data or theoretical analysis. Includes compilations of significant scientific and technical data and information deemed to be of continuing reference value. NASA counterpart of peer-reviewed formal professional papers but has less stringent limitations on manuscript length and extent of graphic presentations.

- TECHNICAL MEMORANDUM. Scientific and technical findings that are preliminary or of specialized interest, e.g., quick release reports, working papers, and bibliographies that contain minimal annotation. Does not contain extensive analysis.

- CONTRACTOR REPORT. Scientific and technical findings by NASA-sponsored contractors and grantees.

- CONFERENCE PUBLICATION. Collected papers from scientific and technical conferences, symposia, seminars, or other meetings sponsored or co-sponsored by NASA.

- SPECIAL PUBLICATION. Scientific, technical, or historical information from NASA programs, projects, and missions, often concerned with subjects having substantial public interest.

- TECHNICAL TRANSLATION. English-language translations of foreign scientific and technical material pertinent to NASA's mission.

Specialized services also include organizing and publishing research results, distributing specialized research announcements and feeds, providing information desk and personal search support, and enabling data exchange services.

For more information about the NASA STI program, see the following:

- Access the NASA STI program home page at http://www.sti.nasa.gov

- Help desk contact information:

https://www.sti.nasa.gov/sti-contact-form/
and select the "General" help request type.

NASA/TM–20210025992

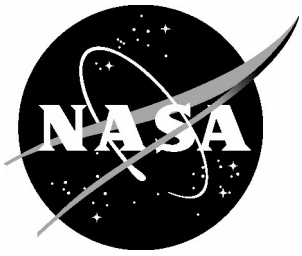

# Application of a Developmental Composite Material Model to Predict the Crush Response of Two Energy Absorbers

*Karen E. Jackson*
*National Institute of Aerospace, Hampton, Virginia*

*Robert K. Goldberg and Trenton M. Ricks*
*Glenn Research Center, Cleveland, Ohio*

*Rudy T. Haluza*
*Penn State University, State College, Pennsylvania*

*Javier Buenrostro*
*University of California at San Diego, California*

National Aeronautics and
Space Administration

Langley Research Center
Hampton, Virginia 23681-2199

December 2021

Available from:

NASA STI Program / Mail Stop 148
NASA Langley Research Center
Hampton, VA 23681-2199
Fax: 757-864-6500

# Application of a Developmental Composite Material Model to Predict the Crush Response of Two Energy Absorbers

## OUTLINE

## OUTLINE (Completed)

## List of Acronyms

| | |
|---|---|
| ACP | Advanced Composites Program |
| ASU | Arizona State University |
| ASTM | American Society for Testing and Materials |
| AWG | Aerospace Working Group |
| CH | Cargo Helicopter |
| CPU | Central Processing Unit |
| DAS | Data Acquisition System |
| DIC | Digital Image Correlation |
| FAA | Federal Aviation Administration |
| ft | foot, unit of length |
| g | gravitational force |
| GMU | George Mason University |
| GRC | Glenn Research Center |
| GTFC | Generalized Tabulated Failure Criteria |
| GWU | George Washington University |
| HRI | Honda Research Institute |
| ID | Identification |
| in | inch, unit of length |
| LandIR | Landing and Impact Research facility |
| LaRC | Langley Research Center |
| lb or lbf | pound, unit of force |
| LCID | Load Curve Identification |
| LSTC | Livermore Software Technology Corporation |
| MPP | Massively Parallel Processing |
| MSU | Michigan State University |
| NASA | National Aeronautics and Space Administration |
| OSU | Ohio State University |
| PFC | Puck Failure Criteria |
| PMD | Principal Material Direction |
| PMP | Principal Material Planes |
| QS-RT | Quasi Static - Room Temperature |
| RW | Rotary Wing |
| s | second, unit of time |
| SPC | Single Point Constraint |
| SSCS | Specific Sustained Crush Stress |
| TRACT | Transport Rotorcraft Airframe Crash Testbed |
| TWFC | Tsai-Wu Failure Criteria |
| WWFE-II | World-Wide Failure Exercise (Second) |

## List of Figures

## List of Figures in Appendix C.

## List of Tables

**Application of a Developmental Composite Material Model to Predict the Crush Response of Two Energy Absorbers**

## 1.0 ABSTRACT

In 2012, a consortium was formed with the goal of creating a new composite material model capable of predicting the wide range of properties, accumulated damage behavior, and the many different types of failure in composites under impact loading. The material model was developed for execution in the commercially available nonlinear, explicit transient dynamic finite element code, LS-DYNA®. This material model incorporates three submodels for deformation, damage, and failure. In addition, the model accounts for strain rate and temperature effects and relies heavily on the input of tabulated material response data. The model is designated *MAT_COMPOSITE_TABULATED_PLASTICITY_DAMAGE, or *MAT_213. Initially, *MAT_213 was developed for use with solid elements only; however, a thin shell element formulation for *MAT_213 has been adapted recently. The objective of this project was to find a suitable modeling example to investigate the capabilities and performance of *MAT_213. In 2012, two composite energy absorbers were designed and evaluated at NASA Langley Research Center through multi-level testing and simulation. The first was a conical-shaped energy absorber, designated the conusoid, which consisted of four layers of hybrid carbon-Kevlar® plain-weave fabric oriented at [+45°/-45°/-45°/+45°] with respect to the vertical direction. The second was a sinusoidal-shaped energy absorber, designated the sinusoid, which consisted of hybrid carbon-Kevlar® plain-weave fabric face sheets, two layers for each face sheet oriented at ±45° with respect to the vertical direction, and a closed-cell ELFOAM® P200 polyisocyanurate foam core. Finite element models were developed of the energy absorbers and simulations were performed using LS-DYNA®. In this paper, the development of a *MAT_213 model of a hybrid carbon-Kevlar® plain-weave fabric is presented. Next, comparisons with material characterization tests are presented. Then, test-analysis results are documented for each energy absorber as comparisons of time-history responses, as well as predicted and experimental structural deformations and progressive damage under impact loading using the *MAT_213 material model. Since a prior *MAT_58, or *MAT_LAMINATED_COMPOSITE_FABRIC material model was used in previous simulations of the energy absorbers, comparisons are made between *MAT_58 and *MAT_213 model predictions with test data. Finally, the paper includes a comprehensive list of “lessons learned,” in which a series of parametric studies are documented that were performed to investigate specific issues related to the material model. These “lessons learned” are included in hopes that they may help future *MAT_213 users.

## 2.0 INTRODUCTION

Composite materials are gaining increased usage in the aerospace industry due to their improved stiffness- and strength-to-weight ratios compared with metals. As an example, the Boeing 787 transport aircraft contains 50 percent composites by weight [1]. However, a major factor that is limiting additional gains in the application of composite materials is that it is extremely challenging to predict accurately the onset of damage and progressive failure response, especially under transient dynamic loading conditions. Composite materials can fail in a variety of macroscopic modes, including fiber fracture, matrix cracking, and delamination. Mechanisms of failure at the microscopic level include tensile, compressive, or shear fracture of the matrix; bond failure of the fiber-matrix interface; and, tensile or compressive (buckling) failure of the fibers. Adding further complication, these failure modes can occur separately or in combination with one another.

Many failure theories have been developed to simulate damage onset and progressive failure of composite materials and structures. In fact, the Second World-Wide Failure Exercise (WWFE-II) is an international effort to examine 12 different failure theories and assess their maturity and capabilities [2-4] through detailed test-analysis comparisons. Results of this multiyear, multiorganizational effort have proved that one criterion cannot predict all observed failure mechanisms in composites.

### 2.1 Motivation for Material Model Development

A meeting of the LS-DYNA® Aerospace Working Group (AWG) was held in 2012 during which the development of a new composite material model, to be incorporated into the commercial, nonlinear transient dynamic finite element code LS-DYNA® [5] was proposed. The LS-DYNA® AWG is a partnership of federal agencies, corporations, and universities working together to support the use, development, and reliability of LS-DYNA® for aerospace numerical analyses. The primary motivation for the development of a new composite material model was that existing LS-DYNA® material models have been found to have limitations in some aspect of their capabilities. For example, a table of current composite material models available in LS-DYNA® is provided in Table 1, along with a list of their capabilities. Note that only *MAT_213 has all capabilities such as applicability to shell and solid elements, damage and failure predictive capabilities, strain rate effects and temperature effects listed as ‘yes.’ Even though *MAT_213 is applicable to solid elements, only the shell element formulation of *MAT_213 was exercised in this project. Development of the model has continued over the past decade with close cooperation of Livermore Software Technology Corporation (LSTC), which was the parent company of LS-DYNA®. Recently, LSTC was purchased by Ansys, Inc. [6]. As of today, the material model has not yet been generally released and access is available only through a developmental version

of LS-DYNA®. However, general release is expected in 2022. Currently, *MAT_213 is undergoing final quality checks.

Table 1. List of Current Composite Material Models in LS-DYNA®.
(Reprinted from Reference 7 with permission)

| MAT No. | Title | Shells | Damage | Failure | Rate Effects | Temp Effects |
|---|---|---|---|---|---|---|
| 22 | *MAT_COMPOSITE_ DAMAGE | Yes | No | Yes | No | No |
| 54 | *MAT_ENHANCED_ COMPOSITE_DAMAGE | Yes | Yes | Yes | Yes | No |
| 55 | | Yes | Yes | Yes | Yes | No |
| 58 | *MAT_LAMINATED_ COMPOSITE_FABRIC | Yes | Yes | Yes | Yes | No |
| 59 | *MAT_COMPOSITE_ FAILURE_{OPTION}_MODEL | Yes | Yes | Yes | No | No |
| 116 | *MAT_COMPOSITE_LAYUP | Yes | No | No | No | No |
| 117 | *MAT_COMPOSITE_MATRIX | Yes | No | No | No | No |
| 118 | *MAT_COMPOSITE_DIRECT | Yes | No | No | No | No |
| 158 | *MAT_RATE_SENSITIVE_ COMPOSITE_FABRIC | Yes | Yes | Yes | Yes | No |
| 161/162 | *MAT_COMPOSITE_MSC/ *MAT_COMPOSITE_DMG_MSC | Yes | Yes | Yes | Yes | No |
| 213 | *MAT_COMPOSITE_TABULATED_ PLASTICITY_DAMAGE | Yes | Yes | Yes | Yes | Yes |
| 219 | *MAT_CODAM2 | Yes | Yes | Yes | No | No |
| 221 | *MAT_ORTHOTROPIC_ SIMPLIFIED_DAMAGE | No | Yes | Yes | No | No |
| 261 | *MAT_LAMINATED_ FRACTURE_DAIMLER_PINHO | Yes | Yes | Yes | No | No |
| 262 | *MAT_LAMINATED_ FRACTURE_DAIMLER_ CAMANHO | Yes | Yes | Yes | No | No |

## 2.2 Description of the Two Energy Absorbers

At about the same time that development began on *MAT_213, NASA Langley Research Center (LaRC) initiated design and evaluation of two composite energy absorbers through multilevel testing and simulations performed under the Transport Rotorcraft Airframe Crash Testbed (TRACT) research program [8]. One of the energy absorbers was a conical-shaped design that consisted of a series of righ side up and upside down cones. This energy absorber was fabricated of four layers of hybrid carbon-Kevlar® plain-weave fabric oriented at [+45°/-45°/-45°/+45°] with respect to the vertical, or crush, direction and was designated the “conusoid” [9]. A sinusoidal-shaped energy absorber, designated the “sinusoid,” was developed that consisted of hybrid carbon-Kevlar® plain-weave fabric face sheets, two layers for each face sheet oriented at ±45° with respect to the vertical direction and a closed-cell ELFOAM® P200 polyisocyanurate (2.0 lb/ft$^3$) foam core [10]. Additional information on the

development, testing, and simulation of the two energy absorbers is documented in References 8-13.

A building block approach was used in the evaluation of the energy absorbers. This approach included basic material testing of the constituent materials including both the hybrid carbon-Kevlar® plain-weave fabric and the closed-cell ELFOAM® P200 polyisocyanurate foam. Next components of the energy absorbers were fabricated and tested under impact loading. Each component was 12-in. long, 7.5-in. high, and 1.5-in. wide. Following successful component testing, larger subfloor-level components were manufactured and retrofitted into a barrel section of a CH-46E helicopter, which was tested under vertical impact. Finally, the energy absorbers were retrofitted into a full-scale CH-46E helicopter that was crash tested at the Landing and Impact Research (LandIR) Facility at NASA Langley Research Center [12]. Please note that only the energy absorber component tests are presented in the current paper.

### 2.3 Objectives of the Paper

This paper will describe *MAT_213 including its three submodels for deformation, damage, and failure and will document the development of *MAT_213 to represent hybrid carbon-Kevlar® plain-weave fabric, based on limited material characterization data. Comparisons of predicted and experimental material responses were generated. Next, the existing finite element models of the conusoid and sinusoid energy absorbers were modified to utilize *MAT_213 to represent the composite layers in both energy absorbing concepts. Crush simulations were conducted, and test-analysis results are presented for each energy absorber as comparisons of time-history responses, as well as predicted and experimental structural deformations and progressive damage under impact loading. Previous simulations of the conusoid and sinusoid were performed in which the hybrid carbon-Kevlar® plain-weave fabric was simulated using a continuum damage mechanics-based composite material model called *MAT_LAMINATED_COMPOSITE_FABRIC or *MAT_58, see Reference 13. Consequently, comparisons were made between *MAT_213 and *MAT_58 analytical predictions and test data.

## 3.0 DESCRIPTION OF *MAT_213

The development of *MAT_213 began during a meeting of the LS-DYNA® AWG in 2012. A consortium was created with charter members: the Federal Aviation Administration (FAA), the National Aeronautics and Space Administration (NASA) Glenn Research Center (GRC), Arizona State University (ASU), George Mason University (GMU), Ohio State University (OSU), and Livermore Software Technology Corporation (LSTC). Since its initial creation, the consortium has grown to include George Washington University (GWU) and NASA Langley Research Center (LaRC). The initial goal of the consortium was to create a material

model flexible enough to represent the wide range of properties, accumulated damage behavior, and the many different types of failure in composites. Some of the desired features of the new material model were:

- Deformation and Damage Model with generalized, tabulated input, stress-strain curves for nondamage related behavior
- Input parameters based upon standard mechanical property tests
- Explicit modeling of interlaminar delamination via tiebreak contact and cohesive zone elements
- Strain rate and temperature effects included
- Strain based damage and failure parameters
- Implemented for both shell and solid elements
- Extremely fast computationally

The initial development of *MAT_213 started with funding from the FAA in 2012. Subsequently, additional funding was obtained from NASA as a part of the Advanced Composites Project (ACP) in 2015. The ACP project was undertaken with a goal to develop theory, algorithms, experimental techniques, and analysis methods to reduce the total time taken for the development and certification of new composite structures. Currently, the certification process can take 10 to 20 years. One goal in developing this next generation material model is to reduce certification time to 3 to 5 years.

*MAT_213 was created to be a fully generalized material model suitable for use with any composite architecture (unidirectional, woven or braided). The *MAT_213 algorithm is divided into three components: deformation, damage, and failure. Specifically, the deformation submodel simulates the nonlinear material response of the composite (due to either deformation or damage), the damage submodel simulates the nonlinear unloading/reloading due to stiffness reduction, and the failure submodel predicts when the failure criterion is satisfied and erodes the element appropriately. Additional details of each of these three submodels are provided in the next subsections of the paper. Finally, information on the development and application of *MAT_213 is provided in References 7, 14–35.

However, before describing the *MAT_213 submodels, it is important to examine the input cards for *MAT_213, which are listed in Table 2. The units are lb-in-s for this case. *MAT 213, like any other model, is completely flexible in terms of the units that are used, as long as they are consistent. As mentioned previously, most of the parameters listed in Cards 1 and 2 of Table 2, are used by LS-DYNA® to perform internal computations. For example, setting AOPT = 2.0 tells LS-DYNA® that a local coordinate system is defined as the cross product of two vectors (**a** and **d**) that are defined on Cards 3 and 4. Also, note that in Table

2, lines that begin with $# are comments in an actual input deck. The definition of each parameter is provided in Table 3, which is reprinted from the *MAT_213 User's Guide [35]. Finally, please note that the input values in Table 2 are representative of hybrid carbon-Kevlar® plain-weave fabric. The detailed explanation of how these values were generated is provided in Section 4.0. Additionally, omitted values are assumed to have the specified default values listed in Reference 35. The initial moduli inputs are used in the process of determining the initial time steps in the simulation and other initialization actions. However, moduli used in the core of the analysis are computed based on the input stress-strain data.

Table 2. *MAT_213 Input Cards

| *MAT_213 | | | | | | | |
|---|---|---|---|---|---|---|---|
| $# Card 1 | | | | | | | |
| $# mid | RO | EA | EB | EC | PRBA | PRCA | PRCB |
| 1 | 1.29E-4 | 6.42E6 | 2.68E6 | 2.68E6 | 0.1095 | 0.048 | 0.048 |
| $# Card 2 | | | | | | | |
| $# GAB | GBC | GAC | PTOL | AOPT | MACF | FILT | VEVP |
| 3.26E5 | 3.26E5 | 3.26E5 | 1.0E-6 | 2.0 | 1 | | 0 |
| $# Card 3 | | | | | | | |
| $# XP | YP | ZP | A1 | A2 | A3 | | |
| | | | 1 | 0 | 0 | | |
| $# Card 4 | | | | | | | |
| $# V1 | V2 | V3 | D1 | D2 | D3 | BETA | TCSYM |
| | | | 1 | 1 | 0 | | 0 |
| $# Card 5 | | | | | | | |
| $# H11 | H22 | H33 | H12 | H23 | H13 | H44 | H55 |
| 0.007 | 0.082 | | -.00085 | | | 3.875 | |
| $# Card 6 | | | | | | | |
| $# H66 | LT1 | LT2 | LT3 | LT4 | LT5 | LT6 | LT7 |
| | 1001 | 1002 | | 1004 | 1005 | | 1007 |
| $# Card 7 | | | | | | | |
| $# LT8 | LT9 | LT10 | LT11 | LT12 | YSC | DFLAG | DC |
| | | 1010 | | | 100 | 1 | 50 |
| $# Card 8 | | | | | | | |
| $#FCTYPE | FV0 | FV1 | FV2 | FV3 | FV4 | FV5 | FV6 |
| 3 | 100 | | 2 | 9013 | | | |
| $# Card 9 | | | | | | | |
| $# FV7 | FV8 | FV9 | FV10 | FV11 | FV12 | FV13 | FV14 |
| | | | | | | | |

| $# Card 10 | | | | | | | |
|---|---|---|---|---|---|---|---|
| $#BETA11 | BETA22 | BETA33 | BETA44 | BETA55 | BETA66 | BETA112 | BETA23 |
| | | | | | | | |
| $# Card 11 | | | | | | | |
| $#BETA13 | Cp | TQC | TEMP | PMACC | | | |
| | | | | | | | |

Parameters used by the *MAT_213 plasticity algorithm and the deformation submodel include PRBA, PRCA, PRCB, FILT, VEVP and the parameters on Cards 5-7, excluding DFLAG and DC. These two parameters are the only ones used in the *MAT_213 damage submodel. Parameters listed on Cards 8-11 are used specifically in the MAT_213 failure algorithm. All parameters are described in the *MAT_213 User's Guide [Reference 35] and are repeated here in Table 3. Please note that the Remarks listed in Table 3 can be found in Appendix A. Additionally, note that multiple parameters point to separate tables and curves that may be required (e.g., LT1 and LT12) or optional input (e.g., DC).

Table 3. Definition of *MAT_213 Parameters

| Parameter | Symbol | Description |
|---|---|---|
| MID | | Material identification number |
| RO | | Mass density |
| EA | $E_A$ | Young's modulus in the A-direction |
| EB | $E_B$ | Young's modulus in the B-direction |
| EC | $E_C$ | Young's modulus in the C-direction |
| PRBA | $\nu_{BA}$ | Elastic Poisson's Ratio, BA |
| PRCA | $\nu_{CA}$ | Elastic Poisson's Ratio, CA |
| PRCB | $\nu_{CB}$ | Elastic Poisson's Ratio, CB |
| GAB | $G_{AB}$ | Shear modulus, A-B plane |
| GBC | $G_{BC}$ | Shear modulus, B-C plane |
| GCA | $G_{CA}$ | Shear modulus, C-A plane |
| PTOL | | Yield function tolerance used during plastic multiplier calculations |
| AOPT | | Material axis option:<br>EQ.0.0: locally orthotropic with material axes determined by element nodes 1, 2, and 4, as with *DEFINE_COORDINATE_NODES.<br>EQ.1.0: locally orthotropic with material axes determined by a point in space and the global location of the element center; this is the a-direction. This option is for solid elements only.<br>EQ.2.0: globally orthotropic with material axes determined by vectors defined below, as with *DEFINE_COORDINATE_VECTOR.<br>EQ.3.0: locally orthotropic material axes determined by rotating the material axes about the element normal by an angle, BETA, from a line in the plane of the element defined by the cross product of the vector v |

| | | |
|---|---|---|
| | | with the element normal.<br>EQ.4.0: locally orthotropic in cylindrical coordinate system with the material axes determined by a vector v, and an originating point, P, which define the centerline axis. This option is for solid elements only.<br>LT.0.0: the absolute value of AOPT is a coordinate system ID number (CID on *DEFINE_COORDINATE_NODES). |
| MACF | | Material axes change flag for brick elements:<br>EQ.1: No change, default,<br>EQ.2: switch material axes A and B,<br>EQ.3: switch material axes A and C,<br>EQ.4: switch material axes B and C. |
| FILT | | Factor for strain rate filtering (optional):<br>$\dot{\varepsilon}i+1\text{avg}=(1-\text{FILT})\times\dot{\varepsilon}i+1\text{cur}+\text{FILT}\times\dot{\varepsilon}i\text{avg}$<br>where i is the previous time step. The value of FILT is between 0 and 1. |
| VEVP | | Flag to control viscoelastic and viscoplastic behavior:<br>EQ.0: viscoplastic only with no rate effects in elastic region (default)<br>EQ.1: viscoelastic and viscoplastic (see cards 10 & 11) |
| XP, YP, ZP | | Coordinates of point p for AOPT = 1 |
| A1, A2, A3 | | Components of vector **a** for AOPT = 2 |
| V1, V2, V3 | | Components of vector **v** for AOPT = 3 |
| D1, D2, D3 | | Components of vector **d** for AOPT = 2 |
| BETA | | Material angle in degrees for AOPT = 3, may be overridden on the element card, see *ELEMENT_SHELL_BETA or *ELEMENT_SOLID_ORTHO. |
| TCSYM | | Flag for handling tension-compression asymmetry in all three material directions:<br>EQ.0: Do not adjust user-defined data (default)<br>EQ.1: Compute and use average of tension and compression elastic moduli in adjusting the stress-strain curve. See Remark 7.<br>EQ.2: Use compression modulus as user-defined tension modulus in adjusting the stress-strain curve. See Remark 7.<br>EQ.3: Use tension modulus as user-defined compression modulus in adjusting the stress-strain curve. See Remark 7.<br>EQ.4: Use user-defined tensile curve as the compressive curve overriding the user-defined compressive curve. This implies that the normal stress-strain curves are symmetric including yield values.<br>EQ.5: Use user-defined compressive curve as the tensile curve overriding the user-defined tensile curve. This implies that the normal stress-strain curves are symmetric including yield values. |
| H11, H22, H33, H12, H23, H13, H44, H55, H66 | | Plastic flow rule coefficients. H33, H55 and H66 are not required for shell elements.<br>**See Remark 1.** |
| LT*i*, i=1,12 | | TABLE_3D ID's containing temperature and strain rate dependent stress-strain input curves for the 12 separate tests (LT: 3D Load Tables):<br>LT1-3: Tension A, B, C directions,<br>LT4-6: Compression A, B, C directions,<br>LT7: Shear a-b plane, |

| | | |
|---|---|---|
| | | LT8: Shear b-c plane,<br>LT9: Shear a-c plane,<br>LT10: 45° Off-axis a-b plane Tension or Compression,<br>LT11: 45° Off-axis b-c Tension or Compression,<br>LT12: 45° Off-axis a-c Tension or Compression.<br>For shell elements: LT3, LT6, LT8, LT9, LT11 and LT12 are not required while LT10 is optional.<br>**See Remarks 2, 8 and 9.** |
| YSC | | Load curve ID containing the stress-strain curve ID's and associated initial yield strain values. **See Remark 3.** |
| DFLAG | | Damage formulation flag:<br>EQ.0: Based on effective stress (default)<br>EQ.1: Based on corrected plastic strain |
| DC | | Curve ID that specifies which components of the damage model are active. It contains the damage parameter ID and the corresponding damage versus total strain curve ID. Set this value to zero if damage should not be included in the analysis. **See Remark 4.** |
| FCTYPE | | Failure criterion type:<br>EQ.0: No Failure considered (default)<br>EQ.1: Puck Failure Criterion (PFC) (solid elements only)<br>EQ.2: Tsai-Wu Failure Criterion (TWFC) (solid elements only)<br>EQ.3: Generalized Tabulated Failure Criterion (GTFC)<br>**See Remarks 5 and 6 for FCTYPE, FV1, … FV12 input parameters.** Tsai-Wu Failure Criterion and Generalized Tabulated Failure Criterion are abbreviated TWFC and GTFC, respectively. It should be noted that *DEFINE_ELEMENT_ EROSION_SHELL keyword is required for element erosion for shell elements. |
| FV0 – FV14 | | These parameters depend on the selected failure criteria Please find additional information in Reference 35. |
| BETA11-BETA66 | | These parameters are used to define VEVP parameters. |
| $c_p$ | | Specific heat capacity (per unit mass) |
| TQC | | Taylor-Quinney Coefficient |
| TEMP | | This is the reference (initial) temperature used to obtain the corresponding stress-strain curves. |
| PMACC | | Plastic multiplier computational accuracy<br>EQ. 0: Use up to a maximum of 1000 increments (default)<br>EQ. N: Specify a positive value N greater than 1 as the maximum number of increments. An error message is issued if a converged solution cannot be found. |

It should be noted that full implementation (e.g. deformation, damage and failure) of *MAT_213 requires additional input, beyond the parameters shown in Table 2. In fact, for the model simulations performed and documented in this report, four separate files were

created to fully define *MAT_213. These are 12_MAT213.k (master input curve), 13_MAT213_InputCurves_wDamage.k (input curves and yield strains), 14_DAMAGE.k (damage parameters), and 15_FAILURE_SURFACE.k (failure parameters). Consequently, these four files are reprinted in Appendix B.

### 3.1 Deformation Submodel

The deformation submodel is a strain-hardening orthotropic plasticity model which is generated by utilizing a yield function with the functional form of the Tsai-Wu composite failure criteria [36] and a nonassociative flow law. The input needed for the plasticity-based deformation submodel can be derived from a set of twenty experiments performed under uniaxial stress conditions: uniaxial tension in each of the three Principal Material Directions (PMDs), uniaxial compression in each of the three PMD, pure shear in each of the three Principal Material Planes (PMP), and optionally-defined 45° off-axis tension or compression in each of the three PMP. The PMDs are referred to as the 1, 2, and 3 directions, respectively (analogous to the a, b, and c material directions in the LS-DYNA® keyword user's manual [5]). For a general orthotropic material, the twenty experiments are expected to be performed under Quasi Static and Room Temperature (QS-RT) conditions during laboratory testing or virtual testing. Each of the experiments may be performed at various combinations of temperature and strain rate to provide additional input to *MAT_213. However, if shell elements are used, the required number of experiments can be reduced to five. These five experiments are uniaxial tension in each of the two in-plane PMDs, uniaxial compression in each of the in-plane PMDs and in-plane pure shear. The requirement for in-plane off-axis test data is optional for shell and solid elements.

The plasticity algorithm relies heavily on input of the constant flow rule coefficients, H11 through H66, which are found on cards 5 and 6 of the input deck (see Tables 2 and 3). The flow rule coefficients are used to reflect the development of plastic strain in the material. Note that a software program was developed at ASU to assist in calculating the flow rule coefficients based on tabulated input curves [37]. In fact, the flow rule coefficients listed in Table 2 for the hybrid carbon-Kevlar® plain-weave fabric were provided by ASU, based on the available test data.

In addition to plasticity, the deformation submodel also supports viscoelastic/viscoplastic behavior and thermomechanical effects using optional user-supplied input. The input stress-strain curves are converted into effective stress-effective plastic strain during the pre-processing step, which is later used to compute the yield function coefficients during the simulation. The effective plastic strain is used as a tracking parameter to see where the current load state lies on each of the stress-strain curves. Both the effective stress versus total strain and the effective stress versus effective plastic strain need to have positive

slopes. It should be noted that beyond the end of each curve, an extrapolation is conducted using the last two points in each curve. For additional information on the deformation submodel, the reader is referred to References 7, 20, 25, 28-29, and 31.

### 3.2 Damage Submodel

In a practical sense, the damage submodel is a “wrapper” around the deformation model. The damage model converts the stresses from the true stress space to the effective stress space. The deformation/plasticity model then utilizes the effective stresses to track the evolution of the material response. The new stresses computed using the deformation model are then converted back into the true stress space to reflect the actual material response. The damage model can be used both to capture nonlinear unloading before the peak stress is reached and stress degradation after the peak stress is reached. Unloading tests and simulations can be used to distinguish between softening due to plasticity and damage.

For *MAT_213, only two parameters are required to initiate the damage submodel: DFLAG and DC. These parameters are found on Card 7 of the *MAT_213 input, as shown in Table 2. DFLAG serves as a damage formulation flag. If it is set to 0 (default), then damage is based on effective stress. If it is set to 1, then damage is based on the corrected plastic strain. The DC parameter identifies a curve ID that specifies which components of the damage model are active. It contains the damage parameter ID and the corresponding damage versus total strain curve ID. If damage is not to be included in the analysis, then DC should be set to 0.

Finally, the damage model is optional. If a user truly just wants a deformation only analysis, damage is not needed. Also, even though only two parameters are included in the input deck, setting up the tabulated curves required for the damage model can be complex, particularly for the prepeak stiffness reduction. Consequently, users should be aware that setting up and using the damage model is not a trivial process.

### 3.3 Failure Submodel

Three different failure models are implemented in *MAT_213 and they can be activated one at a time. These are: Puck Failure Criteria (PFC), Tsai-Wu Failure Criteria (TWFC) and Generalized Tabulated Failure Criteria (GTFC). Of these three failure models, only GTFC utilizes tabulated parameters. Note that Puck and Tsai-Wu are existing failure criteria, while GTFC was developed for *MAT_213. The number of parameters required are different for each of the implemented failure submodels. The selection of the failure criteria to be used is designated by the parameter FCTYPE, which can be set to 0 for no failure, 1 for the PFC, 2 for TWFC, and 3 for GTFC. As indicated in Table 2, the failure criterion selected for the

present simulations was GTFC, or FCTYPE equal 3. Additional information on the failure submodel can be found in References 7, 15-16, 18.

## 4.0 DEVELOPMENT OF A *MAT_213 MODEL FOR HYBRID CARBON-KEVLAR® PLAIN-WEAVE FABRIC BASED ON MATERIAL CHARACTERIZATION TEST DATA

As mentioned previously, *MAT_213 is based on tabulated test data, and, as a reminder, the shell formulation of *MAT_213 requires input from five tests: longitudinal tension, transverse tension, longitudinal compression, transverse compression, and shear. The off-axis test input is optional. For the hybrid carbon-Kevlar® plain-weave fabric, only a limited set of test data were available including longitudinal tension, transverse tension, and biaxial tension. In this case, the compression properties were assumed to be identical to the tensile properties. Also, the biaxial tension data were used to derive shear properties, as well as for the optional off-axis curve. This section of the report will describe the available test data and show test-analysis comparisons between test data and *MAT_213 predicted responses.

### 4.1 Material Characterization Data

A close-up photograph of the hybrid carbon-Kevlar® plain-weave fabric is shown in Figure 1, in which the carbon fibers are oriented vertically (warp direction) and the Kevlar® fibers are oriented horizontally (fill direction). The hybrid material is composed of T300 carbon and Kevlar® 49. The resin is a West System 105 resin with 205 hardener. Specimen fabrication was performed using a wet layup with curing at room temperature for a minimum of 24 hours. This hybrid material was used to fabricate all coupons and the energy absorbers described herein. Note that *MAT_213 does not represent the individual fibers within a layer of fabric material, and, instead, represents each layer in the composite laminate with overall effective properties.

A limited set of material characterization tests were performed on the hybrid carbon-Kevlar® fabric, including tensile tests of coupons in which the carbon fibers were oriented in the 0° longitudinal (axial) direction, tensile tests of coupons in which the carbon fibers were oriented in the 90° transverse direction, and tensile tests of coupons in which the carbon fibers were oriented in a ±45° direction. These tests were performed on 10 in. x 1 in. coupons with a gauge length of 6 in., and a 4-ply stacking sequence, with total thickness of approximately 0.04 in. Tensile tests were conducted in accordance with the American Society of Testing and Materials (ASTM) 3039 [38], and in-plane shear tests were conducted in accordance with ASTM 3518 [39].

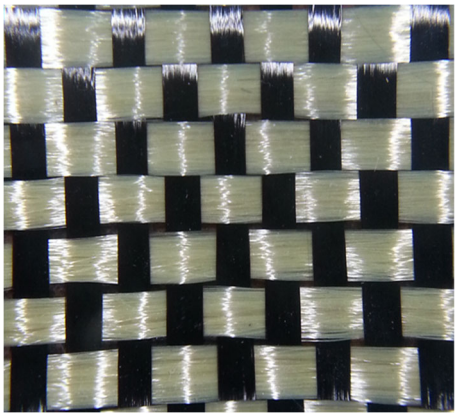

Figure 1. Hybrid carbon-Kevlar® plain-weave fabric.

The longitudinal tensile stress versus strain response is plotted in Figure 2(a), which represents the average response obtained from three repeated tests of coupons in which the carbon fibers are oriented at 0° with respect to the axial direction. Stress was determined by dividing the measured load, recorded on a MTS load-test machine, by the cross-sectional area of the specimen. Strain was determined at three locations along the length of the gauge section using Digital Image Correlation (DIC) in conjunction with a speckle pattern that was sprayed onto the specimen. The three strain measurements were averaged for each test. The longitudinal tension response is nearly perfectly linear elastic until a maximum stress of 89,386 psi, at which point a load drop occurs indicating loss of load-carrying capability in the coupon. Unfortunately, the test was stopped at this point and no additional "post-peak degradation" response was measured. The parameter EA, Young's modulus in the A-direction, was obtained from this plot (see Table 2). Also, the data shown in Figure 2(a) were input as tabulated data assigned to LT1, which is a *DEFINE_TABLE_3D identification (ID) containing temperature and strain rate dependent stress-strain input curves (ID 1001). Please note that the longitudinal tension data, shown in Figure 2(a), were input without filtering or smoothing. In addition, since no longitudinal compression data were available, the tabulated data from Figure 2(a) were also assigned to LT4 (*DEFINE_TABLE_3D, ID 1004).

Test results are plotted in Figure 2(b) for transverse tensile stress versus strain from coupons in which the carbon fibers are oriented at 90° with respect to the axial direction. Two coupon responses were averaged to obtain the response. A reference line is added in the plot which begins at the origin and matches the elastic response of the test curve. Unlike the longitudinal tension curve, the transverse response exhibits a short period of linear elastic response followed by a nonlinear response. The transition between linear and nonlinear behavior initiates at a strain of 0.006 in/in. A load drop occurs at 53,315 psi indicating initial failure of the coupon. Unfortunately, the test was stopped at this point and no additional post-peak degradation was recorded. The parameter EB, Young's modulus in

the B-direction, was obtained from this plot (see Table 2). The data shown in Figure 2(b) were input as tabulated data assigned to LT2 (*DEFINE_TABLE_3D, ID 1002), without filtering or smoothing. In addition, since no transverse compression data were available, the tabulated data from Figure 2(b) were also assigned to LT5 (*DEFINE_TABLE_3D, ID 1005).

Average test results are plotted in Figure 2(c) for two coupons in which the carbon fibers are oriented at ±45° with respect to the axial direction. This biaxial tension test is used to derive shear properties of the material. Also, the averaged curve was filtered to remove high frequency oscillations. Shear stresses and shear strains (and the corresponding shear stress versus shear strain curve) were approximated using procedures based on standards and equations discussed in References 40-42. Given the lack of shear test data and transverse strain data, these curves are most likely approximations and can be refined based on the results of future testing. Obviously, both the biaxial tension and shear responses, shown in Figures 2(c) and 2(d), are highly nonlinear. The data shown in Figure 2(c) were converted to shear stress versus shear strain and are plotted in Figure 2(d). The parameter GAB, shear modulus in the A-B plane, was obtained from this plot (see Table 2). The data shown in Figure 2(d) were input as tabulated data assigned to LT7 (*DEFINE_TABLE_3D, ID 1007). In addition, since *MAT_213 allows for input of off-axis data, the tabulated data from Figure 2(c) were also assigned to LT10 (*DEFINE_TABLE_3D, ID 1010).

To further clarify how the test curves, shown in Figure 2, are input into *MAT_213, lines of code from the LS-DYNA® file containing the tabulated curves are listed in Figure 3. The example shown is for the longitudinal tension load curve. While temperature dependency can be easily ignored, strain rate dependency must be included, even if strain rate test data are not available. For example, in Figure 3, the *DEFINE_TABLE_3D card establishes the base temperature as 21° C. Next, the *DEFINE_TABLE card establishes two input load curves, Load Curve ID (LCID) 1111 at a strain rate of 0.0 $s^{-1}$ and LCID 10000001 at a strain rate of 1.0 $s^{-1}$. Since no strain rate data were available for the hybrid carbon-Kevlar® plain-weave fabric, LCID 1111 and LCID 10000001 are identical. Note that all load curves were input to the 13_MAT213_InputCurves_wDamage.k file.

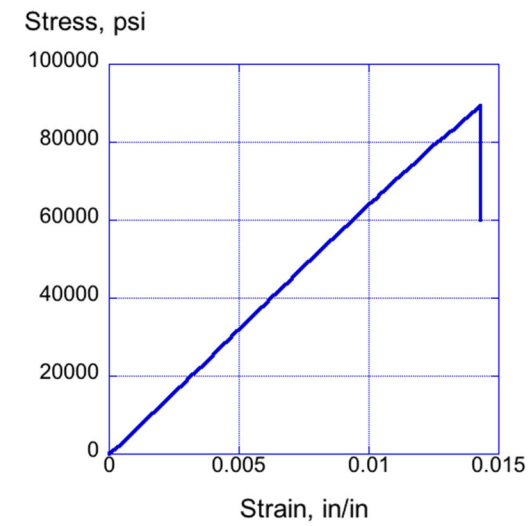


(a) Longitudinal response.

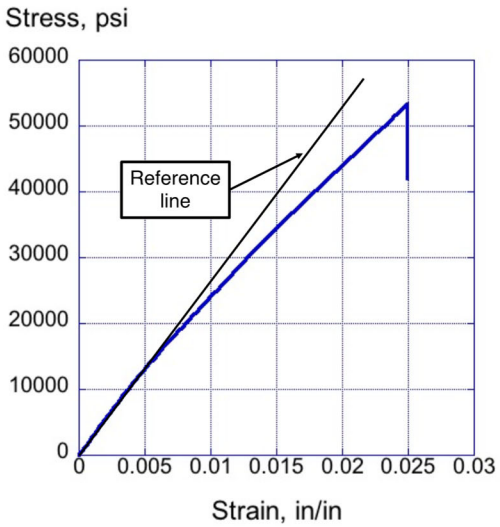


(b) Transverse tensile response.

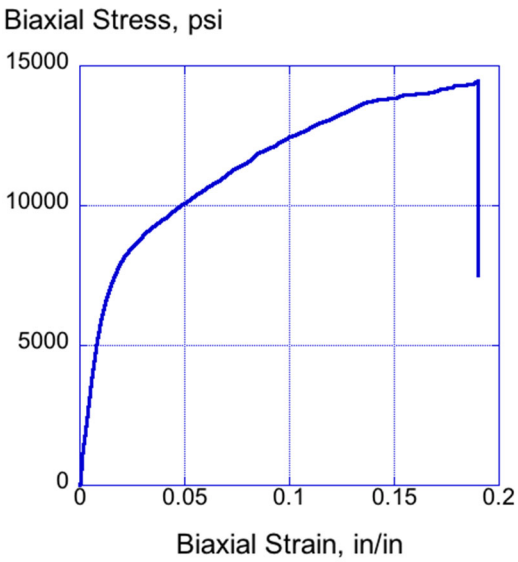


(c) Biaxial tension response.

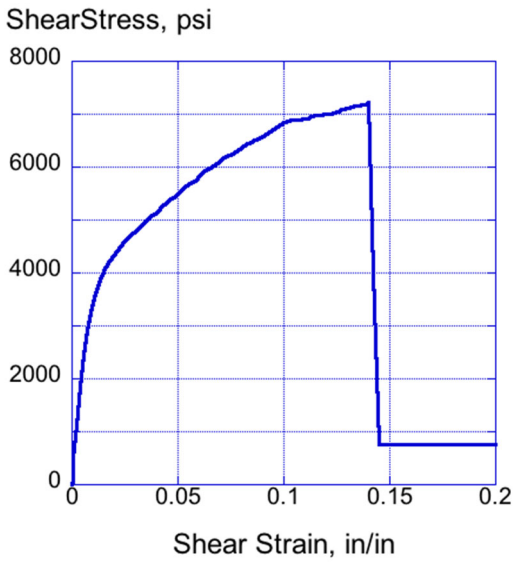


(d) Shear response.

Figure 2. Material characterization test results.

Before moving on, it is worth mentioning that beginning users of *MAT_213 should know that entering tabulated test data from load curves can present numerous difficulties. First, the tabulated data must be input in ascending order. Often it may be necessary to filter the test data to remove oscillations. Second, it may be best to input the test data for a fixed number of points. For example, one hundred points per load curve is sometimes used. When error messages occur, it is best to refer to the *MAT_213 User's Guide [35].

### 4.2 Test-Analysis Comparison with Material Characterization Data

This section of the paper presents test-analysis comparisons between material test data and model predictions. The section is divided into four subsections: Comparison with Longitudinal Tension Test Data, Comparison with Transverse Tension Test Data, Comparison with Biaxial Tension Test Data, and Comparison with Shear Test Data. For all simulations, the *MAT_213 model, shown in Table 2, was used with no changes. The GTFC was specified for each simulation and three modes of failure were enabled including longitudinal tension, transverse tension, and shear.

```
*DEFINE_TABLE_3D
$ Tension_1
$#     tbid         sfa         offa
      1001
$# temperature                    table_id
                    21                 1013
$
*DEFINE_TABLE
$ Tension_1, Temperature = 21 degrees
$#     tbid         sfa         offa
     1013
$#         strain_rate            curve_id
                   0.0                1111
                   1.0            10000001
$
*DEFINE_CURVE
$ Tension_1, Temperature = 21 degrees, Strain Rate = 0.0/s
$#     lcid         sidr        sfa             sfo       offa       offo     dattyp
      1111
$#                strain                  stress
                0.0000                  0.0000
             0.0001575                  800.00
            0.00032473                  1937.7
                 -----                   .....
```

A simple finite element model was developed and executed to represent the material characterization tests previously described. Instead of simulating the actual 1-in. x 6-in. gauge section of the coupon, a 1-in. x 1-in. model was developed, which provided a more uniform stress distribution across the width of the specimen. The model, shown in Figure 4, contained 289 Belytschko-Tsay shell elements, 329 nodes, and 1 material property (*MAT_213) and had a nominal element edge length of 0.0588 in. Four layers were input using the *PART_COMPOSITE feature in LS-DYNA® which allows the user to assign ply thickness, orientation, and material property for each layer in the composite. A Single Point Constraint (SPC) was defined to fix the nodes on the left side of the model. In addition, the nodes on the right side of the model were assigned a boundary prescribed motion card such

that, at the start time, the displacement in the x-direction was zero and at the end time (0.5 s) it was a prescribed value based on the test being simulated. The model was loaded slowly to minimize the kinetic energy of the simulation, thus recreating the quasi-static conditions used during the test. Output from the model included the SPC force at each node on the left side of the model. These forces were summed and divided by the cross-sectional area of the specimen to obtain stress. Strain was derived as a ratio of the time and displacement and was divided by the original length (1 in.) of the specimen. To further clarify this statement, an example illustrating the method used to determine strain is described, as follows.

The end time of the simulation (0.5 s) and the maximum displacement (0.02 in.) are known values. A ratio is formed, as shown in Eqn. 1:

$$\frac{\text{Time(s)}}{0.5} = \frac{\text{Displ(in)}}{0.02} \tag{1}$$

Then, solving for displacement as a function of time yields Eqn. 2:

$$\text{Displ (in)} = \frac{0.02 \times \text{Time(s)}}{0.5} \tag{2}$$

Calculating displacement for the example case is shown in Eqn. 3:

$$\text{Displ(in)} = 0.04 \times \text{Time(s)} \tag{3}$$

Finally, since strain is displacement/length, then:

$$\text{Strain} = \frac{0.04 \times \text{Time(s)}}{\text{1.0-in.}} \tag{4}$$

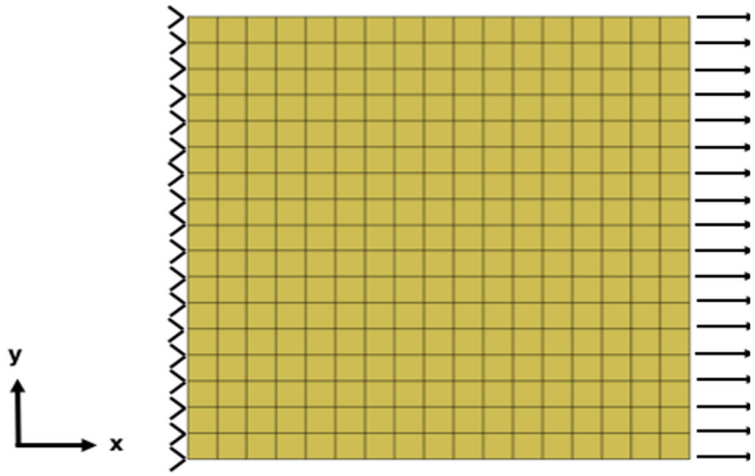

Figure 4. Tensile coupon model.

4.2.1 Comparison with Longitudinal Tension Test Data

For the longitudinal tension simulation, four plies were input using *PART_COMPOSITE. Each ply was 0.0117-in. thick, giving the laminate a total thickness of 0.047 in. The model was executed for an end time of 0.5 s and a maximum displacement of 0.02 in. The model required 36 hours and 56 minutes of Central Processing Unit (CPU) running the Massively Parallel Processing (MPP) developmental version of LS-DYNA® on a Linux-based workstation with 8 processors. The excessively long run time was attributed to the fact that the parameter TSSFAC, which is used to control the time step, was mistakenly set to 0.1. Note that the default value of TSSFAC is 0.9.

A plot showing the longitudinal tensile test response and the *MAT_213 predicted response is shown in Figure 5(a). The model matches the linear elastic stiffness of the test response exactly. The *MAT_213 model predicts the maximum stress and failure almost perfectly. The *MAT_213 response shown in Figure 5(a) was generated by summing the SPC forces at the nodes on the left edge of the model and dividing by the cross-sectional area. The strain was calculated as a ratio of time and displacement using the method described previously. Some analysts may not approve of using this approach for calculating stress and strain due to the influence of boundary conditions on the response. Consequently, a plot of element stress and strain in the x-direction is shown in Figure 5(b) for Elm 145, which is located directly in the center of the tension coupon model (see Figure 4), along with the test response. The predicted curve shown in Figure 5(b) is nearly identical to the one shown in Figure 5(a). As a result, the SPC-method will continue to be used to generate predicted response data in the remainder of the paper.

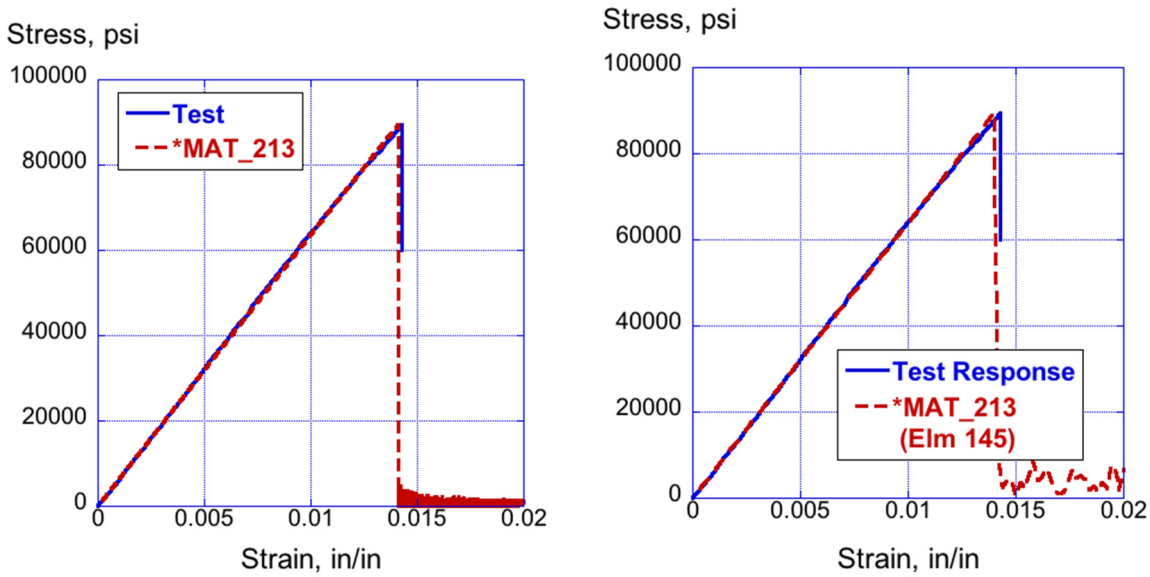


(a) Test versus *MAT_213 using SPC. (b) Test versus element x-stress-strain.

Figure 5. Test-analysis comparisons of longitudinal tension response.

4.2.2 Comparison with Transverse Tension Test Data

For the transverse tension simulation, four plies were input using *PART_COMPOSITE. Each ply was 0.0117-in. thick, giving the laminate a total thickness of 0.047 in. The same tension coupon model, shown in Figure 4, was used for this simulation. The model was executed for an end time of 0.5 s and a maximum displacement of 0.03 in. and required 37 hours and 12 minutes of CPU running the MPP version of LS-DYNA® on a Linux-based workstation with 8 processors. The excessively long run time was again attributed to the fact that the parameter TSSFAC, which is used to control the time step, was set to 0.1. Note that the default value of TSSFAC is 0.9.

A plot showing the transverse tensile test response and the *MAT_213 predicted response is shown in Figure 6. The model matches the initial linear elastic portion of the test response well. As nonlinearity develops in the test response beginning at 0.006 in/in strain, the predicted response exhibits deviations from the test response, which are subsequently restored. The “stair step” behavior is likely due to the influence of damage parameters. The *MAT_213 model over predicts the maximum stress and failure strain. The test response has a maximum stress of 53,315 psi and exhibits failure at a strain of 0.025 in/in. The predicted response has a maximum stress of 61,833.3-psi and a failure strain of 0.028 in/in. Thus, the *MAT_213 predicted response has a 16% higher failure stress than the test and a 12.7% higher failure strain.

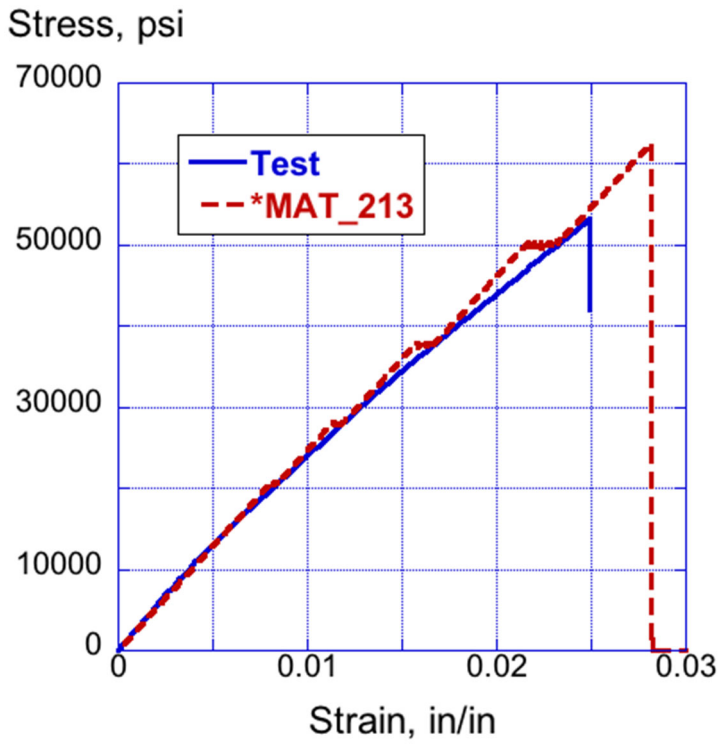

Figure 6. Test and analysis transverse tensile responses.

4.2.3. Comparison with Biaxial Tension Test Data

For the biaxial tension model, four ±45°plies were assigned to the tensile coupon model (see Figure 4) using the *PART_COMPOSITE command. Each ply was 0.0117-in. thick, giving the laminate a total thickness of 0.047 in. The model was executed for an end time of 0.5 s, a maximum displacement of 0.25 in. and required 31 hours and 16 minutes of CPU running the MPP version of LS-DYNA® on a Linux-based workstation with 8 processors. Once again, the excessively long run time was attributed to the fact that the parameter TSSFAC, which is used to control the time step, was set to 0.1. Note that the default value of TSSFAC is 0.9.

Test-analysis comparisons are shown for the biaxial tension model in Figures 7(a) and 7(b). The first plot shows that the *MAT_213 response matches the test response up to a stress of 9,000 psi and a strain of 0.03 in/in. After that point, the predicted stress begins to reduce dramatically until it hits zero at 0.125 in/in strain. As a reminder, the *MAT_213 material parameters listed in Table 2 were used for this simulation, which has three active damage modes (longitudinal tension, transverse tension, and shear). It was determined by examining fringe plots of the damage parameters that both longitudinal tension and transverse tension damage modes were activated and interfering with the shear response. A solution was found that did not involve changing *MAT_213. For the biaxial model, an extra constraint was added along the bottom edge of nodes (see Figure 4) to limit y-displacement. With this added constraint, the *MAT_213 model accurately predicted the

biaxial tension response up to a strain value of 0.06 or 0.07 in/in, as shown in Figure 7(b). During the test, beginning at 0.08 in/in strain, the fibers in the ±45° laminate start to realign themselves with the direction of loading until failure occurs. The *MAT_213 material model does not have the capability of predicting this type of response. Additionally, some of the discrepancies should be expected since *MAT_213 assumes small strains.

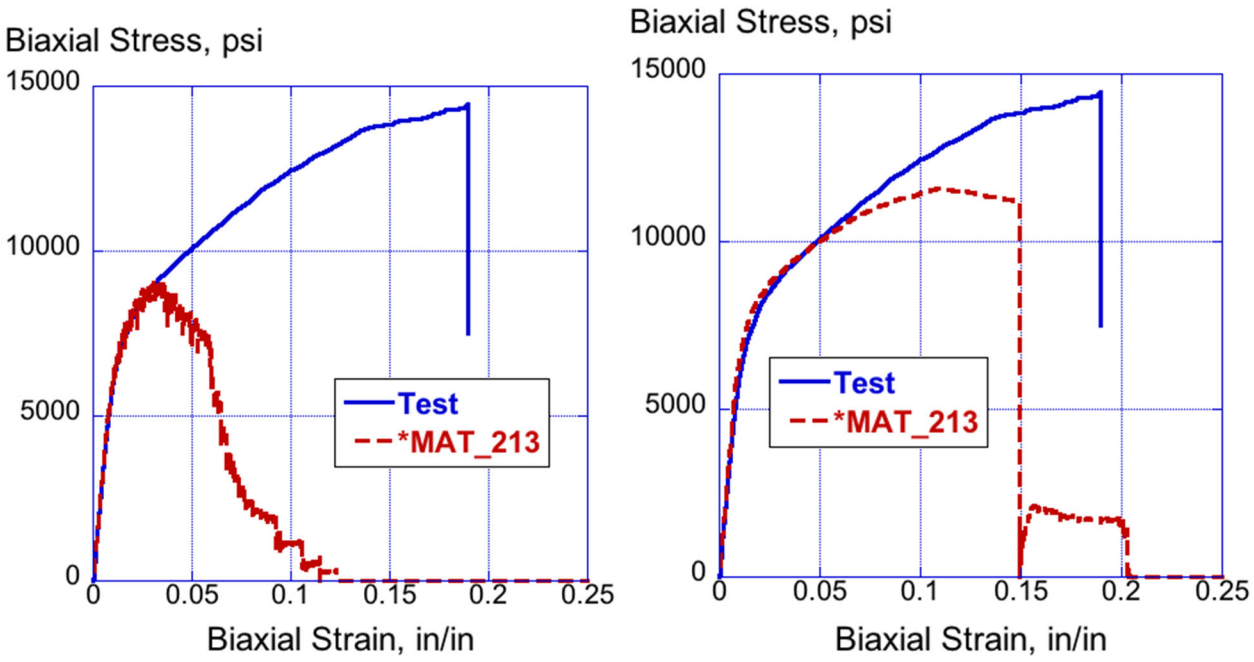


(a) Initial test-analysis comparison. (b) Revised simulation with added constraint.

Figure 7. Test-analysis comparisons for biaxial tension.

For the biaxial tension simulation with added y-displacement constraint, a fringe plot of history variable 18 for shell elements is shown in Figure 8. History variable 18 is strongly associated with shear. The large band of red moving across the coupon resembles a shear wave and is indicative of the loading experienced by the coupon. Note that history variables for shell elements can be different than those used for solid elements.

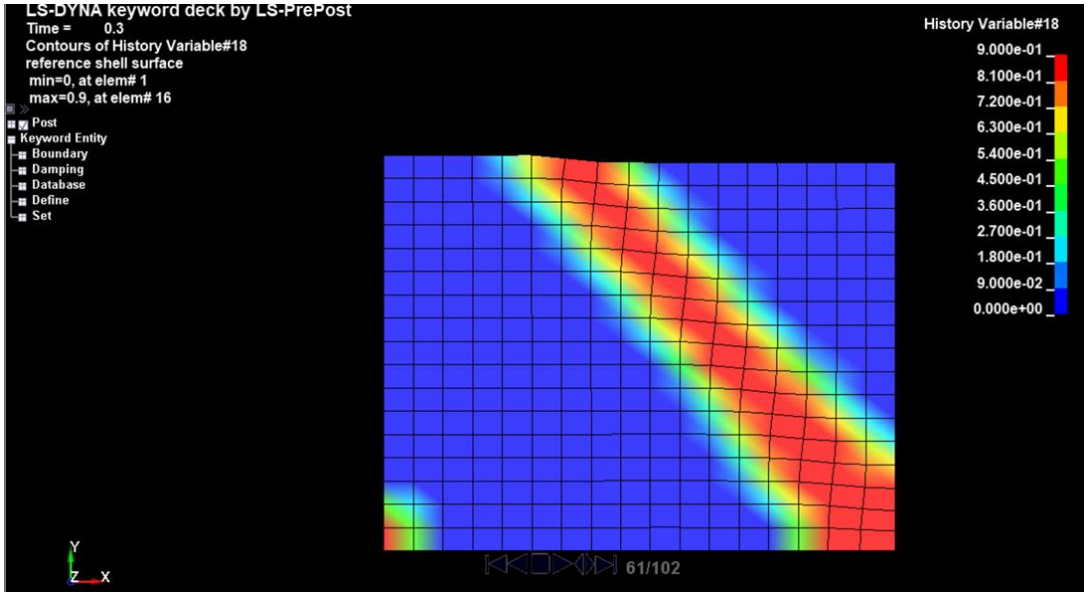


Figure 8. Contour plot of history variable 18.

4.2.4 Comparison with Shear Test Data

The predicted shear response, shown in Figure 9(a), exhibits the same behavior as the initial biaxial tension model. In this case, the stress and strain values at which the load begins to drop are lower due to the shear conversion. However, the simulation that was performed with additional y-displacement constraint of the bottom nodes, shows excellent agreement with the test data up to a stress of 5,300 psi and a strain of 0.05 in/in, as shown in Figure 9(b).

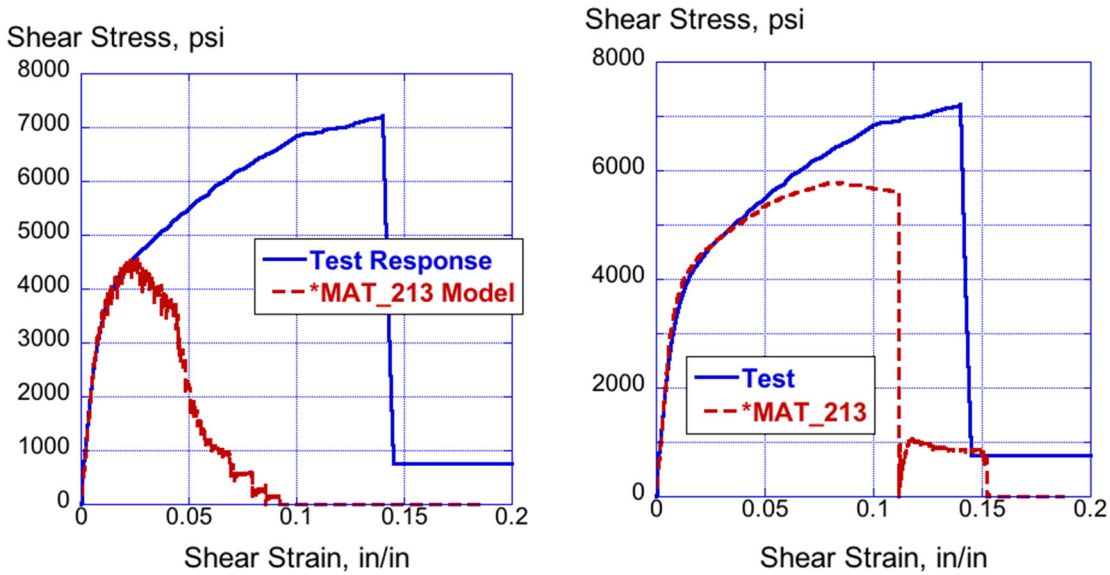


(a) Initial test-analysis comparison. (b) Revised simulation with added constraint.

Figure 9. Test-analysis comparisons for shear.

## 5.0 APPLICATION OF *MAT_213 TO SIMULATE THE CRUSHING RESPONSE OF TWO COMPOSITE ENERGY ABSORBERS

In 2012, the NASA Rotary Wing (RW) Crashworthiness Program [43] initiated the TRACT research program by obtaining two CH-46E helicopter airframes from the Navy CH-46E Program Office (PMA-226) at the Navy Flight Readiness Center in Cherry Point, North Carolina. Full-scale crash tests were conducted to assess dynamic responses of transport-category rotorcraft under combined forward and vertical impact loading. The first crash test, TRACT 1 [44], was performed at the NASA LandIR Facility. Impact tests conducted at LandIR provide data that enable the study of critical interactions between the airframe, seat, and occupant during a controlled crash environment. The CH-46E airframe is categorized as a medium lift rotorcraft with length and width of 45 and 7 ft, respectively, and a capacity for 5 crew and 25 troops. TRACT 1 was conducted in August 2013 under combined conditions of 300-in/s (25-ft/s) vertical and 396-in/s (33-ft/s) forward velocity onto soil, which is characterized as a sand/clay mixture. The primary objectives for TRACT 1 were to assess improvements in occupant loads and flail envelope with the use of crashworthy features such as pretensioning active restraints and load-limiting seats and to develop novel techniques for photogrammetric data acquisition to measure occupant and airframe kinematics [44]. Pre- and post-test photographs of the TRACT 1 crash test are shown in Figure 10.


(a) Pretest photograph. (b) Posttest photograph.

Figure 10. Pre- and post-test photographs of the TRACT 1 full-scale crash test.

The TRACT 1 airframe was tested in a baseline configuration with no changes to the structural configuration, including the discrete aluminum shear panels in the subfloor. It is important to note that the CH-46E does not contain a center keel beam; hence the airframe relies on the aluminum shear panels, the cargo rails in the floor, and the airframe structure to provide longitudinal and torsional stiffness. A final objective of TRACT 1 was to generate crash test data in a baseline configuration for comparison with data obtained from a similar TRACT 2 crash test. The crash test of the second CH-46E airframe (TRACT 2) was conducted on October 1, 2014 and was performed for the same nominal impact velocity

conditions and onto the same sand/clay surface [8]. The difference is that the TRACT 2 airframe was retrofitted with three different composite energy absorbing subfloor concepts located in the midcabin region: a corrugated web design [45, 46] fabricated of carbon fabric; the conusoid fabricated of four layers of hybrid carbon-Kevlar® fabric [9]; and, the sinusoid foam sandwich design, fabricated of the same hybrid fabric face sheets with a foam core [10]. While the TRACT 2 airframe contained similar seat, occupant, and restraint experiments, one of the major goals of the test was to evaluate the performance of novel composite energy absorbing subfloor designs for improved crashworthiness.

Following the TRACT 1 crash test, a research effort was initiated to develop two composite energy absorbers for retrofit into the TRACT 2 test article. The design goals were to limit the average vertical accelerations to between 25 to 40 g on the floor, to minimize peak crush loads, and to generate relatively long crush stroke limits under dynamic loading conditions, typical of those experienced during the TRACT 1 crash test [44]. To further clarify the design goals, it is important to note that the loading conditions on the frames of the TRACT 1 crash test provided dynamic crush loads of approximately 2,500 to 4,000 lb. per linear foot, measured from one side of the floor to the other (a distance of 60 in. or 5 ft). These values are determined by multiplying the design acceleration levels (25 to 40 g) by the floor mass loading of 100 lb per linear foot. Note that the weight times the g-factor equals the force. The loading condition was based on seat and occupant loads that were recorded during the TRACT1 crash test. A schematic drawing is shown in Figure 11 illustrating design conditions for floor loading.

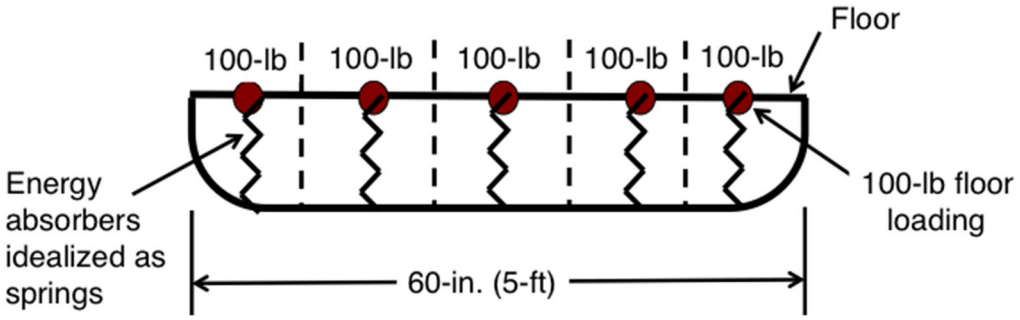


Figure 11. Floor loading condition schematic.

Figure 11 shows an idealized schematic of the floor and subfloor located at an individual fuselage frame. The floor, which is approximately 5 ft wide, is divided into 5 segments of 1 ft. length, each having an associated floor loading of 100 lb. The energy absorbers, depicted as individual springs, are designed to limit floor-level accelerations to 25 to 40 g.

Often, design goals for energy absorbers are defined in terms of Specific Sustained Crush Stress (SSCS). The SSCS is a measure of the energy absorbing capability of the material and is defined in Eqn 5, as

$$SSCS = P_{avg}/(A \times \rho) \quad (5)$$

where $P_{avg}$ is the average sustained crush load, A is the cross-sectional area, and ρ is the density of the material. The SSCS is also the energy absorbed per unit weight of material crushed. Assuming an average acceleration level of 25 g, a floor loading of 100 lb. for a 1-ft. length, a cross-sectional area of 0.98 $in^2$ and a material density of 0.03486 $lb/in^3$, an SSCS value of 72,590 $in^2/s^2$ is obtained for a typical conusoid energy absorber. This value is particularly high. For example, Reference 47 documents the energy absorption capabilities of flat plate composite specimens and reports values of SSCS ranging from 28,710 to 40,200 $in^2/s^2$. Part of the explanation for the high SSCS value is the fact that an average crush load is based on the dynamic design goal. In Reference 9, the average crush load for the conusoid is reported between 900 to 1,500 lb, based on quasistatic loading. Using these averages, SSCS is lowered to values between 26,132 and 43,611 $in^2/s^2$. The SSCS is typically reported in metric units. Thus, a SSCS value of 72,590 $in^2/s^2$ is converted to 18.1 Nm/g. Note that Farley [48] reported SSCS values of between 20 and 75 Nm/g for various composite tubes that were subjected to quasi-static compressive loads.

Farley [48, 49], Kindervater [50], Bannerman [51], and Hanagud [52] have investigated the crushing response of composite structural elements and sine wave beams. Farley [49] has shown that high values of SSCS are obtained when using hybrid carbon-Kevlar® composites in which the carbon fibers are oriented in the same direction as the loading axis and the Kevlar® fibers are oriented at 45° to the loading axis. As stated in Reference 49, “the Kevlar® fibers are positioned in the laminate to provide containment and support for the carbon fibers, which absorb energy through a combination of crushing and fracturing modes.”

### 5.1 Description of the Conusoid Energy Absorber

The geometry of the conusoid is based on alternating right side up and upside down half-cones placed in a repeating pattern. As such, the conusoid combines a simple cone design, which has been extensively studied in the literature [53-56], with sinusoidal beam geometry to create a structure that utilizes the advantages of both configurations. An isometric view of the conusoid is shown in Figure 12(a). Variations in geometry, materials, and laminate stacking sequences were evaluated during development of the conusoid and the final design consisted of four layers of a hybrid carbon-Kevlar® plain-weave fabric oriented at ±45° with respect to the vertical, or crush, direction. A photograph of a typical conusoid component is shown in Figure 12(b). Dimensions of the component are 12-in. long, 7.5-in. high, with an overall width of 1.5 in. Additional information on the development and fabrication of the conusoid energy absorber may be found in Reference 9.

### 5.2 Description of the Sinusoid Energy Absorber

The sinusoid energy absorber consisted of hybrid carbon-Kevlar® plain weave fabric face sheets, two layers for each face sheet oriented at ±45° with respect to the vertical, or crush direction and a closed-cell ELFOAM® P200 polyisocyanurate (2.0 lb/ft$^3$) foam core. Sine wave energy absorbers have been studied extensively because they offer desirable features under compressive loading [57-60]. Energy absorption values from sine wave concepts can be similar to values obtained from crush tubes. In addition, sine wave concepts tend to deform in a stable manner through plastic hinge formation and crushing, rather than global buckling. Often, the actual shape of the energy absorber is not truly a sine wave, but a series of alternating half circles. In fact, the sinusoid concept described in this paper is a series of half circles with a diameter of 1.75 in.; however, the designation of "sinusoid" will continue to be used.

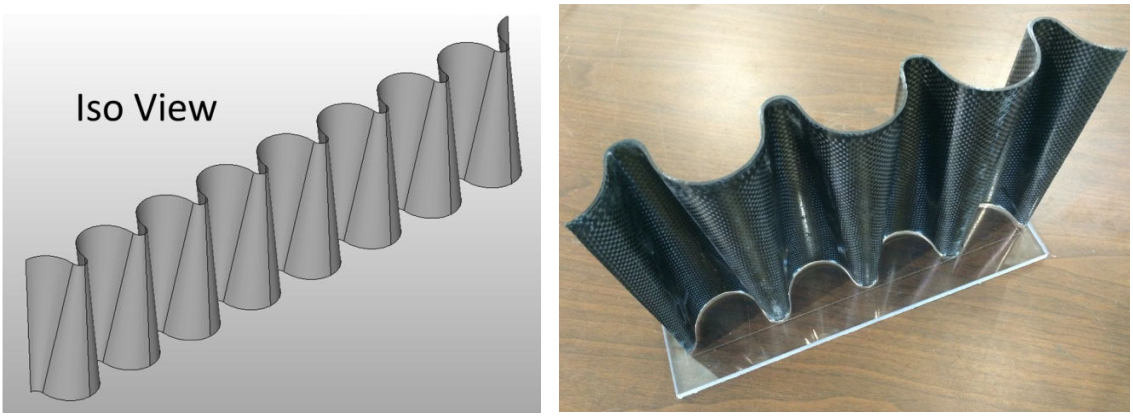


(a) Schematic drawing. (b) Photograph of component.

Figure 12. Isometric view and photograph of a conusoid energy absorber.

The total thickness of a sinusoid component was 1.5 in. with a length of 12 in. and a height of 7.5 in. Design parameters were assessed through component testing including different materials for the face sheets and different laminate stacking sequences. Variations in sinusoid geometry were not evaluated since an existing mold was used in construction. A photograph of a sinusoid foam sandwich specimen is shown in Figure 13. Note that, in preparation for the component drop test, 0.5-in.-thick polycarbonate plates were attached to both the top and bottom surfaces of the specimen.

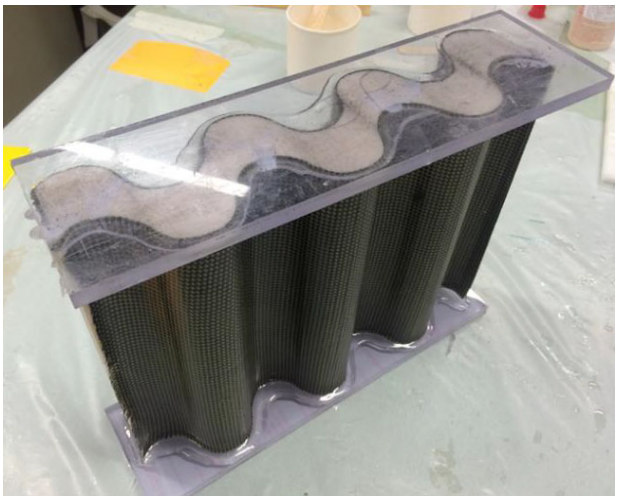

Figure 13. Pretest photograph of a sinusoid foam sandwich component.

### 5.3 Impact Testing and Simulation of the Conusoid Energy Absorber

The conusoid energy absorber component was dynamically crushed in a 14 ft. drop tower with an instrumented 110 lb. falling mass, providing an impact velocity of 264 in/s (22 ft/s). The drop mass was instrumented with a 500 g damped accelerometer and data were acquired using a National Instruments Data Acquisition System (DAS) sampling at 25 kHz. All post-processed acceleration data were filtered using a low-pass 4-pole Butterworth filter with a 500-Hz cut-off frequency. A high-speed camera filming at 1 kHz captured the deformation time history, which is depicted in Figure 14. The identified failure mechanism is folding of the conusoid walls, which is a desirable failure mode that produces a stable and constant crush response within the design level of 25 to 40 g.

A depiction of the baseline finite element model representing the conusoid energy absorber is shown in Figure 15. The model contained: 4 parts; 185,940 nodes; 44,294 Belytschko-Tsay shell elements; 66,380 solid elements, 1 initial velocity card assigned to nodes forming the rigid mass, and 1 body load card defining gravity. The nominal shell element edge length is 0.032 in. The shell elements representing the hybrid carbon-Kevlar® fabric layers were assigned *MAT_213, as listed in Table 2. Once verified through comparison with coupon test data, these properties were unchanged for all subsequent simulations of the energy absorbers. It should be noted that during initial conusoid simulations it was discovered that the model was 9 in. tall. Thus, the model was trimmed in the vertical direction to match the component height of 7.5 in. Also, initial simulations exhibited a buckling failure model, not seen in the test. As a result, a ply-drop crush trigger was implemented on the upper edge of the conusoid, as shown in Figure 16.

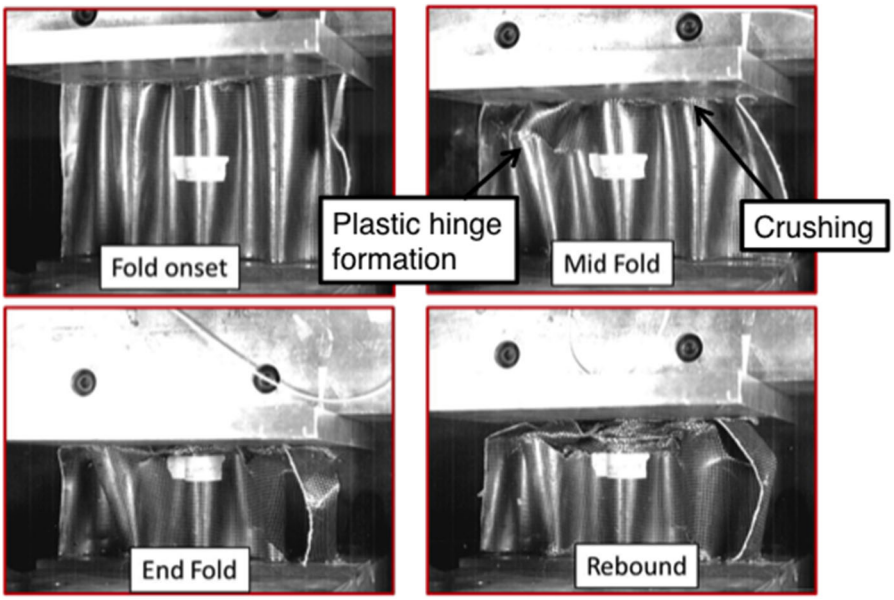


Figure 14. High speed video clips of conusoid deformation.

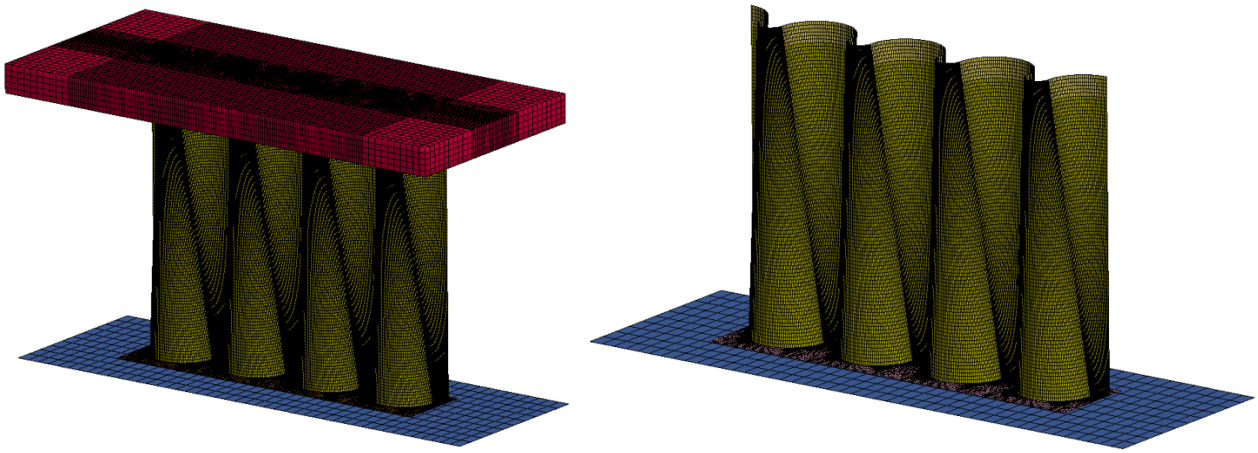

(a) Model with impact mass. (b) Model without impact mass.

Figure 15. Pictures of the original conusoid component model.

As shown in Figure 16, the ply-drop trigger was created by generating a new part for the two upper rows of elements (shaded red), which were assigned one ply thickness. The two rows of elements below that (shaded blue), were also assigned a new part and were given the thickness of two plies. The next two rows of elements (shaded green) were also assigned a new part with a thickness of three plies. All remaining elements were assigned four ply layers. The ply-drop trigger proved to be an effective means to enable stable crushing of the conusoid. The 7.5-in.-high ply-drop conusoid model contained 137,654 nodes; 56,474 shell elements; 66,380 solid elements; 7 parts; 1 initial velocity card; and, 1 automatic contact. The nominal element edge length is 0.032 in. Also, note that all of the solid elements were used to create the drop mass and were not used in the conusoid model.

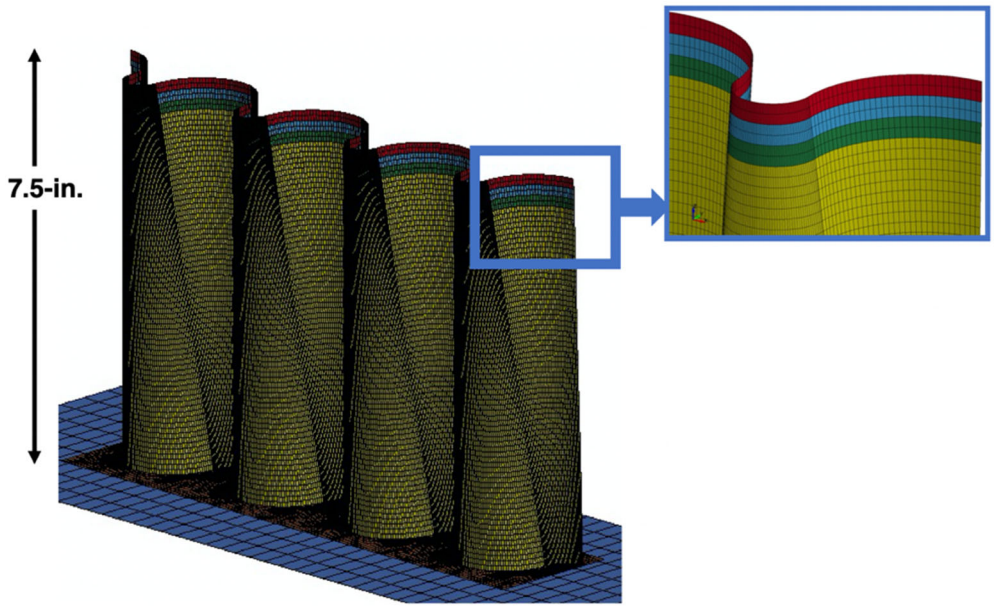


(a) Conusoid model with ply-drop crush trigger.

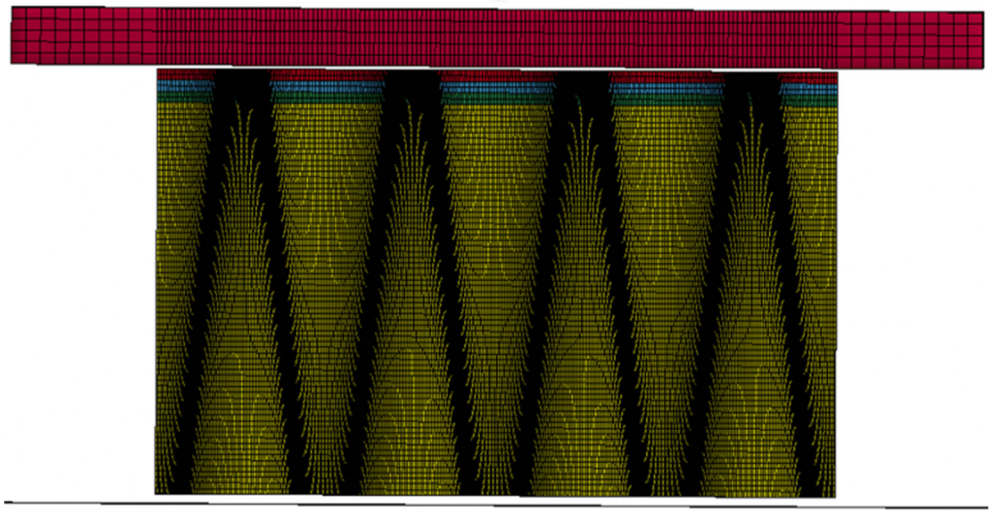

(b) Front view.

Figure 16. Updated pictures of the conusoid model.

For the conusoid, individual ply layers were input using the *PART_COMPOSITE feature in LS-DYNA®. SPCs were used to constrain the nodes forming the bottom plate. In addition, the nodes forming the impact mass were assigned an initial velocity of 264 in/s, matching the test condition. The conusoid model was executed using the developmental version of LS-DYNA® MPP on a Linux-based workstation with 8 processors and required 163 hours and 53 minutes of clock time to execute the simulation for 0.035 seconds. The excessively long run time was attributed to the fineness of the mesh, since TSSFAC was set to 0.9. Model output included time-history responses of the drop mass, and image sequences of structural deformation.

Comparisons of predicted and experimental acceleration and displacement time histories of the drop mass are shown in Figures 17(a) and (b), respectively. Since the design goal for the energy absorbers was based on average acceleration, these values were determined for the test and simulation. The average acceleration for the test is 28.06 g and for model it is 30.2 g, for a pulse duration of 0.0 to 0.025 s, which is a difference of 7.6%. In addition, the *MAT_213 simulation closely matched the peak acceleration, 61.5 g for the test and 63.7 g for the simulation. However, the timing of the predicted peak acceleration occurs later in time with a delay of 0.0018 s. The explanation of the delay is the extra time required to initially crush the ply-drop trigger. Maximum crush displacement for the test is 2.9 in. and for the model it is 2.7 in., which is a difference of 6.9%. Thus, the *MAT_213 model did an excellent job of predicting the test response.

A sequence of model deformation is shown in Figure 18. Stable crushing occurs through plastic hinge formation and folding, along with some tearing of the conusoid walls. The predicted response matches the model deformation captured by the high-speed camera, as shown in Figure 14.

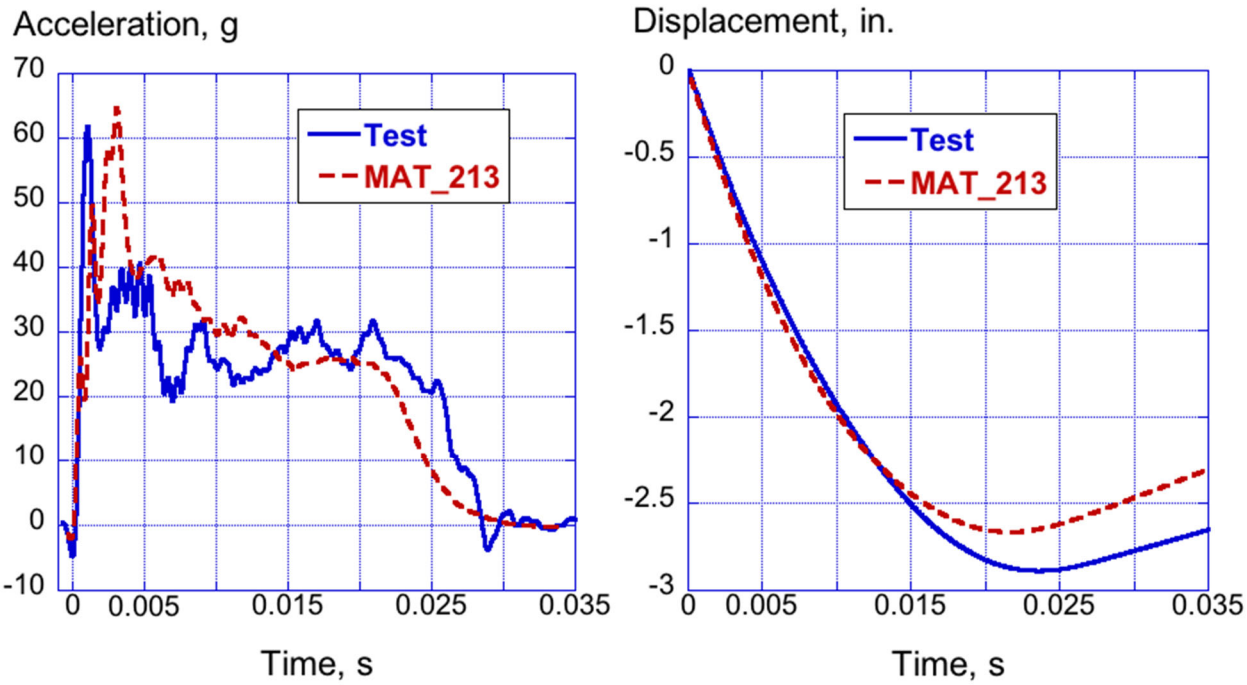


(a) Acceleration responses. (b) Displacement responses.

Figure 17. Test-analysis comparisons for the drop test of the conusoid.

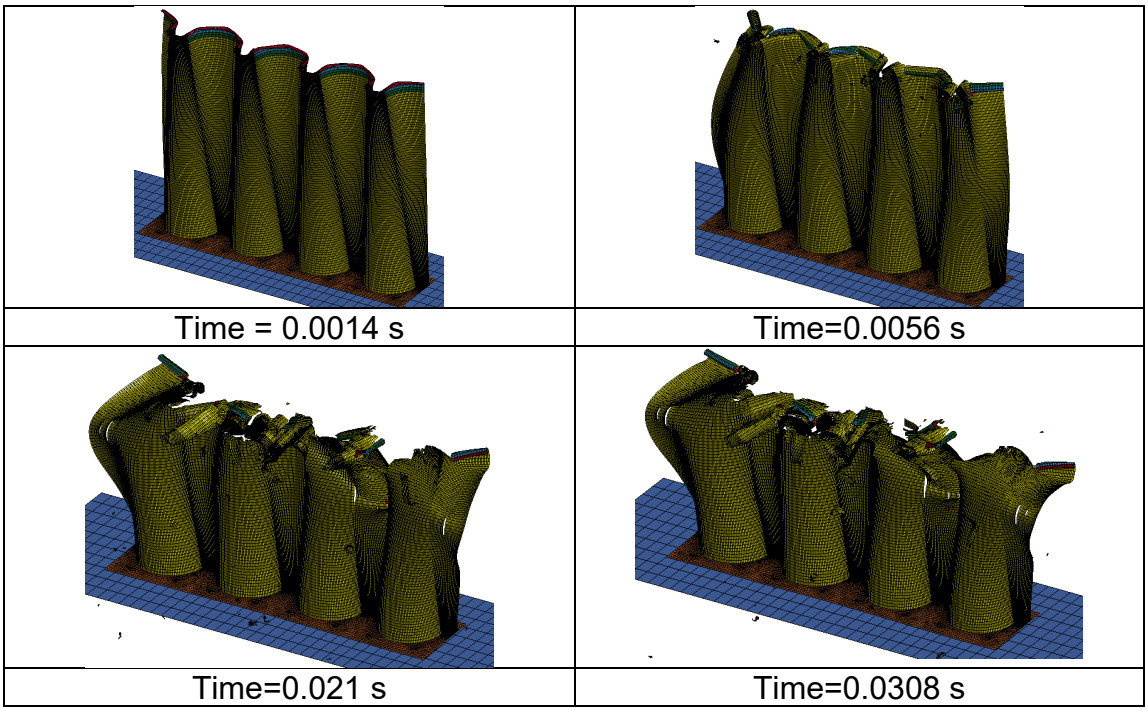


Figure 18. Deformation sequence of the conusoid.

### 5.4 Impact Testing and Simulation of the Sinusoid Energy Absorber

The sinusoid foam sandwich energy absorber was initially evaluated through quasistatic and dynamic crush testing of components. A post-test photograph of a typical sinusoid component is shown in Figure 19 for a dynamic crush test in which a 113.5 lb mass impacted the sinusoid at 265 in/s (22.08 ft/s). The sinusoid component is approximately 12 in. long, 7.5 in. high, and 1.5 in. wide. A flat 0.5-in.-thick polycarbonate plate was glued to both the top and bottom surfaces of the specimen. As shown in Figure 19, the specimen exhibits stable, plastic-like deformation with uniform folding of the face sheets and crushing of the foam core. Crushing initiates along the top edge of the specimen. Note that the sides of the specimen were not covered with face sheets, which allowed splaying of the foam core.

The LS-DYNA® finite element model representing the sinusoid component drop test is shown in Figure 20. The model contained: 53,540 nodes; 7,380 Belytschko-Tsay shell elements; 37,515 solid elements; a rigid drop mass; SPCs to fully constrain the bottom nodes of the sinusoid; 1 automatic single surface contact; and 3 material definitions. The nodes forming the impact mass were assigned an initial velocity of 265 in/s, matching the test condition. As with the conusoid, the shell elements were assigned *MAT_213, using the properties listed in Table 2. The nominal element edge length in the sinusoid model was 0.2 inches.

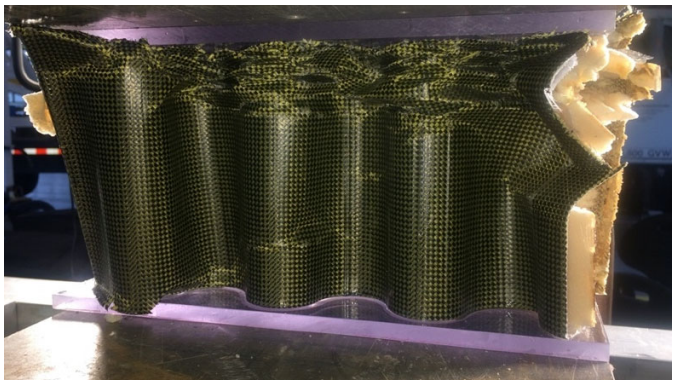

Figure 19. Post-test photograph of a sinusoid foam sandwich energy absorber.

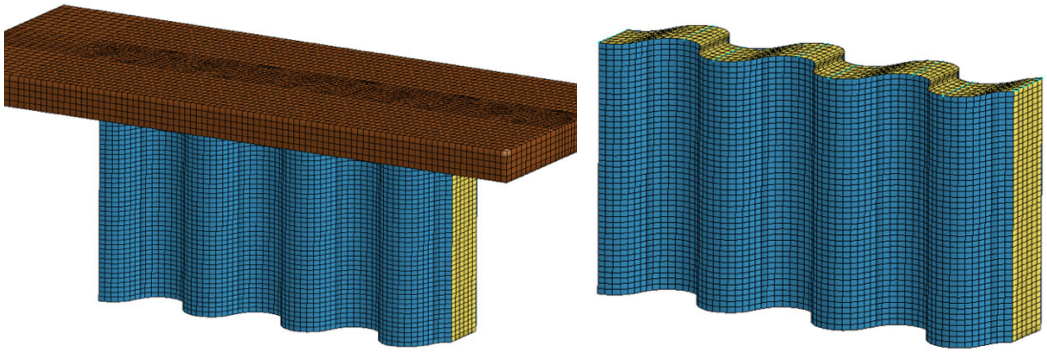

(a) Sinusoid component model. (b) Model without drop mass.

Figure 20. Depictions of the finite element model of the sinusoid component.

The solid elements representing the foam core were assigned *MAT_63 or *MAT_CRUSHABLE_FOAM, which is a crushable foam material model in LS-DYNA® that allows user input of the stress-strain response of the material in tabular format. The stress-strain response of the P200 foam was determined through quasistatic testing of 4 in. x 4 in. x 3 in. rectangular blocks. A plot of the experimental curve obtained at a crush rate of 1.0 in/minute is shown in Figure 21, along with the stress-strain response used as input to *MAT_63. Note that the input curve matches the test data to a strain of 0.67 in/in. At this point, the test data ends, yet the *MAT_63 input response continues and increases dramatically up to 100,000 psi at 1 in/in (note that this data point is not shown in the plot). The large “tail” added to the end of the stress-strain response represents compaction of the foam and is needed to stabilize the response of the solid elements for high values of volumetric strain.

The sinusoid model was executed using the developmental version of LS-DYNA® MPP on a Linux-based workstation with 4 processors and a termination time of 0.06 s, which required 21 hours and 6 minutes to achieve normal termination. Note that TSSFAC was set to 0.9. Model output included time-history responses of the drop mass, and image sequences of structural deformation.

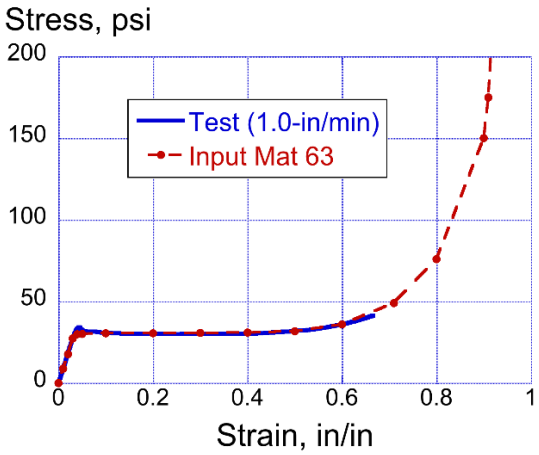


Figure 21. Plot of P200 foam stress-strain response.

Test-analysis comparisons of time-history acceleration and displacement responses are plotted in Figure 22 for the sinusoid component crush test. Based on a pulse duration of 0.0- to 0.03 s, the average acceleration for the test is 22.11 g and for model it is 22.04 g, which is a difference of 0.32%. Maximum crush displacement for the test is 4.0 in. and for the model it is 3.83 in., which is a difference of 4.25%. Thus, the *MAT_213 model did another excellent job of predicting the test response, including the peak acceleration, the average sustained crush acceleration, the unloading response, and the maximum crush displacement.

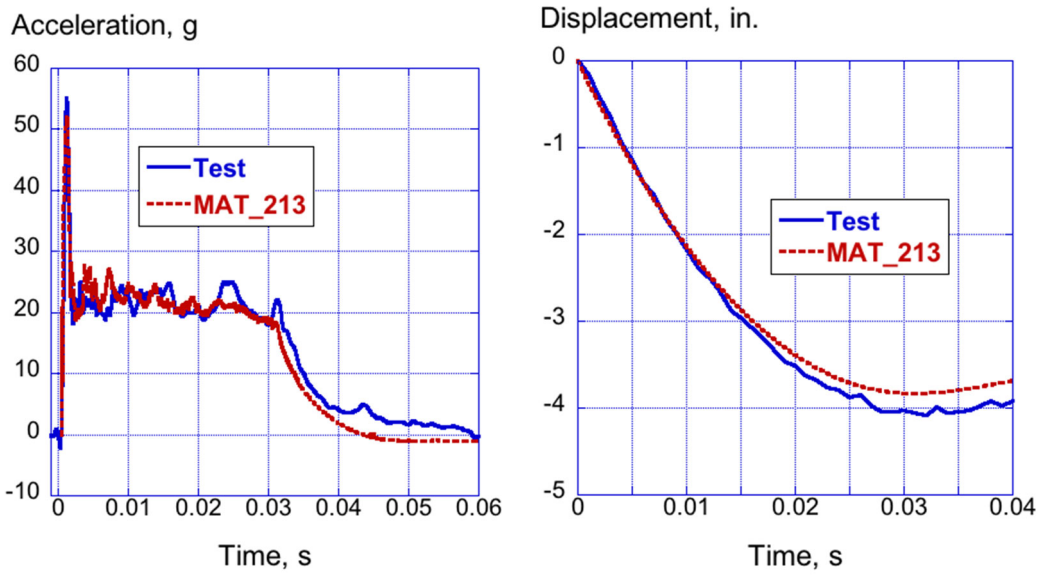


(a) Acceleration responses. (b) Displacement responses.

Figure 22. Test-analysis time history comparisons for the sinusoid component.

The predicted sinusoid model deformation is shown in Figure 23 for six discrete time steps. The model exhibits stable crushing through folding and plastic-like deformation of the face sheets and crushing of the foam core. The deformation pattern matches the post-test response shown in Figure 19.

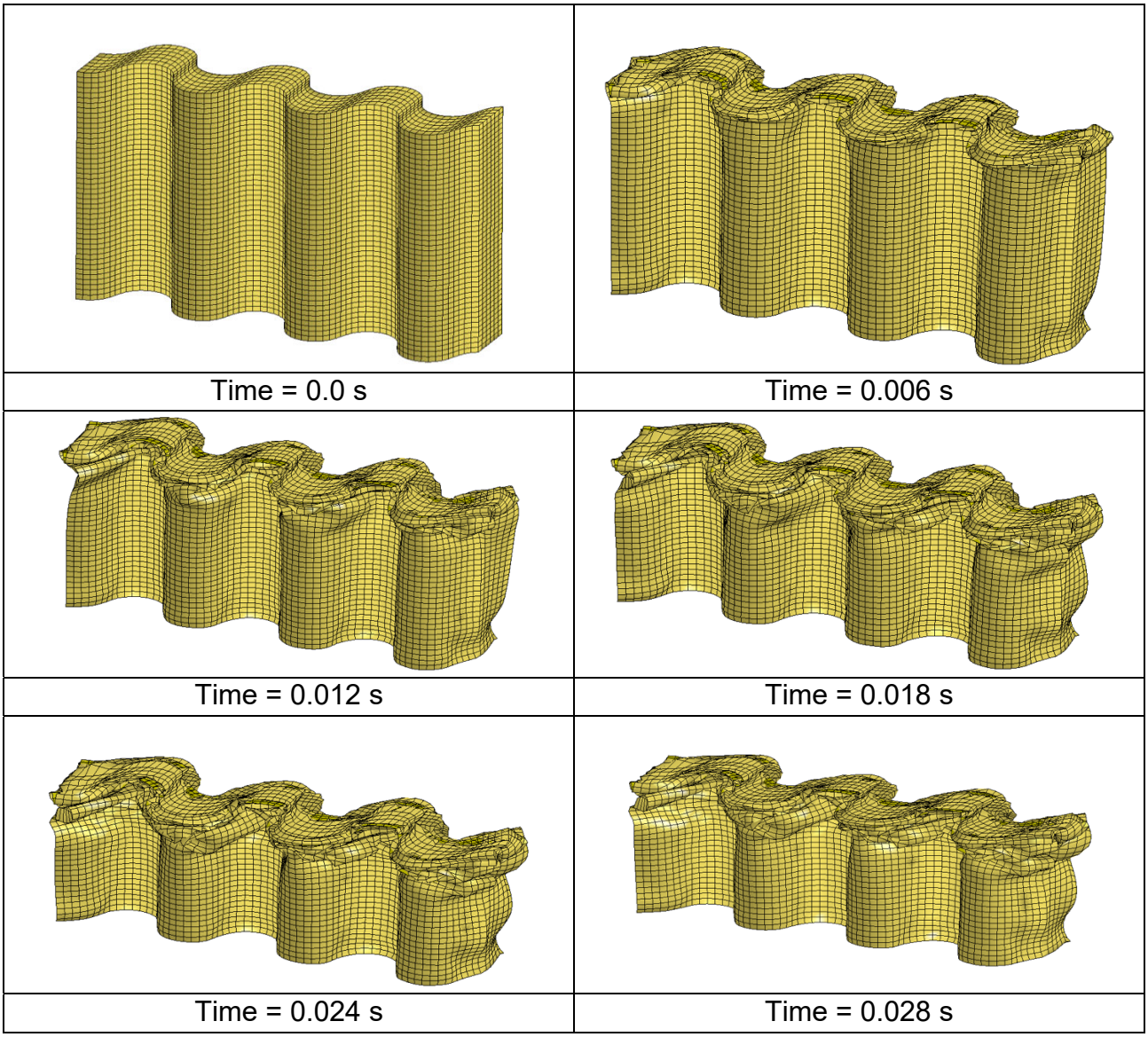


Figure 23. Predicted sinusoid model deformation.

## 6.0 COMPARISON OF *MAT_213 RESULTS WITH RESULTS FROM A PRIOR SIMULATION USING MATERIAL MODEL *MAT_58

During the TRACT research program at NASA LaRC, finite element simulations were conducted to represent all structural impact testing, as documented in Reference 11. As

part of that effort, a material model was developed of the hybrid carbon-Kevlar® plain-weave fabric that is described in Reference 13. The model selected was *MAT_58 or *MAT_LAMINATED_COMPOSITE_FABRIC, which is a continuum damage mechanics material model used in LS-DYNA® for representing composite laminates and fabrics [61]. The *MAT_58 model input is listed in Table 4. Please note that certain parameters, such as EA, EB, GAB, etc. were modified slightly from those reported in Reference 13 to match those in *MAT_213. Additionally, the *MAT_58 SLIM and ERODS parameters were not correlated to match the *MAT_213 input and damage curves.

Table 4. Input parameters for *MAT_58

| *MAT_LAMINATED_COMPOSITE_FABRIC | | | | | | | |
|---|---|---|---|---|---|---|---|
| $# MID | RO | EA | EB | (EC) | PRBA | TAU1 | GAMMA1 |
| 1 | 1.29E-4 | 6.42E06 | 2.68E06 | 2.68E06 | 0.1095 | 4500.0 | 0.0218 |
| $# GAB | GBC | GCA | SLIMT1 | SLIMC1 | SLIMT2 | SLIMC2 | SLIMS |
| 3.26E05 | 3.26E05 | 3.26E05 | 0.8 | 1.0 | 0.8 | 1.0 | 1.0 |
| $#AOPT | TSIZE | ERODS | SOFT | FS | | | |
| 2.0 | 0.0 | 0.5 | 0.0 | -1 | | | |
| $# xp | yp | zp | A1 | A2 | A3 | | |
| 0.0 | 0.0 | 0.0 | 1.0 | 0.0 | 0.0 | | |
| $# V1 | V2 | V3 | D1 | D2 | D3 | BETA | |
| 0.0 | 0.0 | 0.0 | 1.0 | 1.0 | 0.0 | 0.0 | |
| $# E11C | E11T | E22C | E22T | GMS | | | |
| 0.013 | 0.0143 | 0.025 | 0.025 | 0.45 | | | |
| $# XC | XT | YC | YT | SC | | | |
| 70000.0 | 89000.0 | 40000.0 | 54000.0 | 8000.0 | | | |

The *MAT_58 model requires input of material properties in tension, compression, and shear to define stress-strain behavior within the lamina or laminate. The user specifies the in-plane elastic moduli in two primary directions, designated A (typically used for the longitudinal or fiber direction) and B (typically used for the transverse or perpendicular-to-the-fiber direction) in LS-DYNA®. The maximum strength values in tension, compression, and shear are also specified at corresponding strain values. A representation of the stress-strain curve for in-plane tension is illustrated in Figure 24. The tensile response is initially linear elastic with the modulus specified by EA. Stress increases nonlinearly until XT, the maximum strength, is reached, which also corresponds to the strain at the longitudinal strength, E11T. The nonlinear portion of the response is defined internally by LS-DYNA® based on a continuum damage approach. Once XT is reached, the stress is reduced based on the “stress limiting” factor, SLIMT1, and is then held constant at the reduced value until a strain specified by the ERODS parameter is reached, at which point the individual ply within the composite laminate is removed.

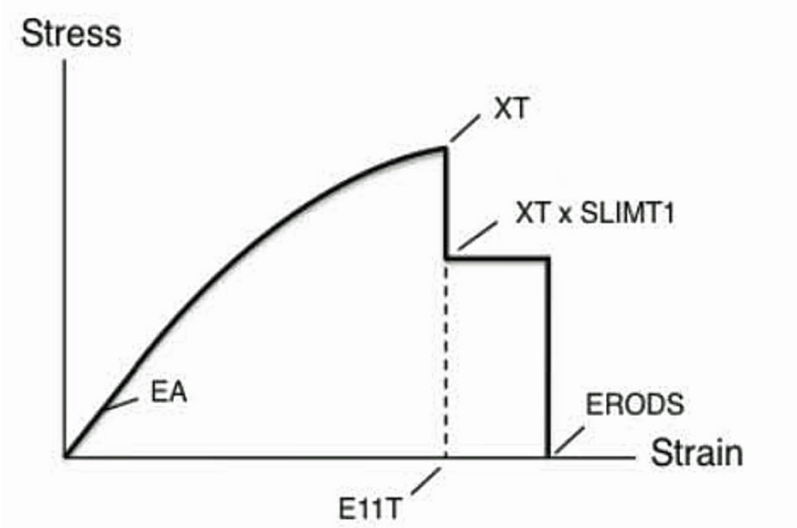


Figure 24. Typical in-plane tension stress-strain curve used in Mat 58 [13].

### 6.1 Comparison of Material Characterization Responses

Test-analysis comparison plots are shown in Figure 25 for longitudinal tension, transverse tension and biaxial tension. Predicted responses were generated from 1-in. by 1-in. model simulations (see Figure 4) using *MAT_213 (Table 2) and *MAT_58 (Table 4).

The stiffness of the longitudinal tension responses (test, *MAT_213, and *MAT_58) match nearly exactly, as shown in Figure 25(a). In addition, the failure of the test response and the *MAT_213 predicted response match closely; however, the *MAT_58 simulation indicates that initial failure occurs at a slightly lower stress and strain. Following initial failure, the *MAT_58 predicted response exhibits a constant, but 20% lower, stress value, which is caused by the SLIMT1 parameter, which is set to 0.8.

The *MAT_58 simulation predicts a nonlinear response, when compared with the test transverse tensile response, shown in Figure 25(b). The failure of the *MAT_58 model occurs at an equivalent stress, but lower strain than the test. Once again, the *MAT_58 response exhibits a 20% drop in stress, based on the SLIMT2 parameter. In contrast, the *MAT_213 model does a better job matching the stiffness of the test response, but over predicts the failure stress and strain.

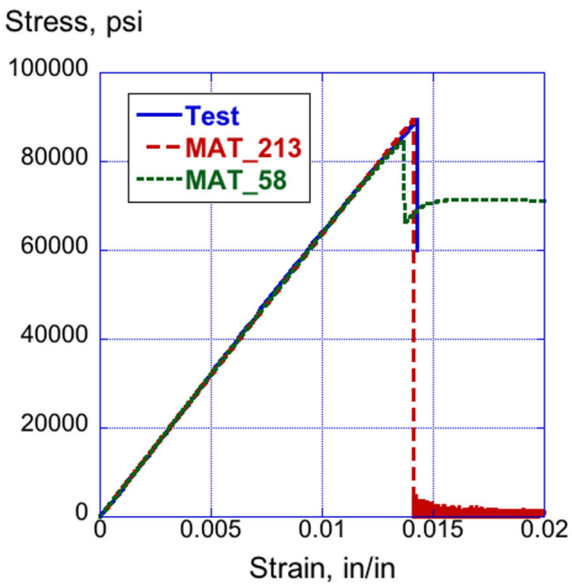


(a) Longitudinal tension.

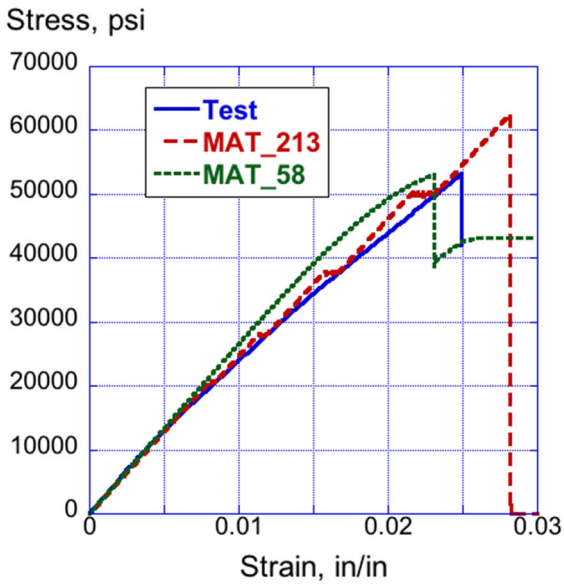


(b) Transverse tension.

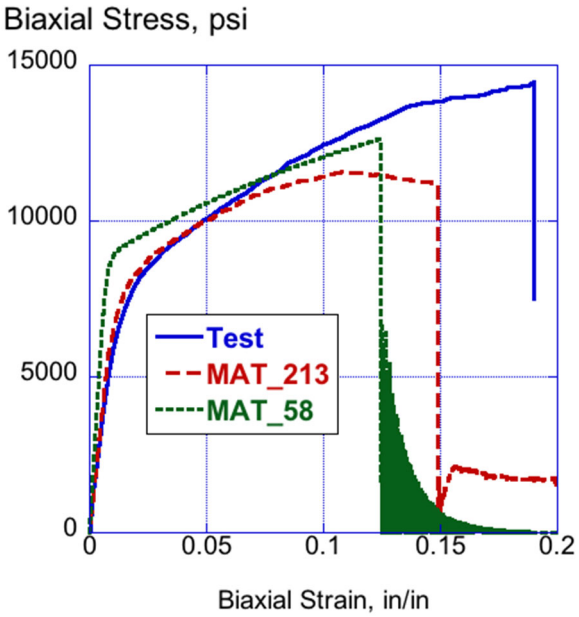


(c) Biaxial tension.

Figure 25. Comparison of material characterization data with predictions from *MAT_213 and *MAT_58.

Finally, the biaxial tension responses (test, *MAT_213, and *MAT_58) are plotted in Figure 25(c). In this case, the *MAT_213 predicted response does an excellent job of matching the test response, up to a strain of 0.06 in/in. The *MAT_213 response matches the “knee” in the test curve nearly exactly, whereas the *MAT_58 response predicts a sharper “knee” and exhibits a response that is close to linear elastic with yielding and strain hardening. The *MAT_58 predicted response fails at a strain of 0.125 in/in with a sudden loss of load.

## 6.2 Comparison of Energy Absorber Crush Responses

The conusoid and sinusoid models were re-executed in which the material model for hybrid carbon-Kevlar® plain-weave fabric is replaced with *MAT_58, as listed in Table 4. As a result, it is possible to compare test responses with analytical predictions from models executed with *MAT_213 and *MAT_58.

### 6.2.1 Conusoid Energy Absorber

Comparisons of the acceleration responses (test, *MAT_213, and *MAT_58) are shown in Figure 26 for the conusoid energy absorber. Average accelerations were determined for each curve based on a pulse duration of 0.0 to 0.025 s. The resulting average acceleration values are shown in the legend of Figure 26. The *MAT_213 simulation is closest to the test (30.2 g for the model compared with 28.6 g for the test). In addition, *MAT_213 does a good job of matching the peak acceleration: 61.5 g for the test, 63.7 g for *MAT_213, and 95.3 g for *MAT_58. Please note that the *MAT_58 model did not incorporate the ply-drop trigger. Consequently, the timing of the predicted peak matched the test response. In addition, as documented in Reference 13, both models did an excellent job of matching the deformation mode of plastic hinge formation and folding.

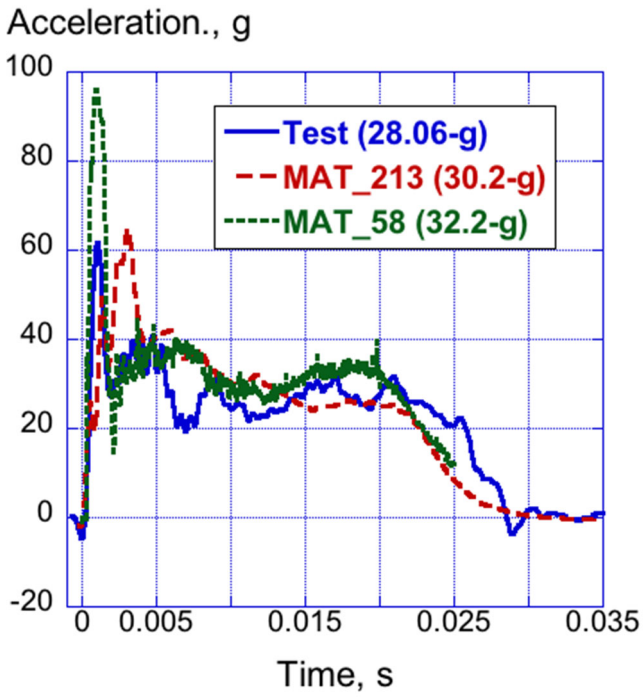


Figure 26. Comparison of test, *MAT_213, and *MAT_58 predictions for the conusoid.

6.2.2 Sinusoid Energy Absorber

A comparison of the acceleration responses (test, *MAT_213, and *MAT_58) is shown in Figure 27 for the sinusoid energy absorber. Average accelerations were determined for each curve using a pulse duration of 0.0 to 0.03 s. Based on these numbers, which are shown in the legend of Figure 27, the simulation with *MAT_213 is slightly lower than the test, 22.04 g versus 22.11 g for the test. The average sustained crush acceleration of the *MAT_58 simulation is slightly over the test, at 22.89 g. Both simulations show excellent agreement with the test response, including peak acceleration, sustained crush acceleration, and unloading. Finally, both simulations matched the experimental deformation modes of folding and plastic-like deformation of the face sheets and crushing of the foam core.

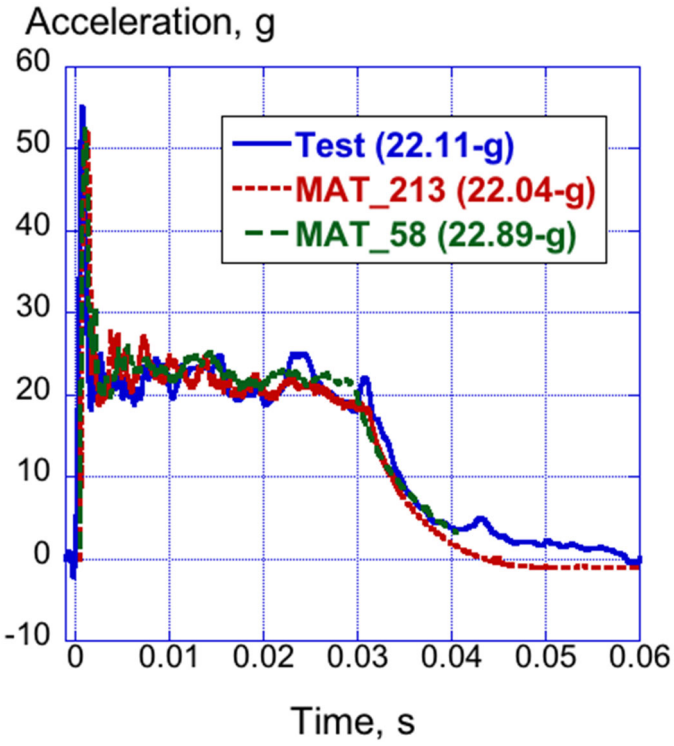


Figure 27. Comparison of test, *MAT_213, and *MAT_58 predictions for the sinusoid.

## 7.0 DISCUSSION OF RESULTS

The new material model, *MAT_213, is multifaceted and offers many additional capabilities when compared with other composite material models available in LS-DYNA®. It is hoped that by reviewing the information contained in the present document, it becomes apparent that the investment required to learn *MAT_213 is well worth the time, based on improvements in model accuracy. Several topics are highlighted in this section of the report including: 7.1 Limitations of the Material Characterization Test Data, 7.2 Test-Analysis Correlation Methods, and 7.3 Potential Future Testing and Simulation. Each topic will be discussed separately. Finally, the paper includes a comprehensive list of “lessons learned,”

in which a series of parametric studies are documented in Appendix C that were performed to investigate specific issues related to the material model. These “lessons learned” are included in hopes that they may help future *MAT_213 users.

### 7.1 Limitations of the Material Characterization Test Data

As stated previously for shell element models, *MAT_213 requires tabulated input from 5 material characterization tests: longitudinal tension and compression, transverse tension and compression, and pure shear. Off-axis data are not required, but may be added, if available. Test data for this project are plotted in Figure 2. The first obvious deficiency is that no compression data are included. Consequently, the compressive responses were assumed to be equivalent to the tension responses. For material stiffness, the “goodness” of this assumption depends upon the level of bimodularity in the material. Most composites exhibit some degree of bimodularity. However, without compression test data for the hybrid carbon-Kevlar® plain-weave fabric, this effect is unknown, and, consequently, is a potential source of error for the model. During a recent internet search of material data sheets for composite fabric materials, it was found that the compressive strength is generally 20 to 40% lower than the tensile strength. However, without compression test data, it is not possible to know the actual response.

In addition to the lack of compression properties, another major deficiency in the test data is that the post-peak degradation response was not collected. For example, as shown in Figure 2, the stress-stain response increases to a maximum value, then initial failure occurs with an accompanying load drop. At this point, the test is stopped. However, had the loading continued, a post-peak degradation response might have been obtained. A stylized stress/strain curve including post-peak degradation data is illustrated in Figure 28. *MAT_213 relies heavily on this information. Without the actual post-peak response, an assumed curve is input, which is a potential source of error in the model.

### 7.2 Test-Analysis Correlation Methods

For the two energy absorbers, test-analysis comparisons were based on average sustained crush acceleration and maximum crush displacement. The reason these metrics were used is that the design goals for the energy absorbers were based on these two factors. However, many, more rigorous, methods exist for performing test-analysis correlations. Model validation is the process of comparing model outputs with test measurements in order to assess the validity of the model. One of the critical tasks to achieve quantitative assessment of models is to develop a validation metric that can quantify the discrepancy between time history responses from a physical test and simulation predictions from a dynamic finite element model. Note that the subject of quantitative model validation methods has attracted considerable interest, with many prior methods documented in References 62-67.

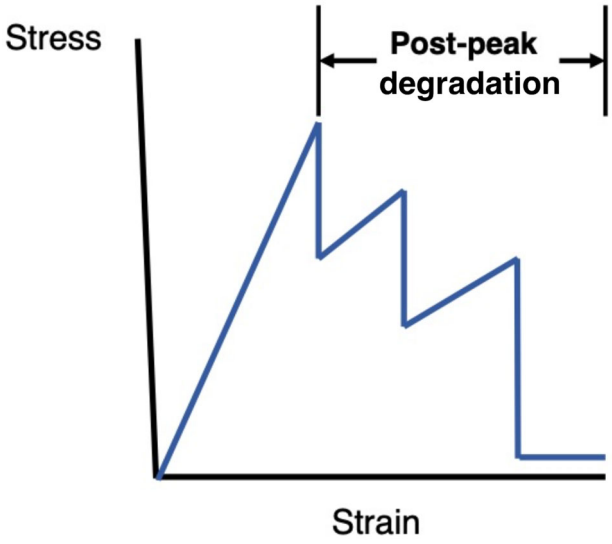


Figure 28. Stylized stress-strain curve with post-peak degradation response.

For the International Standards Organization (ISO) Technical Report ISO/TR 16250 [68], four state-of-the-art objective rating metrics are investigated, and they are: CORrelation and Analysis (CORA) metric, [69-70]**;** Error Assessment of Response Time Histories (EARTH) metric, [71-72]; model reliability metric, [73-75]; and, the Bayesian confidence metric, [72, 76-77]. Further enhancements of the CORA corridor rating and the development of an Enhanced Error Assessment of Response Time Histories (EEARTH) metric have been incorporated to improve the robustness of these metrics. A new combined objective rating, R, metric is developed to standardize the calculation of the correlation between two time-history curves. A Matlab computer program exists that performs the test-analysis correlation and outputs the results in five categories: overall ISO objective rating (R), EEARTH magnitude, EEARTH slope, EEARTH phase, and CORA. The objective ISO rating score ranges from 0 to 1 and the higher the score, the better the correlation between the two time-history curves. In the ISO/TR 16250, a grade is assigned based on the objective rating score, R, as shown in Table 5.

None of the aforementioned test-analysis validation metrics was applied as part of this work. However, they have been used previously with good success [78]. It is highly recommended that the impact dynamics technical community study these test-analysis methods and select one as a standard.

Table 5. Sliding Scale of the Overall ISO Rating.

| Rank | Grade | Rating, R | Description |
|---|---|---|---|
| 1 | Excellent | $R > 0.94$ | Almost perfect characteristics of the reference signal are captured |
| 2 | Good | $0.8 < R \geq 0.94$ | Reasonably good characteristics of the reference signal are captured, but there are noticeable differences between the two curves |
| 3 | Fair | $0.58 < R \geq 0.8$ | Basic Characteristics of the reference signal are captured; but there are significant differences between curves |
| 4 | Poor | $R \leq 0.58$ | Almost no correlation between the two curves |

### 7.3 Potential Future Testing and Simulation

NASA has recently undertaken the action to generate a complete set of material characterization tests of the hybrid carbon-Kevlar® plain-weave fabric. These data will be used in a *MAT_213 material model assigned to solid elements of the conusoid energy absorber, which is depicted in Figures 29 and 30. This model contains: 107,427 nodes; 86,797 solid elements; 6 parts (impact mass, bottom rigid plate, and four parts representing the four composite layers); 6 material cards; 1 initial velocity card; and 1 automatic single surface contact card. The nominal element edge length of the conusoid solid element model is 0.15 in. The component is 12 in. in length, 7.5 in. tall, and 1.5 in. in overall width.

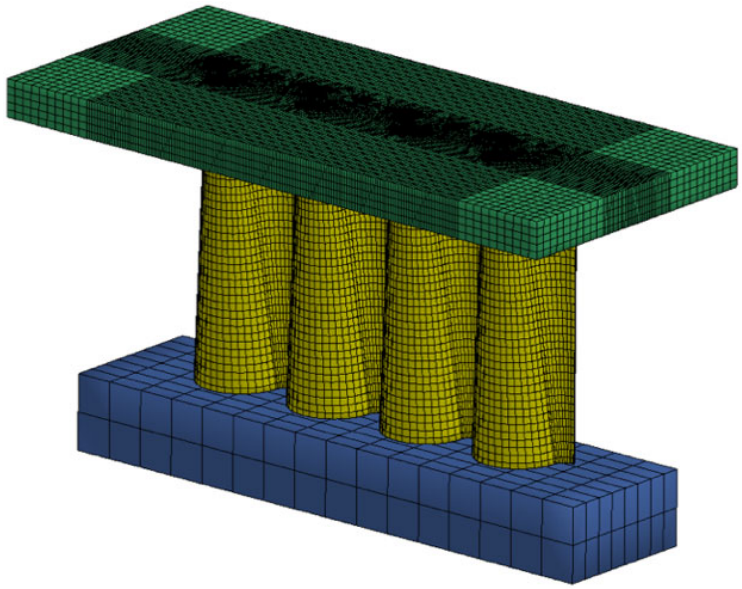

Figure 29. Complete solid-element conusoid model.

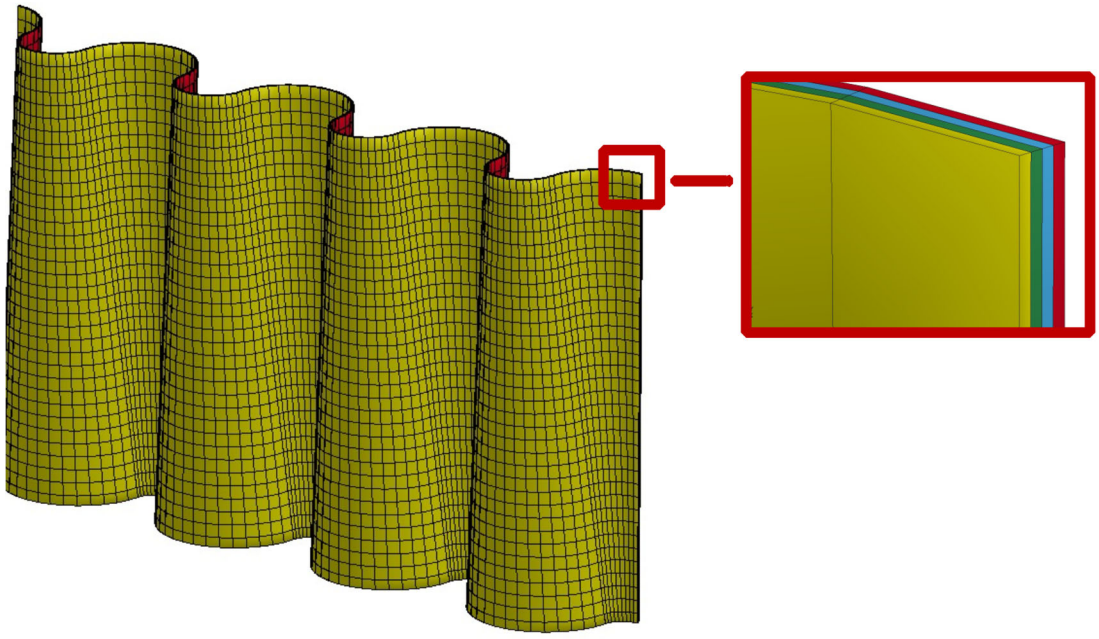

Figure 30. Depiction of the conusoid model showing the edge details.

## 8.0 CONCLUDING REMARKS

This document has focused on the application of a new composite material model that was developed for the commercial nonlinear transient dynamic finite element code, LS-DYNA®. The material is designed *MAT_COMPOSITE_TABULATED_PLASTICITY_DAMAGE, or *MAT_213. The material model incorporates three submodels for deformation, damage, and failure. It is capable of predicting strain rate and temperature effects and it relies heavily on the input of tabulated experimental data. *MAT_213 was originally developed for use with solid elements, but a thin shell element formulation of *MAT_213 has been recently adapted. While the material model is not generally available at this time, a developmental version was used in this exercise.

This paper documents the development of a *MAT_213 material model to represent hybrid carbon-Kevlar® plain-weave fabric. Limited test data were available including: longitudinal tension, transverse tension, and biaxial tension. Compression properties were assumed to be the same as the tensile properties and the biaxial tension data were converted to shear stress and shear strain.

The hybrid carbon-Kevlar® plain-weave fabric was used in the construction of two energy absorbers. The first energy absorber, designated the conusoid, consisted of four layers of hybrid carbon-Kevlar® plain-weave fabric oriented at [+45°/-45°/-45°/+45°] with respect to the vertical direction. The second energy absorber, designated the sinusoid, consisted of

hybrid carbon-Kevlar® plain-weave fabric face sheets, two layers for each face sheet oriented at ±45° with respect to the vertical direction, and a closed-cell ELFOAM® P200 polyisocyanurate foam core. Components of the energy absorbers were constructed and they were 12 in. long, 7.5 in. high, and 1.5 in. wide. Testing included material characterization testing of the hybrid carbon-Kevlar® plain-weave fabric and vertical impact testing of the energy absorbing components.

Finite element models were created and executed using a developmental version of the commercial, nonlinear explicit transient dynamic software code, LS-DYNA®. A simple 1-in. x 1-in. model containing 289 Belytschko-Tsay shell elements, 329 nodes, and 1 material property (*MAT_213) was used to simulate the material characterization tests. More detailed models were generated for the energy absorbers. In particular, the conusoid model had a nominal element edge length of 0.032 in. The sinusoid model did not have nearly as fine a mesh with an element edge length of 0.2 in. Test-analysis results are presented for each energy absorber as comparisons of time-history responses, as well as predicted and experimental structural deformations and progressive damage under impact loading. Finally, previous simulations of the conusoid and sinusoid were performed in which the hybrid carbon-Kevlar® plain-weave fabric was simulated using a continuum damage mechanics-based composite material model *MAT_LAMINATED_COMPOSITE_FABRIC or *MAT_58. Consequently, as a last step, comparisons were made between *MAT_213 and *MAT_58 analytical predictions and test data.

Major conclusions are:

- *MAT_213 did an excellent job of matching the longitudinal tension response obtained from coupons, predicting both the stiffness and failure strength almost exactly.
- For the transverse tension test, *MAT_213 matched the stiffness of the response, but over predicted the failure strength by 16%.
- *MAT_213 matched the biaxial tension response very well, once an extra constraint was added to minimize undesirable failure modes. Likewise for the shear response, which is derived from the biaxial tension data. The *MAT_213 model matched the test data just prior to the point at which the fibers begin to realign themselves with the loading direction.
- *MAT_213 simulation did an excellent job of predicting the conusoid crush response. The average crush acceleration was predicted within 7.6%. The model also matched the progressive deformation and failure mode exhibited by the test article. However, it should be noted that a ply-drop trigger mechanism was added to achieve the desired behavior. Without the trigger, the specimen tended to buckle in a global manner with little energy absorption.

- For the conusoid energy absorber, comparisons were made between the test data, the *MAT_213 predicted response and the *MAT_58 predicted response. Average accelerations were determined for each curve using a pulse duration of 0.0 to 0.025 s. The test response had an average acceleration of 28.06 g, the *MAT_213 response had an average acceleration of 30.2 g and the *MAT_58 response had an average acceleration of 32.2 g. Thus, the *MAT_213 response was closest to the test. In addition, the *MAT_213 simulation matched the peak acceleration: 61.5 g for the test, 63.7 g for *MAT_213, and 95.3 g for *MAT_58.
- *MAT_213 did another excellent job of predicting the sinusoid crash response. The average acceleration for the test was 22.11 g and for model it was 22.04 g, for a pulse duration of 0.0 to 0.03 s, which is a difference of 0.32%. The maximum crush displacement for the test was 4.0 in. and for the model it was 3.83 in., which is a difference of 4.25%.
- Based on a pulse duration of 0.03 s, the sinusoid test response had an average crush acceleration of 22.11 g. The *MAT_213 simulation had an average crush acceleration of 22.04 g, while the *MAT_58 simulation predicted an average of 22.89 g. These values are extremely close to one another.

## 9.0 ACKNOWLEDGEMENTS

The authors gratefully recognize the help and support provided by the additional *MAT_213 Telecon participants including Mike Periera and Troy Lyons of NASA Glenn Research Center and Charles Bakis of Penn State University. We also thank Professor Subby Rajan and his team at Arizona State University for answering questions along the way and for generating the flow rule coefficients. This report would not be possible without their support and guidance in developing the *MAT_213 material model. Also, we acknowledge the team of engineers and technicians at NASA Langley Research Center who constructed the two energy absorbers and conducted the tests reported herein.

## 10.0 REFERENCES

1. Hale, J., “Boeing 787 from the Ground Up,” ***Aeromagazine,*** a quarterly publication of Boeing Commercial, September 1, 2006, pp. 17-23.

2. Kaddour A. S. and Hinton M. J. (2013), “Maturity of 3D Failure Criteria for Fibre-Reinforced Composites: Comparison Between Theories and Experiments: Part B of WWFE-II,” ***Journal of Composite Materials***, Vol. 47, pp. 925-966.

3. Kaddour A. S., Hinton M. J., Li S. and Smith P. A., “The World-Wide Failure Exercises: How Can Composites Design and Manufacture Communities Build Their Strength,” European Conference on Composite Materials, Seville, Spain, 22-26 June 2014.

4. Hinton M. J., and Kaddour A. S., “The Second World-Wide Failure Exercise: Benchmarking of Failure Criteria under Triaxial Stresses for Fiber-Reinforced Polymer Composites,” Proceedings of the 16th International Conference on Composite Materials, held in Kyoto, Japan. on July 8-13, 2007.

5. Hallquist J. O., “LS-DYNA® Keyword User’s Manual,” Volume I, Version 971, Livermore Software Technology Company, Livermore, CA, August 2006.

6. Ansys, Inc., https://www.ansys.com.

7. Achstetter T., “Development of a Composite Material Shell-Element Model for Impact Applications,” Ph.D. Dissertation, George Mason University, 2019.

8. Annett M.S., “Evaluation of the Second Transport Rotorcraft Airframe Crash Testbed (TRACT 2) Full Scale Crash Test,” Proceedings of the American Helicopter Society International Annual Forum 71, Virginia Beach, VA, May 3-5, 2015.

9. Littell J. D., “The Development of a Conical Composite Energy Absorber for use in the Attenuation of Crash/Impact Loads,” Proceedings of the American Society for Composites 29th Technical Conference, 16th US-Japan Conference on Composite Materials, September 8-10, 2014, University of California San Diego, La Jolla, CA.

10. Jackson K. E., Fasanella E. L., and Littell J. D., “Impact Testing and Simulation of a Sinusoid Foam Sandwich Energy Absorber,” Proceedings of the American Society of Composites 30th Technical Conference, East Lansing, MI, September 28-30, 2015.

11. Jackson K.E., Littell J. D., Fasanella E. L., Annett M. S., and Seal M. D., “Multi-Level Experimental and Analytical Evaluation of Two Composite Energy Absorbers,” NASA Technical Memorandum, NASA/TM-2015-218772, July 2015.

12. Littell J. D., Jackson K. E., Annett M. S., Seal M. D., and Fasanella E. L., “The Development of Two Composite Energy Absorbers for Use in a Transport Rotorcraft Airframe Crash Testbed (TRACT 2) Full-Scale Crash Test,” Proceedings of the 71st Annual American Helicopter Society Forum, Virginia Beach, VA, May 5-7, 2015.

13. Jackson K. E., Fasanella E. L., and Littell J.D., “Development of a Continuum Damage Mechanics Material Model of a Carbon-Kevlar® Hybrid Fabric for Simulating the Impact Response of Energy Absorbing Subfloor Concepts,” Proceedings of the 73rd Annual AHS Forum, Ft. Worth, Texas, May 9-11, 2017.

14. Shyamsunder L., Khaled B., Rajan S. D., Goldberg R. K., Carney K. S., DuBois P., and Blankenhorn G., “Implementing deformation, damage, and failure in an orthotropic plastic material model,” ***Journal of Composite Materials***, DOI: 10.1177/0021998319865006, 2019.

15. Khaled B., Shyamsunder L., Hoffarth C., Rajan S. D., Goldberg R. K, Carney K. S., DuBois P. and Blankenhorn G., “Damage characterization of composites to support an orthotropic plasticity material model,” ***Journal of Composite Materials***, Vol. 53, Issue 7, pp. 941-967, 2019.

16. Goldberg R. K., Carney K. S., DuBois P., Hoffarth C., Khaled B., Shyamsunder L., Rajan S. D. and Blankenhorn G., “Implementation of a tabulated failure model into a generalized composite material model,” ***Journal of Composite Materials***, Vol. 52, Issue 25, pp. 3445-3460, 2018.

17. Goldberg R. K., Carney K. S., DuBois P., Hoffarth C., Khaled B., Rajan S., and Blankenhorn G., “Analysis and Characterization of Damage Utilizing a Generalized Composite Material Model Suitable for Impact Problems,” ***Journal of Aerospace Engineering***, Vol. 31, No. 4, 10.1061/(ASCE)AS.1943-5525.0000854, 04018025, 2018.

18. Khaled B., Shyamsunder L., Hoffarth C., Rajan S. D., Goldberg R. K, Carney K. S., DuBois P. and Blankenhorn G., “Experimental characterization of composites to support an orthotropic plasticity material model,” ***Journal of Composite Materials***, Vol. 52, Issue 14, pp. 1847-1872, 2018.

19. Hoffarth C., Khaled B., Shyamsunder L., Rajan S. D., Goldberg R. K., Carney K. S., DuBois P. and Blankenhorn G., “Verification and Validation of a Three-Dimensional Orthotropic Plasticity Constitutive Model Using a Unidirectional Composite,” ***Fibers***, Vol. 5, Issue 1, Number 12, 2017.

20. Harrington J., Hoffarth C., Rajan S. D., Goldberg R. K., Carney K. S., DuBois P. and Blankenhorn G., “Using Virtual Tests to Complete the Description of a Three-Dimensional Orthotropic Material,” ***Journal of Aerospace Engineering***, Volume 30, 10.1061/(ASCE)AS.1943-5525.0000737, 04017025,2017.

21. Hoffarth C., Rajan S. D., Goldberg R. K., Revilock D., Carney K. S., DuBois P. and Blankenhorn G., “Implementation and validation of a three-dimensional plasticity-based deformation model for orthotropic composites,” ***Composites: Part A***, Vol. 91, pp. 336-350, 2016.

22. Goldberg R.K., Carney K.S., DuBois P., Hoffarth C., Harrington J., Rajan S., and Blankenhorn G., “Development of an Orthotropic Elasto-Plastic Generalized Composite Material Model Suitable for Impact Problems,” ***Journal of Aerospace Engineering***, Vol. 29, No. 4, 04015083, 2016.

23. Goldberg, R.K.; Carney, K.S.; DuBois, P.; Hoffarth, C.; Khaled, B.; Shyamsunder, L.; Rajan, S.; and Blankenhorn, G.: “Incorporation of Failure Into an Orthotropic Three-Dimensional Model With Tabulated Input Suitable for Use in Composite Impact Problems”, NASA TM-2017-219442, 2017.

24. Goldberg, R.K.; Carney, K.; DuBois, P.; Hoffarth, C.; Rajan, S.; and Blankenhorn, G.: “Analysis and Characterization of Damage Utilizing an Orthotropic Generalized Composite Material Model Suitable for Use in Impact Problems”, NASA TM-2016-218959, 2016.

25. Goldberg, R.K.; Carney, K.; DuBois, P.; Hoffarth, C.; Rajan, S.; and Blankenhorn, G.: “Incorporation of Plasticity and Damage Into an Orthotropic Three-Dimensional Model With Tabulated Input Suitable for Use in Composite Impact Problems”, NASA TM-2015-218849, 2015.

26. Hoffarth, C.; Harrington, J.; Rajan, S.; Goldberg, R.; Carney, K.; DuBois, P.; and Blankenhorn, G., “Verification and Validation of a Three-Dimensional Generalized Composite Material Model”, NASA TM-2015-218446, 2015.

27. Goldberg, R.; Carney, K.; DuBois, P.; Hoffarth, C.; Harrington, J; Rajan, S.; and Blankenhorn, G., “Theoretical Development of an Orthotropic Elasto-Plastic Generalized Composite Material Model”, NASA TM-2014-218347, 2014.

28. Hoffarth C., “A Generalized Orthotropic Elasto-Plastic Material Model for Impact Analysis,” PhD Dissertation, Arizona State University, December 2016. Available: https://repository.asu.edu/attachments/176440/content/Hoffarth_asu_0010E_16434.pdf

29. Khaled B., “Experimental Characterization and Finite Element Modeling of Composites to Support a Generalized Orthotropic Elasto-Plastic Damage Material Model for Impact Analysis,” PhD Dissertation, Arizona State University, 2019.

30. Shyamsunder L., “Failure Modeling in an Orthotropic Plastic Material Model for Impact and Crush Analysis,” Ph.D. Dissertation, School of Sustainability and Built Environment, Arizona State University, 2020.

31. Hoffarth C., “A Generalized Orthotropic Elasto-Plastic Material Model for Impact Analysis,” DOT/FAA/TC-TT17/54, October 2017.

32. Hoffarth C., Khaled B., Shyamsunder L., and Rajan S. D., “Development of a Tabulated Material Model for Composite Material Failure, MAT213, Part 1: Theory, Implementation, Verification and Validation,” DOT/FAA/TC-19/50, P1, January 2020.

33. Khaled B., Shyamsunder L., Schmidt N., Hoffarth C. and Rajan S. D., “Development of a Tabulated Material Model for Composite Material Failure, MAT213, Part 2: Experimental Tests to Characterize the Behavior and Properties of T800-F3900 Toray Composite,” DOT/FAA/TC-19/50, P2, January 2020.

34. Achstetter T., Park C., and Kan C., “Development of a Tabulated Material Model for Composite Material Failure, MAT213, Part 3: Implementation of Probabilistic Modeling Capability in the Tabulated Composite Failure Model MAT213,” DOT/FAA/TC-19/50, P3, January 2020.

35. Rajan S. D., Hoffarth. C., Khaled B., and Shyamsunder L., “MAT_213 User’s Guide, Version 1.3.5 A User Guide for *MAT_COMPOSITE_TABULATED_PLASTICITY_ DAMAGE in LS-DYNA®,” August 2021.

36. Tsai, S. W. and Wu, E. M., “A General Theory of Strength for Anisotropic Materials,” ***Journal of Composite Materials.*** Vol. 5, 1971, pp. 58–80.

37. Rajan S., Hoffarth C., and Khaled B., “Flow Rule Coefficients Program User Guide© 2013-21, Version 2.1, Arizona State University, March 24, 2021.

38. American Society for Testing and Materials, “Standard Test Method for Tensile Properties of Polymer Matrix Composite Materials,” ASTM-D3039M, 2008.

39. American Society for Testing and Materials, “Standard Test Method for In-Plane Shear Response of Polymer Matrix Composite Materials by Tensile Test of a ±45° Composite,” ASTM D3518M, 2013.

40. Whitney J. M., Daniel I. M., and Pipes R. B., Experimental Mechanics of Fiber Reinforced Composite Materials, Revised Edition, SEM Monograph No. 4, Prentice-Hall, New Jersey, 1984, pp.185-190.

41. Daniel I. M, and Ishai O., Engineering Mechanics of Composite Materials (second edition), Oxford University Press, 2006, pp. 323.

42. Agarwal and Broutman, Analysis and Performance of Fiber Composites, second edition, Wiley, 1990, page 375

43. Jackson, K.E., Fuchs, Y. T., and Kellas, S., “Overview of the NASA Subsonic Rotary Wing Aeronautics Research Program in Rotorcraft Crashworthiness,” ***Journal of Aerospace Engineering***, Special Issue on Ballistic Impact and Crashworthiness of Aerospace Structures, Volume 22, No. 3, July 2009, pp. 229-239.

44. Annett M.S., Littell J.D., Jackson K.E., Bark L., DeWeese R., McEntire B.J., “Evaluation of the First Transport Rotorcraft Airframe Crash Testbed (TRACT 1) Full-Scale Crash Test,” NASA Technical Memorandum, NASA/TM-2014-218543, October 2014.

45. Kindervater C., Thomson R., Johnson A., David M., Joosten M., Mikulik Z., Mulcahy L., Veldman S., Gunnion A., Jackson A., and Dutton S., “Validation of Crashworthiness Simulation and Design Methods by Testing of a Scaled Composite Helicopter Frame Section,” Proceedings of the American Helicopter Society 67th Annual Forum, Virginia Beach, VA, May 3-5, 2011.

46. Billac T., David M., Battley M., Allen T., Thomson R., Kindervater C., Das R., “Validation of Numerical Methods for Multi-terrain Impact Simulations of a Crashworthy Composite Helicopter Subfloor,” Proceedings of the American Helicopter Society 70th Annual Forum, Montreal, Quebec, Canada, May 20-22, 2014.

47. Jackson K. E., Morton J., Lavioe A., and Boitnott R.L., "Scaling of Energy Absorbing Composite Plates," ***Journal of the AHS***, Vol. 39, No. 1, January 1994, pp. 17-23.

48. Farley G. L., and Jones R.M., "Energy Absorption Capability of Composite Tubes and Beams," NASA Technical Memorandum NASA/TM-101634, September 1998.

49. Farley G. L., "Energy Absorption of Composite Materials***," Journal of Composite Materials***, 17, (5), May 1983, pp. 267-279.

50. Kindervater C. M., "Crash Impact Behavior and Energy Absorbing Capability of Composite Structural Elements," 30th National SAMPE Symposium, March 1985, pp.1191-2101.

51. Bannerman D. C., and Kindervater C. M., "Crashworthiness Investigation of Composite Aircraft Subfloor Beam Sections," Proceedings of the International Conference on Structural Impact and Crashworthiness, J. Morton, editor, Elsevier Applied Science, London, UK, July 1984, pp. 710-722.

52. Hanagud S., Craig J. I., Sriram P., and Zhou W., "Energy Absorption Behavior of Carbon Epoxy Composite Sine Webs," ***Journal of Composite Materials***, 23, (5), May 1989, pp. 448-459.

53. Price J. N., and Hull D., "Axial Crushing of Glass Fibre-Polyester Composite Cones," ***Composites Science and Technology***, Volume 28, 1987.

54. Feraboli P., et al. "Design and certification of a composite thin-walled structure for energy absorption," ***International Journal of Vehicle Design***, Vol. 44, Nos. 3/4, 2007.

55. Gupta N. K. and Velmurugan, R., "Axial Compression of Empty and Foam Filled Composite Conical Shells," ***Journal of Composite Materials***, Vol. 33, No. 6, 1999.

56. Fleming D. C., and Vizzini A. J., "Tapered Geometries for Improved Crashworthiness Under Side Loads," ***Journal of the American Helicopter Society***, Vol. 38, 1993.

57. Cronkhite J.D., and Berry V.L., "Crashworthy Airframe Design Concepts, Fabrication and Testing," NASA Contractor Report 3603, NASA Contract NAS1-14890, September 1982.

58. Farley G.L., "Crash Energy Absorbing Composite Sub-Floor Structure," AIAA Paper 86-0944, Proceedings of the 27th AIAA/ASME/ASCE/and AHS Structures, Structural Dynamics, and Materials Conference, San Antonio, TX, May 19-21, 1986.

59. Carden H. D., and Kellas S., "Composite Energy-Absorbing Structure for Aircraft Subfloors," Proceedings of the DOD/NASA/FAA Conference, Hilton Head Island, South Caroline, November 1993.

60. Feraboli P., “Development of a Corrugated Test Specimen for Composite Materials Energy Absorption,” ***Journal of Composite Materials***, Vol. 42, No. 3, 2008, pp. 229-256.

61. Matzenmiller A., Lubliner J., and Taylor R. L., “A Constitutive Model for Anisotropic Damage in Fiber Composites,” ***Mechanica of Materials****,* Vol. 20, 1995, pp. 125-152.

62. Jiang X., and Mahadevan S., “Bayesian risk-based decision method for model validation under uncertainty,” ***Reliability Engineering of System Safety***, Vol 92, No. 6, 2007, pp.707-718.

63. Jiang X., and Mahadevan S., “Bayesian wavelet method for multivariate model assessment of dynamical systems,” ***Journal of Sound and Vibration,*** Vol 312 (4-5) 2008, pp. 694–712.

64. Jiang X. et al., “Bayesian probabilistic PCA approach for model validation of dynamic systems,” ***SAE International Journal of Materials & Manufacturing***, 2009, Vol 2, No. 1, 2009, pp. 555-563.

65. Mongiardini M., Ray M.H., Anghileri M., “Development of Software for the Comparison of Curves During the Verification and Validation of Numerical Models,” 7th European LS-DYNA® Conference, 2009, Salzburg, Austria.

66. Schwer L. E., “Validation metrics for response histories: perspectives and case studies,” ***Engineering with Computer***, 2007, Vol 23, pp. 295-309.

67. Sprague M.A. and Geers T. L., “Spectral Elements and Field Separation for an Acoustic Fluid Subject to Cavitation,” ***Journal of Computational Physics***, Vol. 184, 2003, pp: 149162.

68. ISO/TR 16250 (2013). “International Standards Organization (ISO) Technical Report, “Road vehicles – Objective rating metrics for dynamic systems.”

69. Thunert C., “Manual of the program CORA,” Version 3.5; GNS mbH; Braunschweig, Germany, 2010.

70. Thunert C. “CORA Release 3.6 – User’s Manual;” GNS mbH; Braunschweig, Germany, 2012.

71. Sarin H. et al., “A Comprehensive Metric for Comparing Time Histories in Validation of Simulation Models with Emphasis on Vehicle Safety Applications,” ***Transactions of the ASME – Journal of Dynamic Systems: Measurement and Control***; 132(6), 061401, 2010.

72. Zhan Z. et al., “An Enhanced Bayesian Based Model Validation Method for Dynamic Systems,” ***ASME Journal of Mechanical Design***, 133(4), 041005, 2011.

73. Mahadevan S., and Rebba R., “Validation of reliability computational models using Bayes networks,” ***Reliability Engineering of System Safety***, 87 (2), 2005, pp. 223–232.

74. Rebba R. and Mahadevan S., “Model predictive capability assessment under uncertainty,” ***AIAA Journal***, 2006, Vol. 44, No. 10, pp. 2376–2384.

75. Zhan Z. et al., “Development and Application of a Reliability-Based Multivariate Model Validation Method,” ***Int. J. Veh. Des.***, 60 (3/4), 2012, pp.194–205.

76. Jiang X., Yang R. J., Barbat S., Weerappuli P., “Bayesian probabilistic PCA approach for model validation of dynamic systems,” ***SAE International Journal of Materials and Manufacturing***, Vol. 2, No. 1, 2009, pp. 555-563.

77. Kass R. and Raftery A., “Bayes factors,” ***Journal of the American Statistical Association***, Vol. 90 (430), 1995, pp. 773–795.

78. Jackson K. E. and Putnam J. B., **“**Development of a Full-Scale Finite Element Model of the Fokker F28 Fellowship Aircraft and Crash Simulation Predictions**,”** Proceedings of the ASCE 2021 Earth and Space Conference, Seattle, WA, April 21-23, 2021.

## APPENDIX A. REMARKS CITED IN TABLE 3

1. Flow rule coefficients are determined using the plastic Poisson's ratios.

2. A minimum of two sets of (strain rate-temperature) curves are needed. In case the material is not temperature and/or rate sensitive, make the two sets of table data identical. In the case the material is rate and temperature sensitive, the curve corresponding to the smallest total strain rate for the given reference temperature (TEMP in card 11) is assumed to be the quasistatic, room temperature (QS-RT) curve and influences the viscoelastic-plastic computations. An example TABLE_3D (LT*i*) structure for 3 total strain rates and 3 temperatures for Tension a-direction test is provided in Reference 35. The total strain rates are converted within LS-DYNA® into Effective Plastic Strain Rate (EPSR) for each of the input stress-strain curves. The EPSR value assigned for each stress-strain curve is used for yield stress interpolation. Normal (tension and compression) and shear curve data: Use positive stress and positive strain values in the curve data. Off-axis curve data: Use positive stress and positive strain values in the curve data if the off-axis test is a tension test. Use negative stress and positive strain values in the curve data if the off-axis test is a compressive test. The same combination of compression test is assumed for all MAT_213 cards used in a specific model, i. e., if LT10-LT11-LT12 combination is tension-compression-compression for one MAT_213 data, then it is assumed that all other MAT_213 data in the model use tension-compression-compression data. All shear strain values are tensorial, not engineering (total strain rate input has to be tensorial for shear component). For an elastic component, e. g., a-direction in a unidirectional composite, set the initial yield strain value (in YSC) greater than the failure strain (last strain value in the curve).

3. Curve of initial yield strain values (YSC) must list curves in ascending order as abscissa values with the corresponding yield strains given as the ordinate values.

4. Include in this curve, only the active Damage Parameter ID and the corresponding curve ID. It should be noted that damage data are (a) not rate and temperature dependent, and (b) are used with all relevant input stress-strain curves. The Damage Parameter ID definitions are shown in Reference 35. For shell elements, only in-plane damage is considered and only parameters 1, 2, 4, 5, 7, 13, 15, 16, 18, 21, 23, 24, 26, 37, 38, 40, 42, 45, 46, 48, 50, 61, 62, 64, 65 are active.

5. Use cards 8 and 9 for the failure criterion to be included in the failure model. The failure types and the associated values are provided in Reference 35. Generalized Tabulated Failure Criterion (GTFC) for Solid element: FTYPE=3. FV1 is n, the in-plane and out-of-plane interaction term. FV2 and FV3 are the Table IDs of the two tables for the in-plane and the out-of-plane values that define the in-plane and out-of-plane failure surfaces. FV2 is the table ID for the in-plane values. FV3 is the table ID for the out-of-plane values. For the in-

plane failure surface, the table contains the a-direction stress (S11) value-curve ID pairs. For the out-of-plane failure surface, the table contains the normal c-direction stress (S33) value-curve ID pairs. There is no data in card 9.

6. Element is eroded if failure occurs at any one Gauss point.

7. The user-defined stress-strain curves are adjusted for TCSYM=1, 2, and 3 as follows. If EaT0 and EaC0 represent the original a-direction (1-direction) elastic tensile and compressive moduli respectively, then the modified strain values are computed as explained. For (a) TCSYM=1, EaT= EaC=0.5EaT0+EaC0, (b) TCSYM=2, EaT=EaT0 and EaC=EaT0, and (c) TCSYM=3, EaT=EaC0 and EaC=EaC0. The adjusted tensile strain is then computed as Original Tensile Strain divided by RaT, the adjusted compressive strain is computed as Original Compressive Strain divided by RaC, the adjusted tensile yield strain is computed as Original Tensile Yield Strain divided by RaT, and the adjusted compressive yield strain is computed as Original Compressive Yield Strain divided by RaC. The same process is then applied for the other two normal directions.

8. LCINT option to specify the number of discretized points for the input curves can be used only with *CONTROL_SOLUTION (NOT with *DEFINE_CURVE). The default value is 100.

9. If necessary, the input Poisson’s ratios are adjusted internally in LS-DYNA® to satisfy the criteria, as described in Reference 35.

10. The plastic multiplier computations involve finding the root of the yield function. The root is computed numerically, not analytically. The first step is to find the interval bounding the root. The value of N controls the discretization of the interval to find the bound. The larger the value of N, the more accurate the bound. However, the computational time is likely to increase with larger values of N.

## APPENDIX B. MAT_213 INPUT FILES

To assist beginners in better utilizing *MAT_213, the input files needed to execute a complete *MAT_213 model, specifically using the shell element formulation, are included in this appendix. These files can serve as a representative example of what a full MAT 213 deck looks like. The files are:

B-1. 12_MAT213.k,
B-2. 13_MAT213_InputCurves_w/Damage.k,
B-3. 14_DAMAGE.k,
B-4. 15_FAILURE_SURFACE.k

These files are incorporated into the main LS-DYNA® model file using the *INCLUDE command. Please note that if the user does not wish to study damage or failure effects in their model, then they do not need to include 14_DAMAGE.k or 15_FAILURE_SURFACE.k. For information purposes, the four files listed above are reprinted in this appendix. Finally, as a reminder, lines that begin with $# are comments in the deck.

### B-1. File: 12_MAT213.k

| | | | | | | | |
|---|---|---|---|---|---|---|---|
| *MAT_213 | | | | | | | |
| $# Card 1 | | | | | | | |
| $# mid | RO | EA | EB | EC | PRBA | PRCA | PRCB |
| 1 | 1.29E-4 | 6.42E6 | 2.68E6 | 2.68E6 | 0.1095 | 0.048 | 0.048 |
| $# Card 2 | | | | | | | |
| $# GAB | GBC | GAC | PTOL | AOPT | MACF | FILT | VEVP |
| 3.26E5 | 3.26E5 | 3.26E5 | 1.0E-6 | 2.0 | 1 | | 0 |
| $# Card 3 | | | | | | | |
| $# XP | YP | ZP | A1 | A2 | A3 | | |
| | | | 1 | 0 | 0 | | |
| $# Card 4 | | | | | | | |
| $# V1 | V2 | V3 | D1 | D2 | D3 | BETA | TCSYM |
| | | | 1 | 1 | 0 | | 0 |
| $# Card 5 | | | | | | | |
| $# H11 | H22 | H33 | H12 | H23 | H13 | H44 | H55 |
| 0.007 | 0.082 | | -.00085 | | | 3.875 | |
| $# Card 6 | | | | | | | |
| $# H66 | LT1 | LT2 | LT3 | LT4 | LT5 | LT6 | LT7 |
| | 1001 | 1002 | | 1004 | 1005 | | 1007 |
| $# Card 7 | | | | | | | |
| $# LT8 | LT9 | LT10 | LT11 | LT12 | YSC | DFLAG | DC |
| | | 1010 | | | 100 | 1 | 50 |
| $# Card 8 | | | | | | | |
| $#FCTYPE | FV0 | FV1 | FV2 | FV3 | FV4 | FV5 | FV6 |

| | | | | | | | |
|---|---|---|---|---|---|---|---|
| 3 | 100 | | 2 | 9013 | | | |
| $# Card 9 | | | | | | | |
| $# FV7 | FV8 | FV9 | FV10 | FV11 | FV12 | FV13 | FV14 |
| | | | | | | | |
| $# Card 10 | | | | | | | |
| $#BETA11 | BETA22 | BETA33 | BETA44 | BETA55 | BETA66 | BETA112 | BETA23 |
| | | | | | | | |
| $# Card 11 | | | | | | | |
| $#BETA13 | Cp | TQC | TEMP | PMACC | | | |
| | | | | | | | |

**B-2. File: 13_MAT213_InputCurves_wDamage.k**

| | | | | | | | |
|---|---|---|---|---|---|---|---|
| *KEYWORD | | | | | | | |
| *DEFINE_TABLE_3D | | | | | | | |
| $# Tension_1 | | | | | | | |
| $# tbid | Sfa | offa | | | | | |
| 1001 | | | | | | | |
| $# Temperature | | | table_id | | | | |
| | 21 | | 1013 | | | | |
| *DEFINE_TABLE | | | | | | | |
| $# tbid | Sfa | offa | | | | | |
| 1013 | | | | | | | |
| $# strain rate | | | curve_id | | | | |
| | 0.0 | | 1111 | | | | |
| | 1.0 | | 10000001 | | | | |
| *DEFINE_CURVE | | | | | | | |
| $# Tension_1, Temperature = 21 degrees, Strain Rate = 0.0/s | | | | | | | |
| $# lcid | Sidr | sfa | sfo | offa | offo | dattyp | |
| 1111 | | | | | | | |
| $# | | strain | | stress | | | |
| | | 0.0000 | | 0.0000 | | | |
| | | 0.0001575 | | 800.0 | | | |
| | | 0.00032473 | | 1937.7 | | | |
| | | 0.00060879 | | 3602.9 | | | |
| | | 0.00086701 | | 5396.2 | | | |
| | | 0.0011505 | | 7143.5 | | | |
| | | 0.0014173 | | 8859.2 | | | |
| | | 0.0016853 | | 10561.0 | | | |
| | | 0.0019548 | | 12255.0 | | | |
| | | 0.0022169 | | 13932.0 | | | |
| | | 0.0024714 | | 15584 | | | |
| | | 0.0027158 | | 17233 | | | |
| | | 0.0030060 | | 18890 | | | |
| | | 0.0032253 | | 20536 | | | |
| | | 0.0034863 | | 22151 | | | |
| | | 0.0037336 | | 23746 | | | |

| | | | | | | | |
|---|---|---|---|---|---|---|---|
| | | 0.0039979 | | 25343 | | | |
| | | 0.0042142 | | 26925 | | | |
| | | 0.0044669 | | 28492 | | | |
| | | 0.0047070 | | 30071 | | | |
| | | 0.0049272 | | 31652 | | | |
| | | 0.0051910 | | 33210 | | | |
| | | 0.0054154 | | 34748 | | | |
| | | 0.0056373 | | 36261 | | | |
| | | 0.0058924 | | 37750 | | | |
| | | 0.0061201 | | 39245 | | | |
| | | 0.0063459 | | 40756 | | | |
| | | 0.0065709 | | 42250 | | | |
| | | 0.0068057 | | 43703 | | | |
| | | 0.0070327 | | 45142 | | | |
| | | 0.0072506 | | 46599 | | | |
| | | 0.0074723 | | 48050 | | | |
| | | 0.0076884 | | 49448 | | | |
| | | 0.0079091 | | 50811 | | | |
| | | 0.0081243 | | 52181 | | | |
| | | 0.0083381 | | 53554 | | | |
| | | 0.0085502 | | 54884 | | | |
| | | 0.0087429 | | 56137 | | | |
| | | 0.0089177 | | 57313 | | | |
| | | 0.0090926 | | 58434 | | | |
| | | 0.0092771 | | 59502 | | | |
| | | 0.0094448 | | 60511 | | | |
| | | 0.0095842 | | 61494 | | | |
| | | 0.0097445 | | 62481 | | | |
| | | 0.0098946 | | 63441 | | | |
| | | 0.010058 | | 64364 | | | |
| | | 0.010224 | | 65284 | | | |
| | | 0.010370 | | 66198 | | | |
| | | 0.010500 | | 67110 | | | |
| | | 0.010659 | | 68023 | | | |
| | | 0.010791 | | 68925 | | | |
| | | 0.010935 | | 69830 | | | |
| | | 0.011092 | | 70747 | | | |
| | | 0.011232 | | 71638 | | | |
| | | 0.011387 | | 72496 | | | |
| | | 0.011529 | | 73363 | | | |
| | | 0.011666 | | 74240 | | | |
| | | 0.011822 | | 75094 | | | |
| | | 0.011951 | | 75933 | | | |
| | | 0.012100 | | 76791 | | | |
| | | 0.012235 | | 77666 | | | |
| | | 0.012372 | | 78537 | | | |
| | | 0.012518 | | 79402 | | | |
| | | 0.012666 | | 80260 | | | |
| | | 0.012840 | | 81091 | | | |

| | | | | | | | |
|---|---|---|---|---|---|---|---|
| | | 0.013012 | | 81893 | | | |
| | | 0.013116 | | 82702 | | | |
| | | 0.013315 | | 83552 | | | |
| | | 0.013440 | | 84421 | | | |
| | | 0.013580 | | 85265 | | | |
| | | 0.013721 | | 86098 | | | |
| | | 0.013864 | | 86930 | | | |
| | | 0.014011 | | 87760 | | | |
| | | 0.014155 | | 88645 | | | |
| | | 0.015 | | 8864.5 | | | |
| | | 0.016 | | 8864.5 | | | |
| *DEFINE_CURVE | | | | | | | |
| $# Tension_1, Temperature = 21 degrees, Strain Rate = 1.0/s | | | | | | | |
| $# lcid | sidr | sfa | sfo | offa | offo | dattyp | |
| 10000001 | | | | | | | |
| $# | | strain | | stress | | | |
| | | 0.0000 | | 0.0000 | | | |
| | | 0.0001575 | | 800.0 | | | |
| | | 0.00032473 | | 1937.7 | | | |
| | | 0.00060879 | | 3602.9 | | | |
| | | 0.00086701 | | 5396.2 | | | |
| | | 0.0011505 | | 7143.5 | | | |
| | | 0.0014173 | | 8859.2 | | | |
| | | 0.0016853 | | 10561.0 | | | |
| | | 0.0019548 | | 12255.0 | | | |
| | | 0.0022169 | | 13932.0 | | | |
| | | 0.0024714 | | 15584 | | | |
| | | 0.0027158 | | 17233 | | | |
| | | 0.0030060 | | 18890 | | | |
| | | 0.0032253 | | 20536 | | | |
| | | 0.0034863 | | 22151 | | | |
| | | 0.0037336 | | 23746 | | | |
| | | 0.0039979 | | 25343 | | | |
| | | 0.0042142 | | 26925 | | | |
| | | 0.0044669 | | 28492 | | | |
| | | 0.0047070 | | 30071 | | | |
| | | 0.0049272 | | 31652 | | | |
| | | 0.0051910 | | 33210 | | | |
| | | 0.0054154 | | 34748 | | | |
| | | 0.0056373 | | 36261 | | | |
| | | 0.0058924 | | 37750 | | | |
| | | 0.0061201 | | 39245 | | | |
| | | 0.0063459 | | 40756 | | | |
| | | 0.0065709 | | 42250 | | | |
| | | 0.0068057 | | 43703 | | | |
| | | 0.0070327 | | 45142 | | | |
| | | 0.0072506 | | 46599 | | | |
| | | 0.0074723 | | 48050 | | | |
| | | 0.0076884 | | 49448 | | | |

| | | | | | | | |
|---|---|---|---|---|---|---|---|
| | | 0.0079091 | | 50811 | | | |
| | | 0.0081243 | | 52181 | | | |
| | | 0.0083381 | | 53554 | | | |
| | | 0.0085502 | | 54884 | | | |
| | | 0.0087429 | | 56137 | | | |
| | | 0.0089177 | | 57313 | | | |
| | | 0.0090926 | | 58434 | | | |
| | | 0.0092771 | | 59502 | | | |
| | | 0.0094448 | | 60511 | | | |
| | | 0.0095842 | | 61494 | | | |
| | | 0.0097445 | | 62481 | | | |
| | | 0.0098946 | | 63441 | | | |
| | | 0.010058 | | 64364 | | | |
| | | 0.010224 | | 65284 | | | |
| | | 0.010370 | | 66198 | | | |
| | | 0.010500 | | 67110 | | | |
| | | 0.010659 | | 68023 | | | |
| | | 0.010791 | | 68925 | | | |
| | | 0.010935 | | 69830 | | | |
| | | 0.011092 | | 70747 | | | |
| | | 0.011232 | | 71638 | | | |
| | | 0.011387 | | 72496 | | | |
| | | 0.011529 | | 73363 | | | |
| | | 0.011666 | | 74240 | | | |
| | | 0.011822 | | 75094 | | | |
| | | 0.011951 | | 75933 | | | |
| | | 0.012100 | | 76791 | | | |
| | | 0.012235 | | 77666 | | | |
| | | 0.012372 | | 78537 | | | |
| | | 0.012518 | | 79402 | | | |
| | | 0.012666 | | 80260 | | | |
| | | 0.012840 | | 81091 | | | |
| | | 0.013012 | | 81893 | | | |
| | | 0.013116 | | 82702 | | | |
| | | 0.013315 | | 83552 | | | |
| | | 0.013440 | | 84421 | | | |
| | | 0.013580 | | 85265 | | | |
| | | 0.013721 | | 86098 | | | |
| | | 0.013864 | | 86930 | | | |
| | | 0.014011 | | 87760 | | | |
| | | 0.014155 | | 88645 | | | |
| | | 0.015 | | 8864.5 | | | |
| | | 0.016 | | 8864.5 | | | |
| *DEFINE_TABLE_3D | | | | | | | |
| $# Tension_2 | | | | | | | |
| $# tbid | Sfa | offa | | | | | |
| 1002 | | | | | | | |
| $# temperature | | | table_id | | | | |
| | 21 | | 1014 | | | | |

| | | | | | | | |
|---|---|---|---|---|---|---|---|
| *DEFINE_TABLE | | | | | | | |
| $# tbid | Sfa | offo | | | | | |
| $# 1014 | Strain rate | | curve_id | | | | |
| | 0.0 | | 2222 | | | | |
| | 1.0 | | 10000002 | | | | |
| *DEFINE_CURVE | | | | | | | |
| $# Tension_2, Temperature = 21 degrees, Strain Rate = 0.0/s | | | | | | | |
| $# lcid | Sidr | sfa | sfo | offa | offo | dattyp | |
| 2222 | | | | | | | |
| $# | | strain | | stress | | | |
| | | 0.000000 | | 0.00000 | | | |
| | | 0.00017413 | | 450.0 | | | |
| | | 0.00034826 | | 900.0 | | | |
| | | 0.00065327 | | 1744.9 | | | |
| | | 0.00094285 | | 2581.1 | | | |
| | | 0.0012406 | | 3383.1 | | | |
| | | 0.0015309 | | 4182.0 | | | |
| | | 0.0018319 | | 4945.7 | | | |
| | | 0.0021120 | | 5738.4 | | | |
| | | 0.0024157 | | 6555.3 | | | |
| | | 0.0026958 | | 7319.7 | | | |
| | | 0.0029837 | | 7985.5 | | | |
| | | 0.0032713 | | 8920.9 | | | |
| | | 0.0038352 | | 10150 | | | |
| | | 0.0041269 | | 11031 | | | |
| | | 0.0044081 | | 11604 | | | |
| | | 0.0046746 | | 12288 | | | |
| | | 0.0049656 | | 12980 | | | |
| | | 0.0052396 | | 13604 | | | |
| | | 0.0055052 | | 14262 | | | |
| | | 0.0057978 | | 14906 | | | |
| | | 0.0060615 | | 15523 | | | |
| | | 0.0063383 | | 16168 | | | |
| | | 0.0066190 | | 16794 | | | |
| | | 0.0068784 | | 17377 | | | |
| | | 0.0071703 | | 17944 | | | |
| | | 0.0074414 | | 18509 | | | |
| | | 0.0077046 | | 19114 | | | |
| | | 0.0079766 | | 19725 | | | |
| | | 0.0082455 | | 20301 | | | |
| | | 0.0085200 | | 20882 | | | |
| | | 0.0087778 | | 21456 | | | |
| | | 0.0090544 | | 22014 | | | |
| | | 0.0093096 | | 22612 | | | |
| | | 0.0095804 | | 23211 | | | |
| | | 0.0098451 | | 23755 | | | |
| | | 0.010089 | | 24287 | | | |
| | | 0.010377 | | 24821 | | | |
| | | 0.010636 | | 25366 | | | |

| | | | | | | | |
|---|---|---|---|---|---|---|---|
| | | 0.010893 | | 25951 | | | |
| | | 0.011145 | | 26505 | | | |
| | | 0.011410 | | 27008 | | | |
| | | 0.011653 | | 27567 | | | |
| | | 0.011913 | | 28140 | | | |
| | | 0.012166 | | 28656 | | | |
| | | 0.012425 | | 29184 | | | |
| | | 0.012674 | | 29734 | | | |
| | | 0.012925 | | 30270 | | | |
| | | 0.013185 | | 30795 | | | |
| | | 0.013428 | | 31303 | | | |
| | | 0.013679 | | 31812 | | | |
| | | 0.013940 | | 32331 | | | |
| | | 0.014190 | | 32823 | | | |
| | | 0.014450 | | 33319 | | | |
| | | 0.014695 | | 33837 | | | |
| | | 0.014952 | | 34337 | | | |
| | | 0.015199 | | 34854 | | | |
| | | 0.015442 | | 35352 | | | |
| | | 0.015701 | | 35806 | | | |
| | | 0.015943 | | 36291 | | | |
| | | 0.016200 | | 36769 | | | |
| | | 0.016454 | | 37240 | | | |
| | | 0.016704 | | 37732 | | | |
| | | 0.016943 | | 38193 | | | |
| | | 0.017200 | | 38671 | | | |
| | | 0.017444 | | 39175 | | | |
| | | 0.017681 | | 39642 | | | |
| | | 0.017927 | | 40108 | | | |
| | | 0.01817 | | 40580 | | | |
| | | 0.018409 | | 41045 | | | |
| | | 0.018678 | | 41518 | | | |
| | | 0.018917 | | 42001 | | | |
| | | 0.019166 | | 42491 | | | |
| | | 0.019410 | | 42945 | | | |
| | | 0.019646 | | 43378 | | | |
| | | 0.019908 | | 43847 | | | |
| | | 0.020157 | | 44336 | | | |
| | | 0.020388 | | 44824 | | | |
| | | 0.020633 | | 45279 | | | |
| | | 0.020881 | | 45698 | | | |
| | | 0.021137 | | 46159 | | | |
| | | 0.021385 | | 46641 | | | |
| | | 0.021630 | | 47094 | | | |
| | | 0.021875 | | 47553 | | | |
| | | 0.022117 | | 48009 | | | |
| | | 0.022353 | | 48469 | | | |
| | | 0.022597 | | 48927 | | | |
| | | 0.022837 | | 49354 | | | |

| | | | | | | | |
|---|---|---|---|---|---|---|---|
| | | 0.023080 | | 49798 | | | |
| | | 0.023322 | | 50256 | | | |
| | | 0.023561 | | 50685 | | | |
| | | 0.023806 | | 51138 | | | |
| | | 0.024036 | | 51612 | | | |
| | | 0.024282 | | 51996 | | | |
| | | 0.024490 | | 52491 | | | |
| | | 0.024951 | | 53315 | | | |
| | | 0.0250 | | 5331.5 | | | |
| | | 0.0500 | | 5331.5 | | | |
| *DEFINE_CURVE | | | | | | | |
| $# Tension 2, Temperature = 21-degrees, Strain Rate = 1.0/s | | | | | | | |
| $# lcid | Sidr | sfa | sfo | offa | offo | dattyp | |
| 10000002 | | | | | | | |
| $# | | strain | | stress | | | |
| | | 0.000000 | | 0.00000 | | | |
| | | 0.00017413 | | 450.0 | | | |
| | | 0.00034826 | | 900.0 | | | |
| | | 0.00065327 | | 1744.9 | | | |
| | | 0.00094285 | | 2581.1 | | | |
| | | 0.0012406 | | 3383.1 | | | |
| | | 0.0015309 | | 4182.0 | | | |
| | | 0.0018319 | | 4945.7 | | | |
| | | 0.0021120 | | 5738.4 | | | |
| | | 0.0024157 | | 6555.3 | | | |
| | | 0.0026958 | | 7319.7 | | | |
| | | 0.0029837 | | 7985.5 | | | |
| | | 0.0032713 | | 8920.9 | | | |
| | | 0.0038352 | | 10150 | | | |
| | | 0.0041269 | | 11031 | | | |
| | | 0.0044081 | | 11604 | | | |
| | | 0.0046746 | | 12288 | | | |
| | | 0.0049656 | | 12980 | | | |
| | | 0.0052396 | | 13604 | | | |
| | | 0.0055052 | | 14262 | | | |
| | | 0.0057978 | | 14906 | | | |
| | | 0.0060615 | | 15523 | | | |
| | | 0.0063383 | | 16168 | | | |
| | | 0.0066190 | | 16794 | | | |
| | | 0.0068784 | | 17377 | | | |
| | | 0.0071703 | | 17944 | | | |
| | | 0.0074414 | | 18509 | | | |
| | | 0.0077046 | | 19114 | | | |
| | | 0.0079766 | | 19725 | | | |
| | | 0.0082455 | | 20301 | | | |
| | | 0.0085200 | | 20882 | | | |
| | | 0.0087778 | | 21456 | | | |
| | | 0.0090544 | | 22014 | | | |
| | | 0.0093096 | | 22612 | | | |

| | | | | | | | |
|---|---|---|---|---|---|---|---|
| | | 0.0095804 | | 23211 | | | |
| | | 0.0098451 | | 23755 | | | |
| | | 0.010089 | | 24287 | | | |
| | | 0.010377 | | 24821 | | | |
| | | 0.010636 | | 25366 | | | |
| | | 0.010893 | | 25951 | | | |
| | | 0.011145 | | 26505 | | | |
| | | 0.011410 | | 27008 | | | |
| | | 0.011653 | | 27567 | | | |
| | | 0.011913 | | 28140 | | | |
| | | 0.012166 | | 28656 | | | |
| | | 0.012425 | | 29184 | | | |
| | | 0.012674 | | 29734 | | | |
| | | 0.012925 | | 30270 | | | |
| | | 0.013185 | | 30795 | | | |
| | | 0.013428 | | 31303 | | | |
| | | 0.013679 | | 31812 | | | |
| | | 0.013940 | | 32331 | | | |
| | | 0.014190 | | 32823 | | | |
| | | 0.014450 | | 33319 | | | |
| | | 0.014695 | | 33837 | | | |
| | | 0.014952 | | 34337 | | | |
| | | 0.015199 | | 34854 | | | |
| | | 0.015442 | | 35352 | | | |
| | | 0.015701 | | 35806 | | | |
| | | 0.015943 | | 36291 | | | |
| | | 0.016200 | | 36769 | | | |
| | | 0.016454 | | 37240 | | | |
| | | 0.016704 | | 37732 | | | |
| | | 0.016943 | | 38193 | | | |
| | | 0.017200 | | 38671 | | | |
| | | 0.017444 | | 39175 | | | |
| | | 0.017681 | | 39642 | | | |
| | | 0.017927 | | 40108 | | | |
| | | 0.01817 | | 40580 | | | |
| | | 0.018409 | | 41045 | | | |
| | | 0.018678 | | 41518 | | | |
| | | 0.018917 | | 42001 | | | |
| | | 0.019166 | | 42491 | | | |
| | | 0.019410 | | 42945 | | | |
| | | 0.019646 | | 43378 | | | |
| | | 0.019908 | | 43847 | | | |
| | | 0.020157 | | 44336 | | | |
| | | 0.020388 | | 44824 | | | |
| | | 0.020633 | | 45279 | | | |
| | | 0.020881 | | 45698 | | | |
| | | 0.021137 | | 46159 | | | |
| | | 0.021385 | | 46641 | | | |
| | | 0.021630 | | 47094 | | | |

| | | | | | | | |
|---|---|---|---|---|---|---|---|
| | | 0.021875 | | 47553 | | | |
| | | 0.022117 | | 48009 | | | |
| | | 0.022353 | | 48469 | | | |
| | | 0.022597 | | 48927 | | | |
| | | 0.022837 | | 49354 | | | |
| | | 0.023080 | | 49798 | | | |
| | | 0.023322 | | 50256 | | | |
| | | 0.023561 | | 50685 | | | |
| | | 0.023806 | | 51138 | | | |
| | | 0.024036 | | 51612 | | | |
| | | 0.024282 | | 51996 | | | |
| | | 0.024490 | | 52491 | | | |
| | | 0.024951 | | 53315 | | | |
| | | 0.0250 | | 5331.5 | | | |
| | | 0.0500 | | 5331.5 | | | |
| *DEFINE_TABLE_3D | | | | | | | |
| $# Compression_1 | | | | | | | |
| $# tbid | sfa | offa | | | | | |
| 1004 | | | | | | | |
| $# temperature | | | table_id | | | | |
| | 21 | | 1016 | | | | |
| *DEFINE_TABLE | | | | | | | |
| $# tbid | sfa | offa | | | | | |
| 1016 | | | | | | | |
| $# strain_rate | | | curve_id | | | | |
| | 0.0 | | 4444 | | | | |
| | 1.0 | | 10000004 | | | | |
| *DEFINE_CURVE | | | | | | | |
| $# Compression_1, Temperature = 21 degrees, Strain Rate = 0.0/s | | | | | | | |
| $# lcid | sidr | sfa | sfo | offa | offo | dattyp | |
| 4444 | | | | | | | |
| $# | | strain | | stress | | | |
| | | 0.0000 | | 0.0000 | | | |
| | | 0.00015750 | | 800.0 | | | |
| | | 0.00032473 | | 1937.7 | | | |
| | | 0.00060879 | | 3602.9 | | | |
| | | 0.00086701 | | 5396.2 | | | |
| | | 0.0011505 | | 7143.5 | | | |
| | | 0.0014173 | | 8859.2 | | | |
| | | 0.0016853 | | 10561.0 | | | |
| | | 0.0019548 | | 12255.0 | | | |
| | | 0.0022169 | | 13932.0 | | | |
| | | 0.0024714 | | 15584 | | | |
| | | 0.0027158 | | 17233 | | | |
| | | 0.0030060 | | 18890 | | | |
| | | 0.0032253 | | 20536 | | | |
| | | 0.0034863 | | 22151 | | | |
| | | 0.0037336 | | 23746 | | | |

| | | | | | | | |
|---|---|---|---|---|---|---|---|
| | | 0.0039979 | | 25343 | | | |
| | | 0.0042142 | | 26925 | | | |
| | | 0.0044669 | | 28492 | | | |
| | | 0.0047070 | | 30071 | | | |
| | | 0.0049272 | | 31652 | | | |
| | | 0.0051910 | | 33210 | | | |
| | | 0.0054154 | | 34748 | | | |
| | | 0.0056373 | | 36261 | | | |
| | | 0.0058924 | | 37750 | | | |
| | | 0.0061201 | | 39245 | | | |
| | | 0.0063459 | | 40756 | | | |
| | | 0.0065709 | | 42250 | | | |
| | | 0.0068057 | | 43703 | | | |
| | | 0.0070327 | | 45142 | | | |
| | | 0.0072506 | | 46599 | | | |
| | | 0.0074723 | | 48050 | | | |
| | | 0.0076884 | | 49448 | | | |
| | | 0.0079091 | | 50811 | | | |
| | | 0.0081243 | | 52181 | | | |
| | | 0.0083381 | | 53554 | | | |
| | | 0.0085502 | | 54884 | | | |
| | | 0.0087429 | | 56137 | | | |
| | | 0.0089177 | | 57313 | | | |
| | | 0.0090926 | | 58434 | | | |
| | | 0.0092771 | | 59502 | | | |
| | | 0.0094448 | | 60511 | | | |
| | | 0.0095842 | | 61494 | | | |
| | | 0.0097445 | | 62481 | | | |
| | | 0.0098946 | | 63441 | | | |
| | | 0.010058 | | 64364 | | | |
| | | 0.010224 | | 65284 | | | |
| | | 0.010370 | | 66198 | | | |
| | | 0.010500 | | 67110 | | | |
| | | 0.010659 | | 68023 | | | |
| | | 0.010791 | | 68925 | | | |
| | | 0.010935 | | 69830 | | | |
| | | 0.011092 | | 70747 | | | |
| | | 0.011232 | | 71638 | | | |
| | | 0.011387 | | 72496 | | | |
| | | 0.011529 | | 73363 | | | |
| | | 0.011666 | | 74240 | | | |
| | | 0.011822 | | 75094 | | | |
| | | 0.011951 | | 75933 | | | |
| | | 0.012100 | | 76791 | | | |
| | | 0.012235 | | 77666 | | | |
| | | 0.012372 | | 78537 | | | |
| | | 0.012518 | | 79402 | | | |
| | | 0.012666 | | 80260 | | | |
| | | 0.012840 | | 81091 | | | |

| | | | | | | | |
|---|---|---|---|---|---|---|---|
| | | 0.013012 | | 81893 | | | |
| | | 0.013116 | | 82702 | | | |
| | | 0.013315 | | 83552 | | | |
| | | 0.013440 | | 84421 | | | |
| | | 0.013580 | | 85265 | | | |
| | | 0.013721 | | 86098 | | | |
| | | 0.013864 | | 86930 | | | |
| | | 0.014011 | | 87760 | | | |
| | | 0.014155 | | 88645 | | | |
| | | 0.015 | | 8864.5 | | | |
| | | 0.016 | | 8864.5 | | | |
| *DEFINE_TABLE_3D | | | | | | | |
| $# Compression 2 | | | | | | | |
| $# tbid | sfa | offa | | | | | |
| 1005 | | | | | | | |
| $# temperature | | | table_id | | | | |
| | 21 | | 1017 | | | | |
| *DEFINE_TABLE | | | | | | | |
| $# tbid | sfa | offa | | | | | |
| 1017 | | | | | | | |
| $# strain_rate | | | curve_id | | | | |
| | 0.0 | | 5555 | | | | |
| | 1.0 | | 10000005 | | | | |
| *DEFINE_CURVE | | | | | | | |
| $# Compression_2, Temperature = 21 degrees, Strain Rate = 0.0/s | | | | | | | |
| $# lcid | sidr | sfa | sfo | offa | offo | dattyp | |
| 5555 | | strain | | stress | | | |
| $# | | 0.000000 | | 0.00000 | | | |
| | | 0.00017413 | | 450.0 | | | |
| | | 0.00034826 | | 900.0 | | | |
| | | 0.00065327 | | 1744.9 | | | |
| | | 0.00094285 | | 2581.1 | | | |
| | | 0.0012406 | | 3383.1 | | | |
| | | 0.0015309 | | 4182.0 | | | |
| | | 0.0018319 | | 4945.7 | | | |
| | | 0.0021120 | | 5738.4 | | | |
| | | 0.0024157 | | 6555.3 | | | |
| | | 0.0026958 | | 7319.7 | | | |
| | | 0.0029837 | | 7985.5 | | | |
| | | 0.0032713 | | 8920.9 | | | |
| | | 0.0038352 | | 10150 | | | |
| | | 0.0041269 | | 11031 | | | |
| | | 0.0044081 | | 11604 | | | |
| | | 0.0046746 | | 12288 | | | |
| | | 0.0049656 | | 12980 | | | |
| | | 0.0052396 | | 13604 | | | |
| | | 0.0055052 | | 14262 | | | |
| | | 0.0057978 | | 14906 | | | |
| | | 0.0060615 | | 15523 | | | |

| | | | | | | | |
|---|---|---|---|---|---|---|---|
| | | 0.0063383 | | 16168 | | | |
| | | 0.0066190 | | 16794 | | | |
| | | 0.0068784 | | 17377 | | | |
| | | 0.0071703 | | 17944 | | | |
| | | 0.0074414 | | 18509 | | | |
| | | 0.0077046 | | 19114 | | | |
| | | 0.0079766 | | 19725 | | | |
| | | 0.0082455 | | 20301 | | | |
| | | 0.0085200 | | 20882 | | | |
| | | 0.0087778 | | 21456 | | | |
| | | 0.0090544 | | 22014 | | | |
| | | 0.0093096 | | 22612 | | | |
| | | 0.0095804 | | 23211 | | | |
| | | 0.0098451 | | 23755 | | | |
| | | 0.010089 | | 24287 | | | |
| | | 0.010377 | | 24821 | | | |
| | | 0.010636 | | 25366 | | | |
| | | 0.010893 | | 25951 | | | |
| | | 0.011145 | | 26505 | | | |
| | | 0.011410 | | 27008 | | | |
| | | 0.011653 | | 27567 | | | |
| | | 0.011913 | | 28140 | | | |
| | | 0.012166 | | 28656 | | | |
| | | 0.012425 | | 29184 | | | |
| | | 0.012674 | | 29734 | | | |
| | | 0.012925 | | 30270 | | | |
| | | 0.013185 | | 30795 | | | |
| | | 0.013428 | | 31303 | | | |
| | | 0.013679 | | 31812 | | | |
| | | 0.013940 | | 32331 | | | |
| | | 0.014190 | | 32823 | | | |
| | | 0.014450 | | 33319 | | | |
| | | 0.014695 | | 33837 | | | |
| | | 0.014952 | | 34337 | | | |
| | | 0.015199 | | 34854 | | | |
| | | 0.015442 | | 35352 | | | |
| | | 0.015701 | | 35806 | | | |
| | | 0.015943 | | 36291 | | | |
| | | 0.016200 | | 36769 | | | |
| | | 0.016454 | | 37240 | | | |
| | | 0.016704 | | 37732 | | | |
| | | 0.016943 | | 38193 | | | |
| | | 0.017200 | | 38671 | | | |
| | | 0.017444 | | 39175 | | | |
| | | 0.017681 | | 39642 | | | |
| | | 0.017927 | | 40108 | | | |
| | | 0.01817 | | 40580 | | | |
| | | 0.018409 | | 41045 | | | |
| | | 0.018678 | | 41518 | | | |

| | | | | | | | |
|---|---|---|---|---|---|---|---|
| | | 0.018917 | | 42001 | | | |
| | | 0.019166 | | 42491 | | | |
| | | 0.019410 | | 42945 | | | |
| | | 0.019646 | | 43378 | | | |
| | | 0.019908 | | 43847 | | | |
| | | 0.020157 | | 44336 | | | |
| | | 0.020388 | | 44824 | | | |
| | | 0.020633 | | 45279 | | | |
| | | 0.020881 | | 45698 | | | |
| | | 0.021137 | | 46159 | | | |
| | | 0.021385 | | 46641 | | | |
| | | 0.021630 | | 47094 | | | |
| | | 0.021875 | | 47553 | | | |
| | | 0.022117 | | 48009 | | | |
| | | 0.022353 | | 48469 | | | |
| | | 0.022597 | | 48927 | | | |
| | | 0.022837 | | 49354 | | | |
| | | 0.023080 | | 49798 | | | |
| | | 0.023322 | | 50256 | | | |
| | | 0.023561 | | 50685 | | | |
| | | 0.023806 | | 51138 | | | |
| | | 0.024036 | | 51612 | | | |
| | | 0.024282 | | 51996 | | | |
| | | 0.024490 | | 52491 | | | |
| | | 0.024951 | | 53315 | | | |
| | | 0.0250 | | 5331.5 | | | |
| | | 0.0500 | | 5331.5 | | | |
| *DEFINE_CURVE | | | | | | | |
| $# Compression_2, Temperature = 21 degrees, Strain Rate = 1.0/s | | | | | | | |
| $# lcid | sidr | sfa | sfo | offo | offa | dattyp | |
| 10000005 | | | | | | | |
| $# | | strain | | stress | | | |
| | | 0.000000 | | 0.00000 | | | |
| | | 0.00017413 | | 450.0 | | | |
| | | 0.00034826 | | 900.0 | | | |
| | | 0.00065327 | | 1744.9 | | | |
| | | 0.00094285 | | 2581.1 | | | |
| | | 0.0012406 | | 3383.1 | | | |
| | | 0.0015309 | | 4182.0 | | | |
| | | 0.0018319 | | 4945.7 | | | |
| | | 0.0021120 | | 5738.4 | | | |
| | | 0.0024157 | | 6555.3 | | | |
| | | 0.0026958 | | 7319.7 | | | |
| | | 0.0029837 | | 7985.5 | | | |
| | | 0.0032713 | | 8920.9 | | | |
| | | 0.0038352 | | 10150 | | | |
| | | 0.0041269 | | 11031 | | | |
| | | 0.0044081 | | 11604 | | | |
| | | 0.0046746 | | 12288 | | | |

| | | | | | | | |
|---|---|---|---|---|---|---|---|
| | | 0.0049656 | | 12980 | | | |
| | | 0.0052396 | | 13604 | | | |
| | | 0.0055052 | | 14262 | | | |
| | | 0.0057978 | | 14906 | | | |
| | | 0.0060615 | | 15523 | | | |
| | | 0.0063383 | | 16168 | | | |
| | | 0.0066190 | | 16794 | | | |
| | | 0.0068784 | | 17377 | | | |
| | | 0.0071703 | | 17944 | | | |
| | | 0.0074414 | | 18509 | | | |
| | | 0.0077046 | | 19114 | | | |
| | | 0.0079766 | | 19725 | | | |
| | | 0.0082455 | | 20301 | | | |
| | | 0.0085200 | | 20882 | | | |
| | | 0.0087778 | | 21456 | | | |
| | | 0.0090544 | | 22014 | | | |
| | | 0.0093096 | | 22612 | | | |
| | | 0.0095804 | | 23211 | | | |
| | | 0.0098451 | | 23755 | | | |
| | | 0.010089 | | 24287 | | | |
| | | 0.010377 | | 24821 | | | |
| | | 0.010636 | | 25366 | | | |
| | | 0.010893 | | 25951 | | | |
| | | 0.011145 | | 26505 | | | |
| | | 0.011410 | | 27008 | | | |
| | | 0.011653 | | 27567 | | | |
| | | 0.011913 | | 28140 | | | |
| | | 0.012166 | | 28656 | | | |
| | | 0.012425 | | 29184 | | | |
| | | 0.012674 | | 29734 | | | |
| | | 0.012925 | | 30270 | | | |
| | | 0.013185 | | 30795 | | | |
| | | 0.013428 | | 31303 | | | |
| | | 0.013679 | | 31812 | | | |
| | | 0.013940 | | 32331 | | | |
| | | 0.014190 | | 32823 | | | |
| | | 0.014450 | | 33319 | | | |
| | | 0.014695 | | 33837 | | | |
| | | 0.014952 | | 34337 | | | |
| | | 0.015199 | | 34854 | | | |
| | | 0.015442 | | 35352 | | | |
| | | 0.015701 | | 35806 | | | |
| | | 0.015943 | | 36291 | | | |
| | | 0.016200 | | 36769 | | | |
| | | 0.016454 | | 37240 | | | |
| | | 0.016704 | | 37732 | | | |
| | | 0.016943 | | 38193 | | | |
| | | 0.017200 | | 38671 | | | |
| | | 0.017444 | | 39175 | | | |

| | | | | | | | |
|---|---|---|---|---|---|---|---|
| | | 0.017681 | | 39642 | | | |
| | | 0.017927 | | 40108 | | | |
| | | 0.01817 | | 40580 | | | |
| | | 0.018409 | | 41045 | | | |
| | | 0.018678 | | 41518 | | | |
| | | 0.018917 | | 42001 | | | |
| | | 0.019166 | | 42491 | | | |
| | | 0.019410 | | 42945 | | | |
| | | 0.019646 | | 43378 | | | |
| | | 0.019908 | | 43847 | | | |
| | | 0.020157 | | 44336 | | | |
| | | 0.020388 | | 44824 | | | |
| | | 0.020633 | | 45279 | | | |
| | | 0.020881 | | 45698 | | | |
| | | 0.021137 | | 46159 | | | |
| | | 0.021385 | | 46641 | | | |
| | | 0.021630 | | 47094 | | | |
| | | 0.021875 | | 47553 | | | |
| | | 0.022117 | | 48009 | | | |
| | | 0.022353 | | 48469 | | | |
| | | 0.022597 | | 48927 | | | |
| | | 0.022837 | | 49354 | | | |
| | | 0.023080 | | 49798 | | | |
| | | 0.023322 | | 50256 | | | |
| | | 0.023561 | | 50685 | | | |
| | | 0.023806 | | 51138 | | | |
| | | 0.024036 | | 51612 | | | |
| | | 0.024282 | | 51996 | | | |
| | | 0.024490 | | 52491 | | | |
| | | 0.024951 | | 53315 | | | |
| | | 0.0250 | | 5331.5 | | | |
| | | 0.0500 | | 5331.5 | | | |
| *DEFINE_TABLE_3D | | | | | | | |
| $# Shear_12 | | | | | | | |
| $# tbid | sfa | offa | | | | | |
| $# temperature | | | table_id | | | | |
| | 21 | | 1019 | | | | |
| *DEFINE_TABLE | | | | | | | |
| $# tbid | sfa | offa | | | | | |
| 1019 | | | | | | | |
| $# strain_rate | | | curve_id | | | | |
| | 0.0 | | 7777 | | | | |
| | 1.0 | | 10000007 | | | | |
| *DEFINE_CURVE | | | | | | | |
| $# Shear_12, Temperature = 21 degrees, Strain Rate = 0.0/s | | | | | | | |
| $# lcid | sidr | sfa | sfo | offa | offo | dattyp | |
| 7777 | | | | | | | |
| $# | | strain | | stress | | | |
| | | 0.0000 | | 0.0000 | | | |

| | | | | | | | |
|---|---|---|---|---|---|---|---|
| | | 0.00022200 | | 67.293 | | | |
| | | 0.00082948 | | 451.75 | | | |
| | | 0.0024457 | | 1112.1 | | | |
| | | 0.0040950 | | 1848.7 | | | |
| | | 0.0057325 | | 2453.7 | | | |
| | | 0.0073845 | | 2905.7 | | | |
| | | 0.0090185 | | 3252.5 | | | |
| | | 0.010656 | | 3517.6 | | | |
| | | 0.012311 | | 3725.3 | | | |
| | | 0.013997 | | 3907.7 | | | |
| | | 0.015687 | | 4063.0 | | | |
| | | 0.01740 | | 4176.6 | | | |
| | | 0.019124 | | 4262.5 | | | |
| | | 0.020866 | | 4346.1 | | | |
| | | 0.022606 | | 4442.2 | | | |
| | | 0.024351 | | 4542.2 | | | |
| | | 0.026122 | | 4622.7 | | | |
| | | 0.027903 | | 4683.4 | | | |
| | | 0.029661 | | 4744.0 | | | |
| | | 0.031488 | | 4814.9 | | | |
| | | 0.033263 | | 4893.0 | | | |
| | | 0.035072 | | 4965.5 | | | |
| | | 0.036879 | | 5024.3 | | | |
| | | 0.038644 | | 5079.4 | | | |
| | | 0.040469 | | 5141.8 | | | |
| | | 0.042287 | | 5211.3 | | | |
| | | 0.044121 | | 5282.8 | | | |
| | | 0.045912 | | 5346.0 | | | |
| | | 0.047734 | | 5393.1 | | | |
| | | 0.049546 | | 5437.4 | | | |
| | | 0.051316 | | 5502.2 | | | |
| | | 0.053167 | | 5580.8 | | | |
| | | 0.055000 | | 5642.6 | | | |
| | | 0.056681 | | 5681.1 | | | |
| | | 0.058496 | | 5722.9 | | | |
| | | 0.060287 | | 5787.8 | | | |
| | | 0.062143 | | 5864.6 | | | |
| | | 0.063965 | | 5933.3 | | | |
| | | 0.065849 | | 5987.1 | | | |
| | | 0.067634 | | 6029.2 | | | |
| | | 0.069431 | | 6067.7 | | | |
| | | 0.071295 | | 6116.7 | | | |
| | | 0.073018 | | 6177.5 | | | |
| | | 0.074900 | | 6226.3 | | | |
| | | 0.076707 | | 6253.7 | | | |
| | | 0.078556 | | 6286.8 | | | |
| | | 0.080437 | | 6342.2 | | | |
| | | 0.082349 | | 6400.4 | | | |
| | | 0.083987 | | 6444.5 | | | |

| | | | | | | | |
|---|---|---|---|---|---|---|---|
| | | 0.085889 | | 6478.1 | | | |
| | | 0.087616 | | 6506.6 | | | |
| | | 0.089419 | | 6536.5 | | | |
| | | 0.091323 | | 6576.8 | | | |
| | | 0.093113 | | 6627.6 | | | |
| | | 0.094875 | | 6677.4 | | | |
| | | 0.096695 | | 6718.5 | | | |
| | | 0.098440 | | 6758.7 | | | |
| | | 0.099888 | | 6803.4 | | | |
| | | 0.10176 | | 6840.2 | | | |
| | | 0.10323 | | 6862.6 | | | |
| | | 0.10530 | | 6880.0 | | | |
| | | 0.10704 | | 6895.1 | | | |
| | | 0.10913 | | 6905.3 | | | |
| | | 0.11281 | | 6921.8 | | | |
| | | 0.11454 | | 6952.7 | | | |
| | | 0.11628 | | 6981.6 | | | |
| | | 0.11807 | | 6992.6 | | | |
| | | 0.12197 | | 6995.7 | | | |
| | | 0.12345 | | 7007.9 | | | |
| | | 0.12559 | | 7030.3 | | | |
| | | 0.12772 | | 7049.9 | | | |
| | | 0.12917 | | 7062.1 | | | |
| | | 0.13126 | | 7082.6 | | | |
| | | 0.13286 | | 7114.9 | | | |
| | | 0.13411 | | 7132.6 | | | |
| | | 0.13614 | | 7140.5 | | | |
| | | 0.13729 | | 7145.7 | | | |
| | | 0.13850 | | 7151.6 | | | |
| | | 0.14031 | | 7172.5 | | | |
| | | 0.14178 | | 7191.2 | | | |
| | | 0.1418 | | 719.12 | | | |
| | | 0.200 | | 719.12 | | | |
| *DEFINE_CURVE | | | | | | | |
| $# Shear_12, Temperature = 21 degrees, Strain Rate = 1.0/s | | | | | | | |
| $# lcid | sidr | sfa | sfo | offa | offo | dattyp | |
| 10000007 | | | | | | | |
| $# | | strain | | stress | | | |
| | | 0.0000 | | 0.0000 | | | |
| | | 0.00022200 | | 67.293 | | | |
| | | 0.00082948 | | 451.75 | | | |
| | | 0.0024457 | | 1112.1 | | | |
| | | 0.0040950 | | 1848.7 | | | |
| | | 0.0057325 | | 2453.7 | | | |
| | | 0.0073845 | | 2905.7 | | | |
| | | 0.0090185 | | 3252.5 | | | |
| | | 0.010656 | | 3517.6 | | | |
| | | 0.012311 | | 3725.3 | | | |
| | | 0.013997 | | 3907.7 | | | |

| | | | | | | | |
|---|---|---|---|---|---|---|---|
| | | 0.015687 | | 4063.0 | | | |
| | | 0.01740 | | 4176.6 | | | |
| | | 0.019124 | | 4262.5 | | | |
| | | 0.020866 | | 4346.1 | | | |
| | | 0.022606 | | 4442.2 | | | |
| | | 0.024351 | | 4542.2 | | | |
| | | 0.026122 | | 4622.7 | | | |
| | | 0.027903 | | 4683.4 | | | |
| | | 0.029661 | | 4744.0 | | | |
| | | 0.031488 | | 4814.9 | | | |
| | | 0.033263 | | 4893.0 | | | |
| | | 0.035072 | | 4965.5 | | | |
| | | 0.036879 | | 5024.3 | | | |
| | | 0.038644 | | 5079.4 | | | |
| | | 0.040469 | | 5141.8 | | | |
| | | 0.042287 | | 5211.3 | | | |
| | | 0.044121 | | 5282.8 | | | |
| | | 0.045912 | | 5346.0 | | | |
| | | 0.047734 | | 5393.1 | | | |
| | | 0.049546 | | 5437.4 | | | |
| | | 0.051316 | | 5502.2 | | | |
| | | 0.053167 | | 5580.8 | | | |
| | | 0.055000 | | 5642.6 | | | |
| | | 0.056681 | | 5681.1 | | | |
| | | 0.058496 | | 5722.9 | | | |
| | | 0.060287 | | 5787.8 | | | |
| | | 0.062143 | | 5864.6 | | | |
| | | 0.063965 | | 5933.3 | | | |
| | | 0.065849 | | 5987.1 | | | |
| | | 0.067634 | | 6029.2 | | | |
| | | 0.069431 | | 6067.7 | | | |
| | | 0.071295 | | 6116.7 | | | |
| | | 0.073018 | | 6177.5 | | | |
| | | 0.074900 | | 6226.3 | | | |
| | | 0.076707 | | 6253.7 | | | |
| | | 0.078556 | | 6286.8 | | | |
| | | 0.080437 | | 6342.2 | | | |
| | | 0.082349 | | 6400.4 | | | |
| | | 0.083987 | | 6444.5 | | | |
| | | 0.085889 | | 6478.1 | | | |
| | | 0.087616 | | 6506.6 | | | |
| | | 0.089419 | | 6536.5 | | | |
| | | 0.091323 | | 6576.8 | | | |
| | | 0.093113 | | 6627.6 | | | |
| | | 0.094875 | | 6677.4 | | | |
| | | 0.096695 | | 6718.5 | | | |
| | | 0.098440 | | 6758.7 | | | |
| | | 0.099888 | | 6803.4 | | | |
| | | 0.10176 | | 6840.2 | | | |

| | | | | | | | |
|---|---|---|---|---|---|---|---|
| | | 0.10323 | | 6862.6 | | | |
| | | 0.10530 | | 6880.0 | | | |
| | | 0.10704 | | 6895.1 | | | |
| | | 0.10913 | | 6905.3 | | | |
| | | 0.11281 | | 6921.8 | | | |
| | | 0.11454 | | 6952.7 | | | |
| | | 0.11628 | | 6981.6 | | | |
| | | 0.11807 | | 6992.6 | | | |
| | | 0.12197 | | 6995.7 | | | |
| | | 0.12345 | | 7007.9 | | | |
| | | 0.12559 | | 7030.3 | | | |
| | | 0.12772 | | 7049.9 | | | |
| | | 0.12917 | | 7062.1 | | | |
| | | 0.13126 | | 7082.6 | | | |
| | | 0.13286 | | 7114.9 | | | |
| | | 0.13411 | | 7132.6 | | | |
| | | 0.13614 | | 7140.5 | | | |
| | | 0.13729 | | 7145.7 | | | |
| | | 0.13850 | | 7151.6 | | | |
| | | 0.14031 | | 7172.5 | | | |
| | | 0.14178 | | 7191.2 | | | |
| | | 0.1418 | | 719.12 | | | |
| | | 0.200 | | 719.12 | | | |
| *DEFINE_TABLE_3D | | | | | | | |
| $# Off-Axis_12 | | | | | | | |
| $# tbid | sfa | offa | | | | | |
| 1010 | | | | | | | |
| $# temperature | | | table_id | | | | |
| | 21 | | 1022 | | | | |
| *DEFINE_TABLE | | | | | | | |
| $# tbid | sfa | offa | | | | | |
| 1022 | | | | | | | |
| $# strain rate | | | curve_id | | | | |
| | 0.0 | | 1110 | | | | |
| | 1.0 | | 10000010 | | | | |
| *DEFINE_CURVE | | | | | | | |
| $# Off_Axis_12, Temperature = 21 degrees, Strain Rate = 0.0/s | | | | | | | |
| $# lcid | sidr | sfa | sfo | offa | offo | dattyp | |
| 1110 | | | | | | | |
| $# | | strain | | stress | | | |
| | | 0.000 | | 0.000 | | | |
| | | 0.00055500 | | 125.76 | | | |
| | | 0.0011060 | | 962.65 | | | |
| | | 0.0032610 | | 2235.4 | | | |
| | | 0.0054600 | | 3654.4 | | | |
| | | 0.0076434 | | 4881.6 | | | |
| | | 0.0098459 | | 5814.9 | | | |
| | | 0.012025 | | 6509.7 | | | |
| | | 0.014208 | | 7036.8 | | | |

| | | | | | | | |
|---|---|---|---|---|---|---|---|
| | | 0.016415 | | 7457.3 | | | |
| | | 0.018659 | | 7817.8 | | | |
| | | 0.020917 | | 8119.5 | | | |
| | | 0.023204 | | 8348.8 | | | |
| | | 0.025499 | | 8528.0 | | | |
| | | 0.027821 | | 8699.3 | | | |
| | | 0.030141 | | 8887.5 | | | |
| | | 0.032467 | | 9078.7 | | | |
| | | 0.034829 | | 9239.8 | | | |
| | | 0.037211 | | 9368.4 | | | |
| | | 0.039548 | | 9492.7 | | | |
| | | 0.041984 | | 9632.7 | | | |
| | | 0.044350 | | 9784.1 | | | |
| | | 0.046763 | | 9926.6 | | | |
| | | 0.049173 | | 10048 | | | |
| | | 0.051525 | | 10162 | | | |
| | | 0.053959 | | 10287 | | | |
| | | 0.056383 | | 10424 | | | |
| | | 0.058828 | | 10563 | | | |
| | | 0.061216 | | 10686 | | | |
| | | 0.063645 | | 10785 | | | |
| | | 0.066061 | | 10883 | | | |
| | | 0.068422 | | 11010 | | | |
| | | 0.070889 | | 11156 | | | |
| | | 0.073334 | | 11277 | | | |
| | | 0.075574 | | 11364 | | | |
| | | 0.077995 | | 11454 | | | |
| | | 0.080382 | | 11579 | | | |
| | | 0.082858 | | 11726 | | | |
| | | 0.085287 | | 11863 | | | |
| | | 0.08779 | | 11972 | | | |
| | | 0.090179 | | 12058 | | | |
| | | 0.092575 | | 12140 | | | |
| | | 0.095061 | | 12239 | | | |
| | | 0.097357 | | 12350 | | | |
| | | 0.099866 | | 12444 | | | |
| | | 0.10228 | | 12509 | | | |
| | | 0.10474 | | 12582 | | | |
| | | 0.10725 | | 12685 | | | |
| | | 0.10980 | | 12796 | | | |
| | | 0.11198 | | 12887 | | | |
| | | 0.11452 | | 12956 | | | |
| | | 0.11682 | | 13014 | | | |
| | | 0.11923 | | 13076 | | | |
| | | 0.12176 | | 13158 | | | |
| | | 0.12415 | | 13256 | | | |
| | | 0.12650 | | 13353 | | | |
| | | 0.12893 | | 13438 | | | |
| | | 0.13125 | | 13521 | | | |

| | | | | | | | |
|---|---|---|---|---|---|---|---|
| | | 0.13318 | | 13606 | | | |
| | | 0.13569 | | 13677 | | | |
| | | 0.13763 | | 13723 | | | |
| | | 0.14040 | | 13758 | | | |
| | | 0.14272 | | 13796 | | | |
| | | 0.15041 | | 13845 | | | |
| | | 0.15272 | | 13906 | | | |
| | | 0.15504 | | 13969 | | | |
| | | 0.16459 | | 14019 | | | |
| | | 0.16746 | | 14059 | | | |
| | | 0.17029 | | 14103 | | | |
| | | 0.17223 | | 14162 | | | |
| | | 0.17714 | | 14229 | | | |
| | | 0.17881 | | 14279 | | | |
| | | 0.18171 | | 14311 | | | |
| | | 0.18708 | | 14355 | | | |
| | | 0.18904 | | 14417 | | | |
| | | 0.18990 | | 14466 | | | |
| *DEFINE_CURVE | | | | | | | |
| $# Off_Axis_12, Temperature = 21 degrees, Strain Rate = 1.0/s | | | | | | | |
| $# lcid | sidr | sfa | sfo | offa | offo | dattyp | |
| 10000010 | | | | | | | |
| $# | | strain | | stress | | | |
| | | 0.000 | | 0.000 | | | |
| | | 0.00055500 | | 125.76 | | | |
| | | 0.0011060 | | 962.65 | | | |
| | | 0.0032610 | | 2235.4 | | | |
| | | 0.0054600 | | 3654.4 | | | |
| | | 0.0076434 | | 4881.6 | | | |
| | | 0.0098459 | | 5814.9 | | | |
| | | 0.012025 | | 6509.7 | | | |
| | | 0.014208 | | 7036.8 | | | |
| | | 0.016415 | | 7457.3 | | | |
| | | 0.018659 | | 7817.8 | | | |
| | | 0.020917 | | 8119.5 | | | |
| | | 0.023204 | | 8348.8 | | | |
| | | 0.025499 | | 8528.0 | | | |
| | | 0.027821 | | 8699.3 | | | |
| | | 0.030141 | | 8887.5 | | | |
| | | 0.032467 | | 9078.7 | | | |
| | | 0.034829 | | 9239.8 | | | |
| | | 0.037211 | | 9368.4 | | | |
| | | 0.039548 | | 9492.7 | | | |
| | | 0.041984 | | 9632.7 | | | |
| | | 0.044350 | | 9784.1 | | | |
| | | 0.046763 | | 9926.6 | | | |
| | | 0.049173 | | 10048 | | | |
| | | 0.051525 | | 10162 | | | |
| | | 0.053959 | | 10287 | | | |

| | | | | | | | |
|---|---|---|---|---|---|---|---|
| | | 0.056383 | | 10424 | | | |
| | | 0.058828 | | 10563 | | | |
| | | 0.061216 | | 10686 | | | |
| | | 0.063645 | | 10785 | | | |
| | | 0.066061 | | 10883 | | | |
| | | 0.068422 | | 11010 | | | |
| | | 0.070889 | | 11156 | | | |
| | | 0.073334 | | 11277 | | | |
| | | 0.075574 | | 11364 | | | |
| | | 0.077995 | | 11454 | | | |
| | | 0.080382 | | 11579 | | | |
| | | 0.082858 | | 11726 | | | |
| | | 0.085287 | | 11863 | | | |
| | | 0.08779 | | 11972 | | | |
| | | 0.090179 | | 12058 | | | |
| | | 0.092575 | | 12140 | | | |
| | | 0.095061 | | 12239 | | | |
| | | 0.097357 | | 12350 | | | |
| | | 0.099866 | | 12444 | | | |
| | | 0.10228 | | 12509 | | | |
| | | 0.10474 | | 12582 | | | |
| | | 0.10725 | | 12685 | | | |
| | | 0.10980 | | 12796 | | | |
| | | 0.11198 | | 12887 | | | |
| | | 0.11452 | | 12956 | | | |
| | | 0.11682 | | 13014 | | | |
| | | 0.11923 | | 13076 | | | |
| | | 0.12176 | | 13158 | | | |
| | | 0.12415 | | 13256 | | | |
| | | 0.12650 | | 13353 | | | |
| | | 0.12893 | | 13438 | | | |
| | | 0.13125 | | 13521 | | | |
| | | 0.13318 | | 13606 | | | |
| | | 0.13569 | | 13677 | | | |
| | | 0.13763 | | 13723 | | | |
| | | 0.14040 | | 13758 | | | |
| | | 0.14272 | | 13796 | | | |
| | | 0.15041 | | 13845 | | | |
| | | 0.15272 | | 13906 | | | |
| | | 0.15504 | | 13969 | | | |
| | | 0.16459 | | 14019 | | | |
| | | 0.16746 | | 14059 | | | |
| | | 0.17029 | | 14103 | | | |
| | | 0.17223 | | 14162 | | | |
| | | 0.17714 | | 14229 | | | |
| | | 0.17881 | | 14279 | | | |
| | | 0.18171 | | 14311 | | | |
| | | 0.18708 | | 14355 | | | |
| | | 0.18904 | | 14417 | | | |

| | | | | | | | |
|---|---|---|---|---|---|---|---|
| | | 0.18990 | | 14466 | | | |
| *DEFINE_CURVE | | | | | | | |
| $# Curve ID vs. Yield strain | | | | | | | |
| $# lcid | sidr | Sfa | sfo | offa | offo | dattyp | |
| 100 | | | | | | | |
| $# | curve_id | | yield_strain | | | | |
| | 1110 | | 0.0075 | | | | |
| | 1111 | | 0.01 | | | | |
| | 2222 | | 0.00575 | | | | |
| | 4444 | | 0.010875 | | | | |
| | 5555 | | 0.00575 | | | | |
| | 7777 | | 0.0075 | | | | |
| | 10000001 | | 0.01 | | | | |
| | 10000002 | | 0.00575 | | | | |
| | 10000004 | | 0.10875 | | | | |
| | 10000005 | | 0.00575 | | | | |
| | 10000007 | | 0.0075 | | | | |
| | 10000010 | | 0.0075 | | | | |
| *END | | | | | | | |

**B-3. File: 14_DAMAGE.k**

| | | | | | | | |
|---|---|---|---|---|---|---|---|
| *KEYWORD | | | | | | | |
| $# DAMAGE VS CURVE ID | | | | | | | |
| *DEFINE_CURVE_TITLE | | | | | | | |
| Damage Parameter vs. Curve ID | | | | | | | |
| $# lcid | sidr | sfa | Sfo | Offa | offo | dattyp | |
| 50 | | | | | | | |
| $# damage parameter | | curve_id | | | | | |
| $# Damage in T1 due to loading in T1 | | | | | | | |
| | 1 | | 100001 | | | | |
| $# Damage in T2 due to loading in T2 | | | | | | | |
| | 2 | | 100002 | | | | |
| $# Damage in S12 due to loading in S12 | | | | | | | |
| | 7 | | 100007 | | | | |
| *DEFINE_CURVE_TITLE | | | | | | | |
| Damage in Tension 1, due to loading in Tension 1 | | | | | | | |
| $# lcid | sidr | sfa | Sfo | Offa | offo | dattyp | |
| 100001 | | | | | | | |
| $# | strain | | stress | | | | |
| | 0.0 | | 0.0 | | | | |
| | 0.014155 | | 0.0 | | | | |
| | 0.015 | | 0.9 | | | | |
| | 0.016 | | 0.9 | | | | |
| *DEFINE_CURVE_TITLE | | | | | | | |
| Damage in Tension 2, due to loading in Tension 2 | | | | | | | |
| $# lcid | sidr | sfa | Sfo | Offa | offo | dattyp | |
| 100002 | | | | | | | |
| $# | strain | | stress | | | | |

| | | | | | | | |
|---|---|---|---|---|---|---|---|
| | 0.0 | | 0.0 | | | | |
| | 0.024951 | | 0.0 | | | | |
| | 0.025 | | 0.9 | | | | |
| | 0.05 | | 0.9 | | | | |
| *DEFINE_CURVE_TITLE | | | | | | | |
| Damage in Shear 12, due to loading in Shear 12 | | | | | | | |
| $# lcid | sidr | sfa | Sfo | Offa | offo | dattyp | |
| 100007 | | | | | | | |
| $# | strain | | stress | | | | |
| | 0.0 | | 0.0 | | | | |
| | 0.14178 | | 0.0 | | | | |
| | 0.148 | | 0.9 | | | | |
| | 0.20 | | 0.9 | | | | |
| *END | | | | | | | |

## B-4. File: 15_FAILURE_SURFACE.k

| | | | | | | | |
|---|---|---|---|---|---|---|---|
| *KEYWORD | | | | | | | |
| *SET_PART_LIST_TITLE | | | | | | | |
| Composite Parts | | | | | | | |
| $# sid | da1 | da2 | da3 | da4 | solver | | |
| 124 | | | | | | | |
| $# pid1 | pid2 | pid3 | pid4 | pid5 | pid6 | pid7 | pid8 |
| 4 | | | | | | | |
| *DEFINE_ELEMENT_EROSION_SHELL | | | | | | | |
| $# sid | stpy | numfip | Nipf | | | | |
| 124 | 4 | 1 | 1 | | | | |
| *DEFINE_TABLE | | | | | | | |
| $# X-Stress vs Curve ID | | | | | | | |
| $# tbid | sfa | offa | | | | | |
| 9013 | | | | | | | |
| $# | value | curve_id | | | | | |
| | 0 | 52 | | | | | |
| | 366000 | 53 | | | | | |
| *DEFINE_CURVE | | | | | | | |
| $# Theta vs Equivalent Failure Strain for T1/C1 = 0 | | | | | | | |
| $# lcid | sidr | sfa | Sfo | offa | offo | dattyp | |
| 52 | | | | | | | |
| $# | a1 | | o1 | | | | |
| | -180 | | 0.6 | | | | |
| | 180 | | 0.6 | | | | |
| *DEFINE_CURVE | | | | | | | |
| $# Theta vs Equivalent Failure Strain for T1 = 366000 | | | | | | | |
| $# lcid | sidr | sfa | Sfo | offa | offo | dattyp | |
| 53 | | | | | | | |
| $# | a1 | | o1 | | | | |
| | -180 | | 0.6 | | | | |
| | 180 | | 0.6 | | | | |
| *END | | | | | | | |

## APPENDIX C. LESSONS LEARNED

During the development of the *MAT_213 material model to represent hybrid carbon-Kevlar® plain-weave fabric, parametric studies were performed as a means of investigating specific issues related to the material model. Please view these "lessons learned" as steps taken by a beginning user of *MAT_213. These issues are described in this section of the report in hopes that they might help future *MAT_213 users. Also note that the sequence of issues is somewhat random.

### C-1. An Issue Involving Material Directions

The motivation behind this study was the potential conflict in defining material directions using *PART_COMPOSITE and *MAT_213. The card *PART_COMPOSITE provides a simple way to implement a laminated composite for shell elements and it allows input of ply thickness, ply material, and ply orientation for each layer in the composite. The ply orientation is defined by the variable bi, which the LS-DYNA® User's Manual describes as the "material angle of integration point i." In contrast, *MAT_213 specifies input of a parameter identified as "AOPT," which is defined in the LS-DYNA® User's Manual as "material axis option." For the simulations conducted in this study, the value of AOPT was set to 2.0, which indicates that the material is globally orthotropic with material axes determined by the cross product of vectors, **a** and **d**. So, the essential issue is: Should the **a** and **d** vectors be defined in the *MAT_213 card when using *PART_COMPOSITE, i. e., redundant material direction cards?

To answer this question, three simulations were executed based on the tension coupon model, which is shown in Figure C-1. The model is 1 in. x 1 in. and the left edge nodes are fixed in place using a Single Point Constraint (SPC). The right edge nodes are assigned a *BOUNDARY_PRESCRIBED_MOTION card such that at time = 0.0 s the x-direction displacement is 0.0 in. By the end time of the simulation, 0.1 s, the maximum x-displacement is 0.02 in., or 2% strain. The model contains 289 shell elements (fully integrated, type 16), 329 nodes, and 1 part definition.

Three simulations were performed:

- Option 1 was the baseline tension coupon model that had *PART_COMPOSITE input, as well as material direction vectors in *MAT_213 enabled;
- Option 2 had the material direction vectors eliminated in *MAT_213, as well as AOPT on *MAT_ 213 cards; however, *PART_COMPOSITE was present;
- Option 3 had the ply angle directions eliminated that are usually specified on the *PART_COMPOSITE card; however, the AOPT parameter and the material direction vectors were present in *MAT_213.

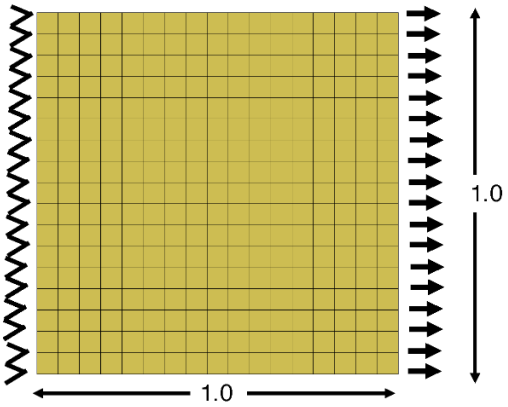


Figure C-1. Tension coupon model.

All three models were executed using the developmental version of LS-DYNA® running MPP on 8 processors of a Linux-based workstation computer and required 1 hour and 45 minutes to achieve normal termination. The results are shown in Figure C-2, as a plot of average SPC force in the x-direction of the left edge nodes versus time. Obviously from the plot, it is evident that Option 1 and Option 3 gave the exact same response. The Option 2 simulation gave quite different results. The maximum loading for Option 2 was 25-lb. in comparison to the maximum load of 550 lb for Options 1 and 3. As a reminder, Option 2 used the *PART_COMPOSITE card to define material directions, as the AOPT parameter and the material direction vectors in*MAT_213 had been disabled.

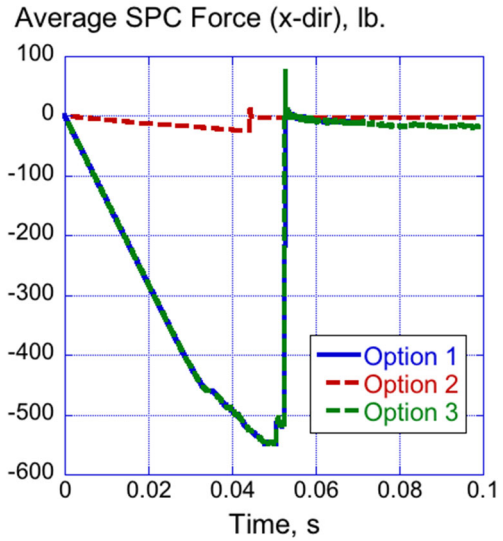


Figure C-2. Average SPC force (x-direction) versus time.

Findings of this study are listed, as follows:

1. Results indicate that the AOPT parameter and material direction vectors within *MAT_213 must be enabled. In this case, the **a** x **d** direction pointed in the normal, z, direction.

2. The *PART_COMPOSITE simulation in which the AOPT and material direction vectors were disabled in *MAT_213 behaved poorly. This finding confirms previous indications that *PART_COMPOSITE is not fully enabled for *MAT_213.
3. These findings lead to another question regarding the appropriate method to use for implementing a multi-ply laminate with *MAT_213. Is the previous method of using *INTEGRATION_SHELL warranted? This issue is under further investigation.

**C-2. An Issue Involving Command Cards**

An initial attempt to run *MAT_213 was made using the tension coupon model, shown in Figure C-1, with assigned properties for IM7/8552. Initially, the model would not execute and there were very few, if any, clues as to why. The model was sent to ASU and their team was able to get the model to execute by commenting out the following eleven LS-DYNA® command cards:

1. *CONTROL_BULK_VISCOSITY,
2. *CONTROL_CONTACT,
3. *CONTROL_COUPLING,
4. *CONTROL_CPU,
5. *CONTROL_DYNAMIC_RELAXATION,
6. *CONTROL_ENERGY,
7. *CONTROL_HOURGLASS,
8. *CONTROL_OUTPUT
9. *CONTROL_SHELL,
10. *DAMPING_PART_STIFFNESS,
11. *HOURGLASS

The goal of this study is to examine the influence of command cards on the response of a tensile coupon with *MAT_213 material properties. Note that all simulations were performed in which *PART_COMPOSITE was enabled. This card defines a four-layer composite in which each layer is assigned a material identification of 1 (*MAT_213), a thickness of 0.011659 in., and an orientation of 0°. The *MAT_213 material properties were representative of IM7/8552, which is a carbon/epoxy prepreg tape manufactured by Hexcel. The material model contains the deformation and damage portions of *MAT_213 but does not include failure. The essential question (Which of the command cards is causing the problem?) was addressed using three different approaches. First, the model generated by ASU was executed as a baseline simulation. This model had the command cards, listed previously, commented out. This simulation is the starting point of this exercise and the average SPC force (x-direction) versus time plot is shown in Figure C-3. Note that the left edge nodes of the model (see Figure C-1) were constrained using SPC's. These forces were output and averaged to generate the plot shown in Figure C-3. Note that the model ended at 0.0696 s, with no indication of why it stopped.

The second step was to uncomment each command card, individually, one at a time, and run the simulations to evaluate the responses of the tension coupon model. Almost all the simulations provided similar average SPC force responses to the response shown in Figure C-3. In addition, all the models failed just after 0.06 seconds, with no explanation. The one

model that gave different results was the *DAMPING_PART_STIFFNESS simulation. In this case, the model executed to normal termination (0.1 s); however, the predicted average SPC force in the x-direction had a lower magnitude response than the other models.

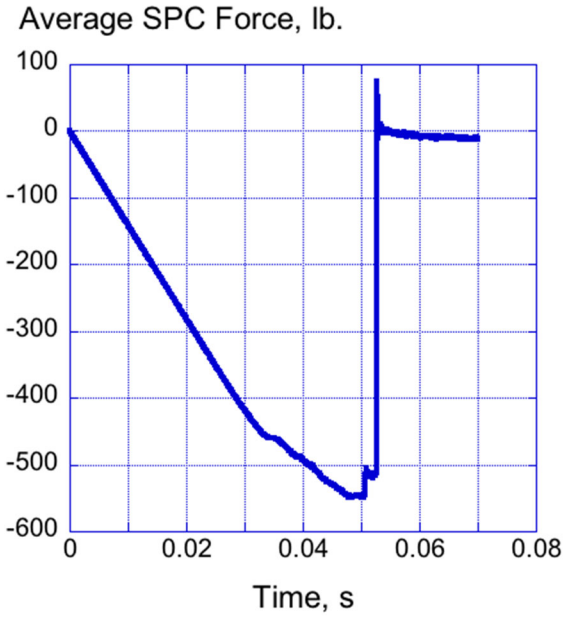


Figure C-3. Average SPC force (x-direction) versus time for the baseline model.

The third approach involved conducting 55 separate simulations, in which two command cards were uncommented at a time. However, before performing these simulations, one change was made that involved replacing the *CONTROL_CONTACT card with the *CONTROL_ACCURACY card. This change was made because no contact is present in the tensile coupon model. The updated command cards used during this third phase of the study are listed in Figure C-4, along with details of the parameters used. Finally, Figure C-5 shows the comparison of all models that were executed in the study. Note that the results of the study are categorized by Round.

Round 2 saw the first failed simulation. A plot of average SPC force (x-direction) versus time is shown in Figure C-6 for all models executed under Round 2, including one outlier model, Case_2_10 (*CONTROL_ACCURACY and *DAMPING_PART_STIFFNESS). The simulation that failed was Case_2_9 (*CONTROL_ACCURACY and *CONTROL_SHELL). For Case_2_9, the model failed almost immediately after starting, with no indication or explanation as to why it failed. The average SPC force for Case_2_9 is shown in Figure C-7. According to the d3hsp file, all of the right column of elements failed at a time step of 1.35E-07. Since the right column of elements contains the nodes through which load is applied, after removal, there is no further possibility of loading.

1. *CONTROL_BULK_VISCOSITY
2. *CONTROL_ACCURACY
3. *CONTROL_COUPLING
4. *CONTROL_CPU
5. *CONTROL_DYNAMIC_RELAXATION
6. *CONTROL_ENERGY
7. *CONTROL_HOURGLASS
8. *CONTROL_OUTPUT
9. *CONTROL_SHELL
10. *DAMPING_PART_ STIFFNESS
11. *HOURGLASS

```
*CONTROL_BULK_VISCOSITY
       1.5     0.06
*CONTROL_ACCURACY
         1       4       0       0
*CONTROL_COUPLING
         1       1       1       0                       1
*CONTROL_CPU
         0
*CONTROL_DYNAMIC_RELAXATION
       250   0.001   0.995   1e+30     0.9          0.04       0
*CONTROL_ENERGY
         1       2                       1       1
*CONTROL_HOURGLASS
         1     0.1
*CONTROL_OUTPUT
         0       3       0       0       0               0
*CONTROL_SHELL
  20.0000       2      -1       0       2       2       1
  1.00000       0       1       1
         0       0
*DAMPING_PART_STIFFNESS
         1    0.05
*HOURGLASS
        50       8
```

Figure C-4. Updated list of command cards (left) and detailed input for the cards (right).

| First Round | Second Round | Third Round | Fourth Round | Fifth Round | Sixth Round |
|---|---|---|---|---|---|
| 1&2 | 2&3 | 3&4 | 4&5 | 5&6 | 6&7 |
| 1&3 | 2&4 | 3&5 | 4&6 | 5&7 | 6&8 |
| 1&4 | 2&5 | 3&6 | 4&7 | 5&8 | 6&9 |
| 1&5 | 2&6 | 3&7 | 4&8 | 5&9 | 6&10 |
| 1&6 | 2&7 | 3&8 | 4&9 | 5&10 | 6&11 |
| 1&7 | 2&8 | 3&9 | 4&10 | 5&11 | |
| 1&8 | 2&9 | 3&10 | 4&11 | | |
| 1&9 | 2&10 | 3&11 | | | |
| 1&10 | 2&11 | | | | |
| 1&11 | | | | | |

| Seventh Round | Eighth Round | Nineth Round | Tenth Round |
|---|---|---|---|
| 7&8 | 8&9 | 9&10 | 10&11 |
| 7&9 | 8&10 | 9&11 | |
| 7&10 | 8&11 | | |
| 7&11 | | | |

Figure C-5. A listing of the models that were executed in which two command cards were enabled. The numbers shown under each heading refer to the list in Figure C-4 (left).

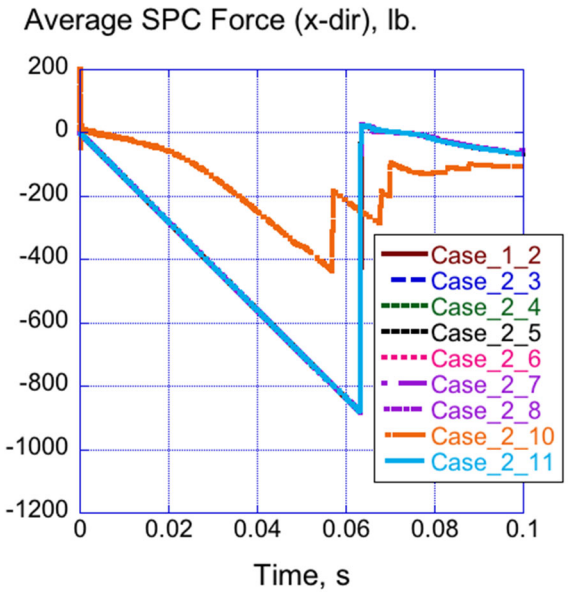


Figure C-6. Average SPC force (x-direction) versus time of all Round 2 simulations, except for Case_2_9.

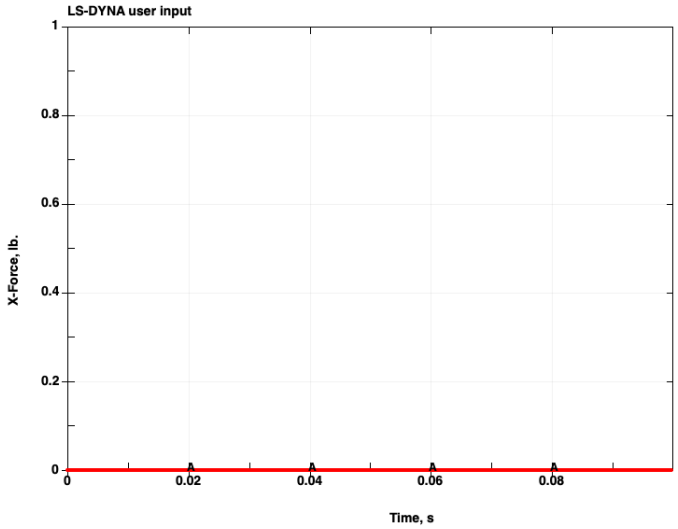


Figure C-7. Average SPC force (x-direction) versus time for Case_2_9.

General findings are listed for the third approach, as follows:

(1) For all simulations, every model with *CONTROL_SHELL enabled failed.

(2) The simulation representing Case 10_11 (*DAMPING_PART_STIFFNESS and *HOURGLASS) failed.

(3) For all simulations, every model with *CONTROL_ACCURACY enabled was an outlier.

(4) For 10 of 11 Rounds, models with *DAMPING_PART_STIFFNESS enabled were outliers. The exception was Case_10_11, which failed.

Based on the results of this investigation, recommendations for bug fixes are made to Ansys:
1. MAT 213 should be enabled as a material card in *PART_COMPOSITE.
2. Model failure is triggered by activation of the laminated shell theory (*CONTROL_SHELL, Card 2, Parameter 3, LAMSHT). LAMSHT is set to 1, which is not the default setting. If LAMSHT is set to 0 (default), there is no erosion in the first 5000 cycles. This finding may constitute a bug and needs to be addressed.

**C-3. Influence of Boundary Conditions**

In March 2021, the influence of boundary constraints on the biaxial tensile response of a 1-in. x 1-in. coupon were evaluated. A picture of the model is shown in Figure C-1. Initially, the left edge nodes were fully constrained, meaning that the nodes were prevented from displacement in the x-, y-, and z-directions, as well as rotations about the x-, y-, and z-axes. The results from the fully constrained simulations were compared with a mid-level reduced constraint and a highly unconstrained case. For the midlevel constraint condition, x-, y-, and z-displacements were fixed, while rotations about the x-, y-, and z-axes were free. For the highly unconstrained condition, only the x-displacement was fixed, and all other constraints were free. Each of these three modeling conditions was evaluated for different flow rule coefficient conditions within *MAT_213. The simulation matrix is shown in Table C-1. Note that each simulation required between 9 and 10 hours of CPU, running the developmental MPP version of LS-DYNA® using 8 processors on a Linux workstation computer. As a final note, a four ply ±45° laminate was simulated to generate shear properties.

Table C-1. Matrix of Simulations Performed.

| Flow Rule Parameter | Fully Constrained | Midlevel Constraint | Highly Unconstrained |
|---|---|---|---|
| Only H11 enabled | X | X | X |
| Only H22 enabled | X | X | X |
| Only H44 enabled | X | X | X |
| Combo (H22 and H44 enabled) | X | X | X |

Results of these simulations are shown in Figures C-8 and C-9. Please note that all models with H11 (only) failed at the first time-step and did not provide any useful information. Also, the models with H22 (only) gave consistent, but anomalous results. For every simulation, the models with H44 (only) ran to normal termination. In several instances, simulations of the Combo model (both H22 and H44 enabled) also failed before achieving normal termination. In general, the H44(only) and the Combo models demonstrated similar results and matched the initial test response well. The results, shown in Figure C-9, demonstrate that only minor variations in response are observed for different constraint conditions.

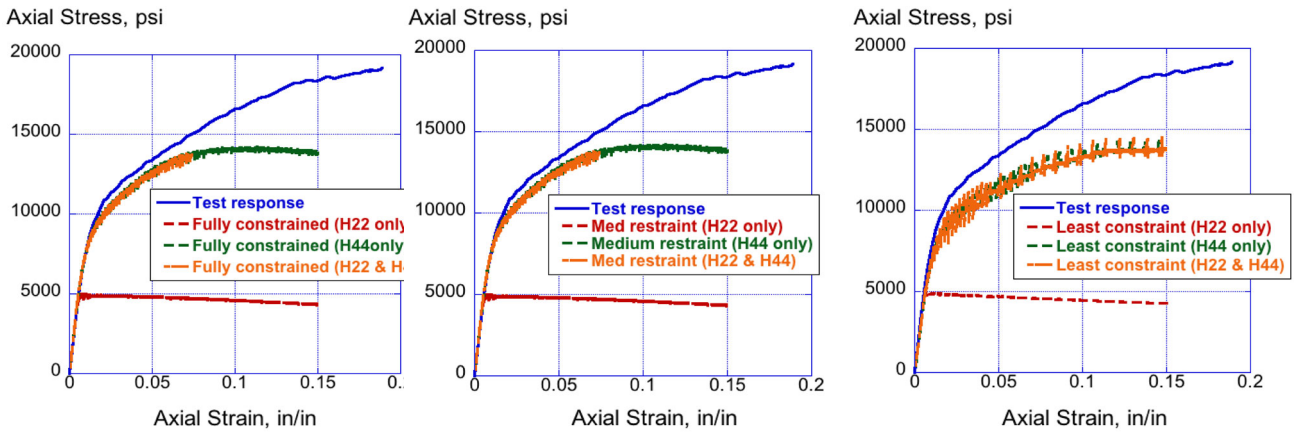


(a) Fully constrained. (b) Medium constraint. (c) Least constraint

Figure C-8. Results of boundary effects simulation study.

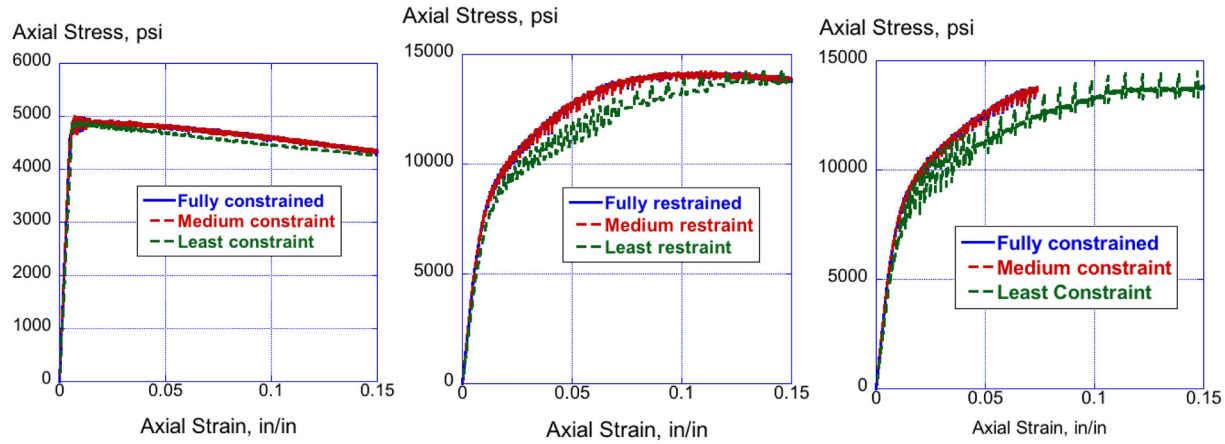


(a) Model results H22 (only). (b) Model results H44 (only) (c) Model results Combo

Figure C-9. Simulation results showing the influence of model constraint.

## C-4. Utilizing *INTEGRATION_SHELL to Simulate a Composite Laminate

As noted previously, the material model, *MAT_213, and the capability used in LS-DYNA® to input composite laminates, *PART_COMPOSITE, do not appear to be fully compatible at this time. If true, this "bug" severely limits the application of the material model for shell element simulations. Until Ansys-LST can "fix" this issue, the only option for simulating composite laminates is *INGEGRATION_SHELL. Consequently, a model of the biaxial tension test of a four-ply [+45°/-45°/-45°/+45°] laminate was simulated using *INTEGRATION_SHELL with properties for plain-weave carbon-Kevlar® fabric. The results, including a comparison with test data, are shown in Figure C-10. Note that the model required 6 hours and 53 minutes of CPU running the developmental version of LS-DYNA® (MPP) on 8 processors of a Linux workstation computer. The model stopped executing at 0.1575 s and no explanation for the stoppage was given. In general, the model matches the test response very well during the initial portion of the response.

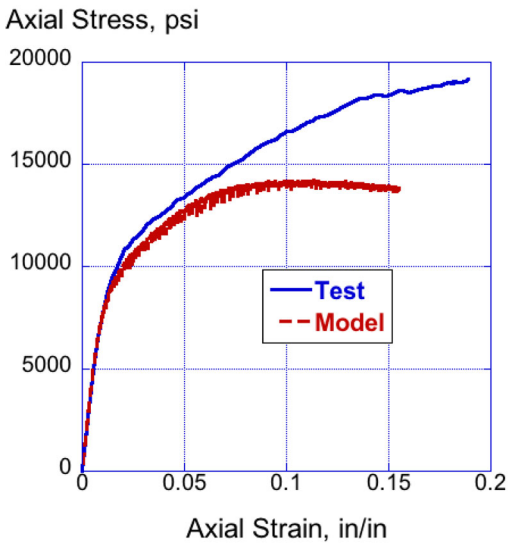


Figure C-10. Comparison of experimental and predicted biaxial stress versus biaxial strain.

**C-5. Comparison of Run Times Between *MAT_58 and *MAT_213**

A study was conducted to answer the question: how do the run times compare between *MAT_213 and *MAT_58? Consequently, six simulations were performed using the tension coupon model, shown in Figure C-1:

- Unidirectional laminate $[0°]_4$ assigned *MAT_213
- Unidirectional laminate $[0°]_4$ assigned *MAT_58
- Transverse laminate [90°]4 assigned *MAT_213
- Transverse laminate [90°]4 assigned *MAT_58
- Biaxial laminate [+45°/-45°/-45°/+45°] assigned *MAT_213
- Biaxial laminate [+45°/-45°/-45°/+45°] assigned *MAT_58

Each simulation was executed for a termination time of 0.5-seconds and run on a Linux-based machine with 8 processors using the MPP developmental version of LS-DYNA®. Each model had the same number of *CONTROL cards and the same *DATABASE output cards. The *MAT_58 material model was copied from an earlier simulation, which is documented in Reference 13.

The comparisons of *MAT_58 model predictions with material characterization data are shown in Figure C-11. Though the test-analysis agreement is not perfect, the run time comparisons, shown in Table C-2, almost rule out the use of *MAT_213. Please note that the *MAT_213 development team is currently exploring methods to improve runtimes.

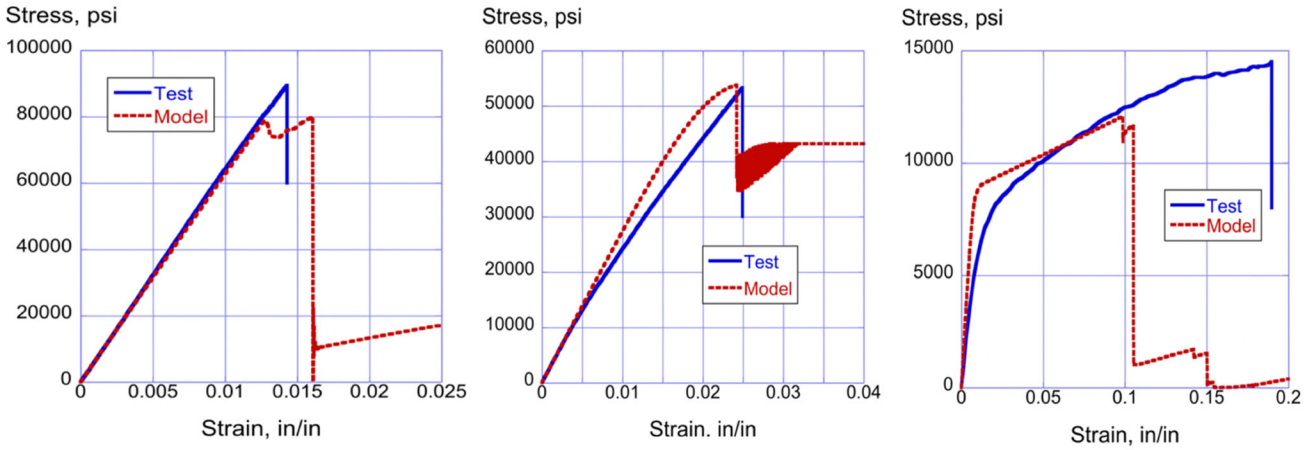


(a) Longitudinal tension. (b) Transverse tension. (c) Shear.

Figure C-11. Material characterization test data compared with *MAT_58 model predictions.

Table C-2. Run Time Comparisons Between *MAT_58 and *MAT_213.

| Laminate | *MAT_213 | *MAT_58 |
|---|---|---|
| Unidirectional $[0°]_4$ | 36 hours & 56 min | 2 hours & 35 min |
| Transverse $[90°]_4$ | 37 hours & 12 min | 2 hours & 53 min |
| Biaxial $[\pm 45°]_2$ | 31 hours & 14 min | 2 hours & 53 min |

### C-6. Variation in H44

A parametric study was executed by varying H44 to obtain better correlation with the shear response. Note that for shell elements, H44 is the flow rule coefficient most associated with shear behavior. H44 was varied from 3.875 (value provided by ASU as optimal) to 11.8. Intermediate values are: 5.8, 7.8, 9.8. Results of this parametric study are depicted in Figure C-12. Obviously, changes in H44 make little or no difference in the longitudinal tension response, shown in Figure C-12(a), or the transverse tensile response, shown in Figure C-12(b). However, changes to the biaxial tension response, shown in Figure C-12(c), are noted based on varying H44. The curve with the highest value of H44 (11.8) exhibits the highest stress, prior to decreasing load and failure.

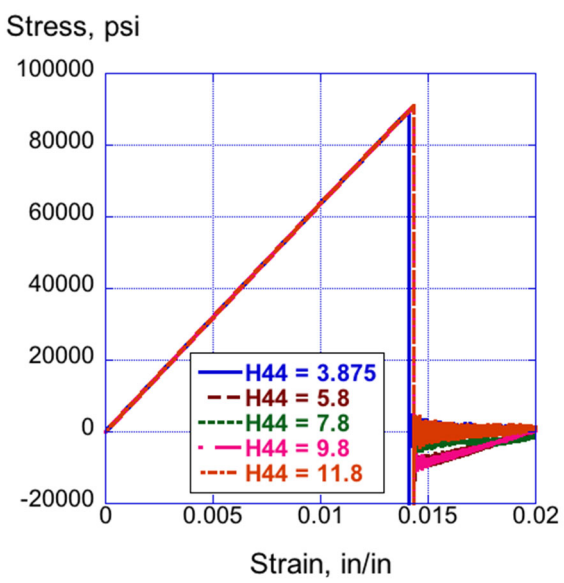


(a) Longitudinal tension.

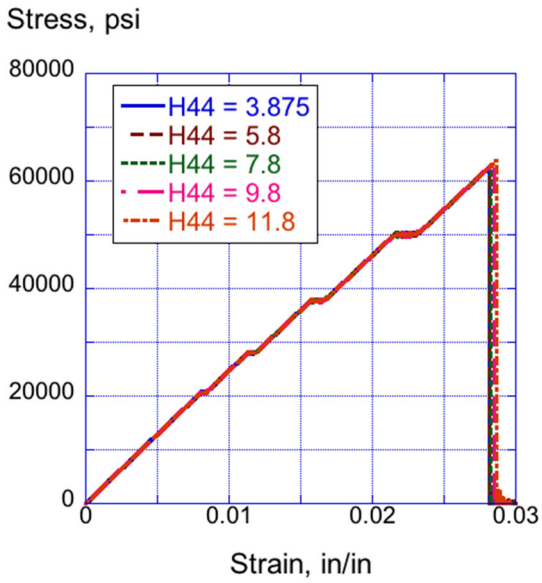


(b) Transverse tension.

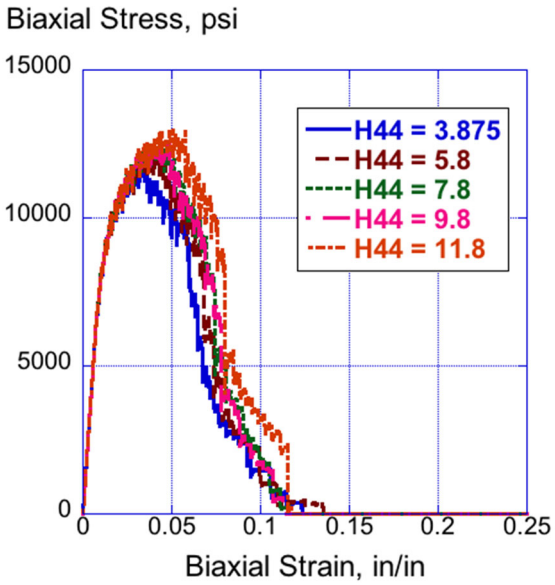


(c) Biaxial tension.

Figure C-12. Results of parametric study on varying H44.

A follow-on study was conducted in which H44 was increased to 25 and 50 for comparison. The predicted results are shown in Figure C-13 along with the test data. Only minor differences were noted in the shear responses for the two extreme cases (H44 = 25 and 50) and the trends were moving in the wrong direction, i.e., higher loads instead of lower.

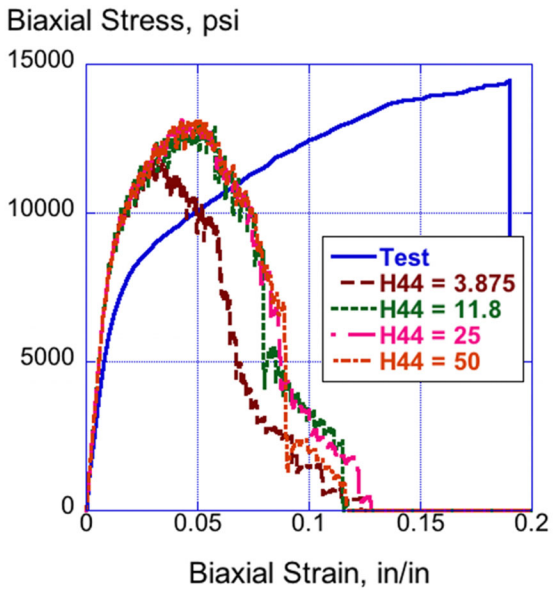


Figure C-13. biaxial stress-strain responses for two cases of high H44.

**C-7. Influence of Varying the Parameter LAMSHT**

In LS-DYNA®, LAMSHT is a flag for turning on laminated shell theory and it is located on the *CONTROL_SHELL card. According to the LS-DYNA® User's Guide, laminated shell theory is available for all thin and thick shell materials. It is activated when LAMSHT = 1, 3, 4, or 5 and by using *PART_COMPOSITE or *INTEGRATION_SHELL to define the integration rule. The various options are listed below:

EQ.0: do not update shear corrections,
EQ.1: activate laminated shell theory,
EQ.3: activate laminated thin shells,
EQ.4: activate laminated shell theory for thick shells,
EQ.5: activate laminated shell theory for thin and thick shells.

A parametric study was executed using the tension coupon model, shown in Figure C-1, in which an eight-ply quasi-isotropic laminate was defined using *PART_COMPOSITE. The model was executed for LAMSHT = 1, 3, and 5. All simulations were executed on a Linux workstation computer, running MPP with 8 processors, using the developmental version of LS-DYNA®. Table C-3 shows a comparison of run times for the three models. The models with LAMSHT = 3 and 5 have similar run times, while the model with LAMSHT = 1 ran to normal termination in a third of the time.

A plot of x-direction stress versus strain for all three LAMSHT cases is depicted in Figure C-14. All of the right-side elements in the LAMSHT=1 simulation failed upon model initiation. Thus, no load response was recorded. Both LAMSHT = 3 and LAMSHT = 5 provided

identical response curves. The major finding of this study is that LAMSHT = 1 should be avoided.

Table C-3. Results of Parametric Study on LAMSHT.

| LAMSHT | Normal Termination | Run Time |
|---|---|---|
| 1 | Yes | 12-min, 53-sec |
| 3 | Yes | 29-hours, 46-min |
| 5 | Yes | 30-hours, 12-min |

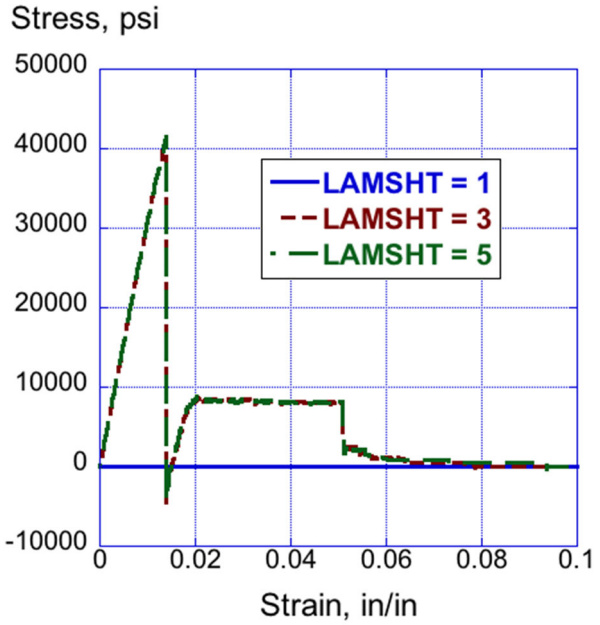


Figure C-14. Plot of x-direction stress versus strain for three LAMSHT cases.

**C-8. Influence of Varying the Damping Coefficient**

The material characterization models for longitudinal tension, transverse tension, and biaxial tension were executed for different values of the damping coefficient, which is input on the *DAMPING_PART_STIFFNESS card. Three values were selected: 0.005, 0.05, and 0.1. The damping coefficient of 0.05 has been used as the baseline value for all previous *MAT_213 simulations. It is also useful to note that one simulation was attempted with a damping coefficient of 0.0, but it failed to execute. The stress-strain results for the longitudinal tension model are shown in Figure C-15. For longitudinal tension, models that were assigned damping of 0.005 and 0.05 gave nearly identical responses and failed at the same maximum stress and strain values. The model with a damping coefficient of 0.1 had the same slope but failed prematurely. The stress-strain results for the transverse tension model are shown in Figures C-16(a) and (b).

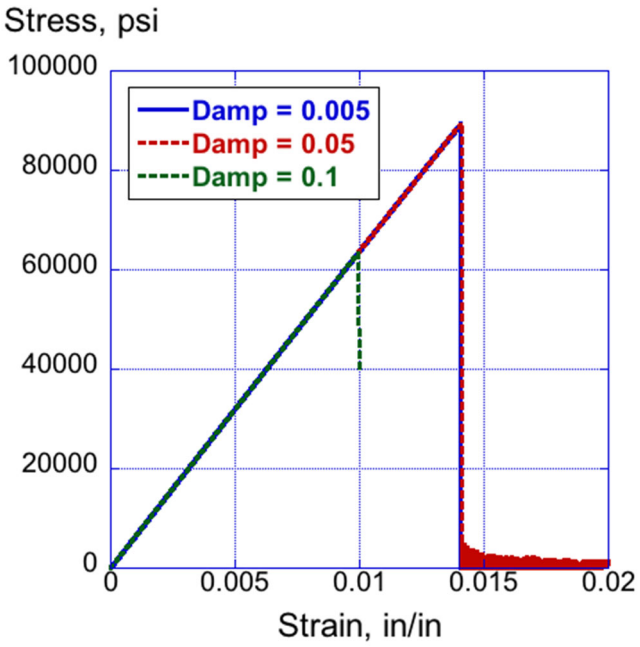


Figure C-15. Stress-strain responses for longitudinal tension with varying damping.

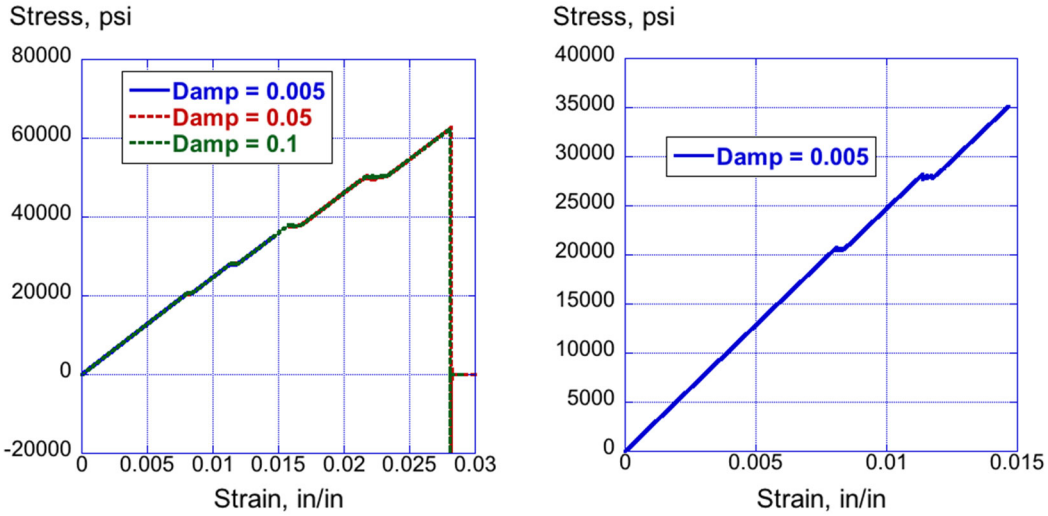


Figure C-16. Stress-strain responses for transverse tension models with varying damping.

Little or no differences are seen in the transverse tension responses for models executed with a damping coefficient of 0.05 and 0.1. These two curves exhibit the same response shape, the same maximum load, and the same failure strain. However, as shown in Figure C-16(b), the model with a damping coefficient of 0.005 did not fail and did not achieve the same maximum load. Finally, the results for the biaxial loading case are shown in Figure C-17. Little or no differences are seen in the biaxial tension responses due to changes in damping coefficient. As an aside, the run times for the biaxial tension models with varying damping coefficients are shown in Table C-4.

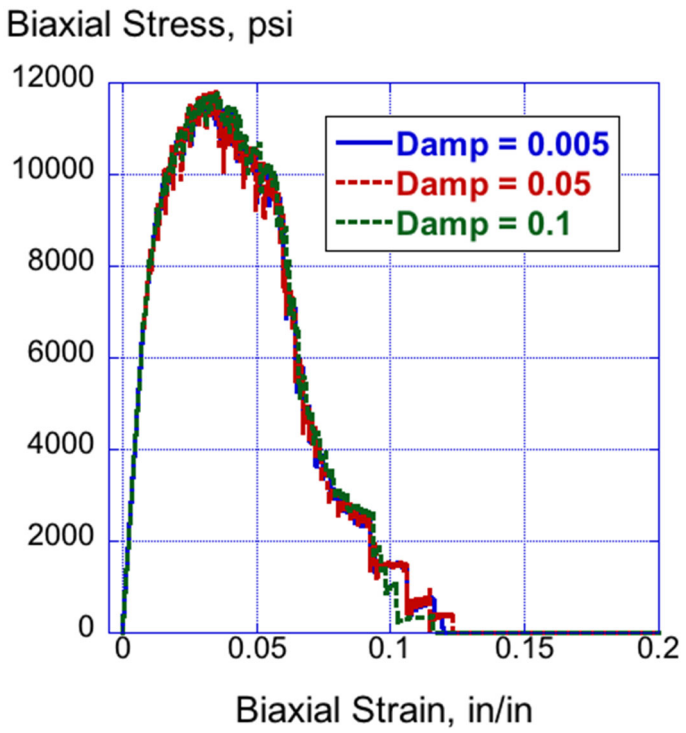


Figure 17. Stress-strain responses for biaxial tension models with varying damping.

Table C-4. Run Times for Biaxial Tension Models.

| Damp Coeff | Normal Termination | Run Time |
|---|---|---|
| 0.005 | Yes | 39 hours 49 min |
| 0.05 | Yes | 31 hours 16 min |
| 0.1 | Yes | 38 hours 49 min |

In conclusion, variations in damping coefficient yielded inconsistent results. The longitudinal tension model with damping coefficient of 0.1 failed prematurely. For transverse tension, the model with a damping coefficient of 0.005 did not fail and did not achieve maximum load. For biaxial tension, all responses were nearly identical with no differences associated with damping coefficient. Based on these results, it is recommended to stick with the baseline damping coefficient of 0.05.

**C-9. Variation in Parameter PTOL**

In many prior simulations using *MAT_213, the value of parameter PTOL was set to 1.0. The default value is 1.0E-6. Consequently, the biaxial tension model was reexecuted with

a value of PTOL set to 1.0E-6. Reducing PTOL from 1.0 to 1.0E-6 reduced the maximum load from 11,500 psi to 9,500 psi, as shown in Figure C-18. The response is now in much better agreement with the test. However, it is still uncertain as to what is causing the load drop-off at a strain of 0.0275 in/in.

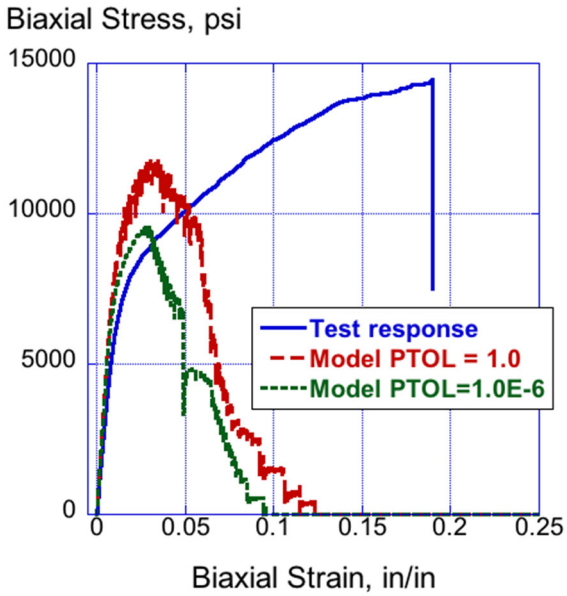


Figure C-18. Biaxial tension test data versus two model results (PTOL = 1.0 and 1.0E-6).

**C-10. Variation in Parameter TSSFAC**

Parameter TSSFAC is found on the *CONTROL_TIMESTEP card and, according to the LS-DYNA® User's Manual, is used as a scale factor for computing the time step. The default value is 0.90. For this parameter study, three discrete values of TSSFAC were evaluated using the tension coupon model, shown in Figure C-1. All simulations were executed on a Linux workstation computer, running MPP with 8 processors, using the developmental version of LS-DYNA®. Table C-5 shows a comparison of run time for the three simulations. A dramatic reduction in run time is shown as TSSFAC is increased from 0.1 to 0.9. Next, the longitudinal tension stress-strain response is shown in Figure C-19.

All curves match the slope of the test response well; however, differences are seen in the maximum stress and failure strain based on TSSFAC, as shown in the inset of Figure C-19. The best match to test data is the model with TSSFAC = 0.1. These results suggest that the best approach might be to use TSSFAC = 0.9 initially during model interrogation and to run the case of TSSFAC = 0.1 as a final simulation.

Table C-5. Comparison of Run Times for Varying TSSFAC.

| TSSFAC | Normal Termination | Run Time |
|---|---|---|
| 0.1 | Yes | 36-hours 56-min |
| 0.5 | Yes | 6-hours 25-min |
| 0.9 | Yes | 4-hours 8-min |

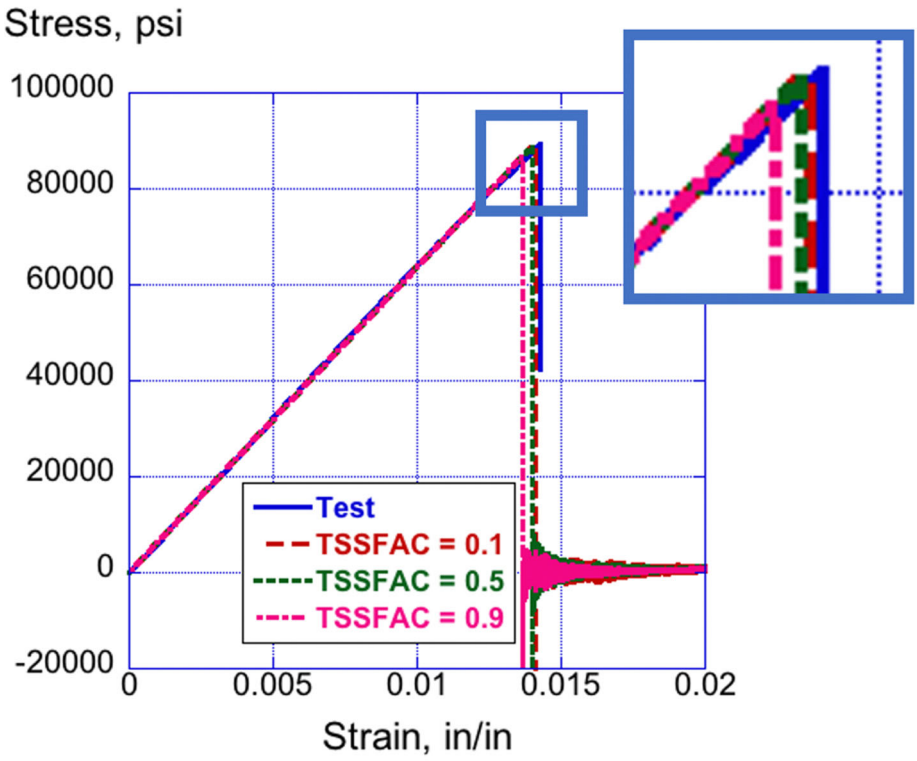


Figure C-19. Longitudinal tension results for varying TSSFAC.

**C-11. New Tension Coupon Model**

A new tension coupon model, shown in Figure C-20, was developed and LS-DYNA® simulations were conducted for three laminates (longitudinal tension, transverse tension, and biaxial tension. The model is 1in. by 6 in. with a nominal element edge length of 0.1 in. It is intended to represent the gauge section of a 1-in x 10-in specimen. The model has: 600 shell elements, 671 nodes, 1 part, and 1 material card (*MAT_213). Left edge nodes are fixed using a SPC, right edge nodes are assigned a boundary prescribed motion definition. As with the 1-in. x 1-in. coupon model, the laminate properties were input using the

*PART_COMPOSITE feature in LS-DYNA®. Output from the model included the SPC forces of the left edge nodes, which were summed and divided by the cross-sectional area to generate stress. Strain was determined as a ratio of time and displacement divided by the gage length of 6 in. Results from the new tension coupon are compared with test data and predictions generated by the 1-in. by 1-in. coupon model, as shown in Figure C-21.

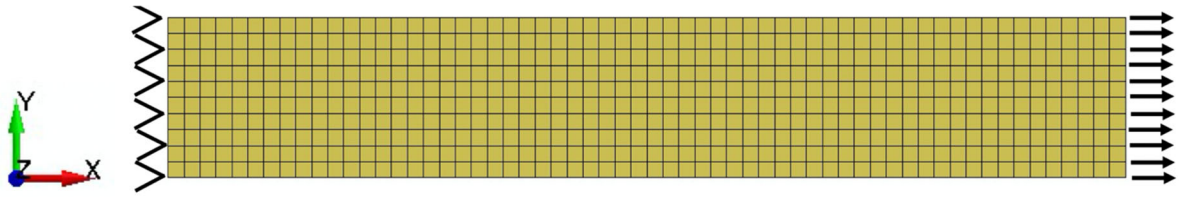


Figure C-20. New tension coupon model, 1 in. x 6 in.

Results of the longitudinal tension simulations are shown in Figure C-21 along with the test response. Both predicted curves match the stiffness and strength of the test extremely well.

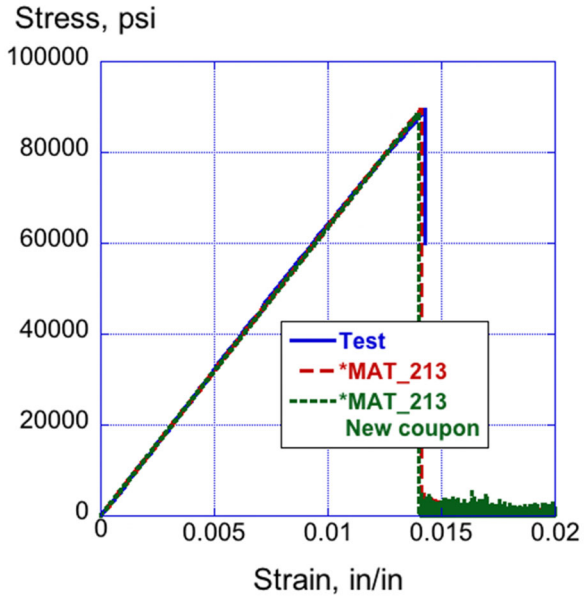


Figure C-21. Test-analysis comparison plot for longitudinal tension. The predicted responses are from two models: 1-in. x 1-in. coupon and the 1-in. x 6-in. coupon.

Results of the transverse tension simulations are shown in Figure C-22 along with the test response. All curves have generally the same initial stiffness. However, both simulations over predict the maximum stress and strain. Both simulations exhibit a “stair step” response, occurring at the same values of stress.

Results of the biaxial tension simulations are shown in Figure C-23 along with the test response. The new coupon model over predicted the magnitude of the test response, but it

also exhibited a sudden drop in load at 0.065-in/in strain, thus exhibiting a similar failure mode as the test, though at a much lower value of strain.

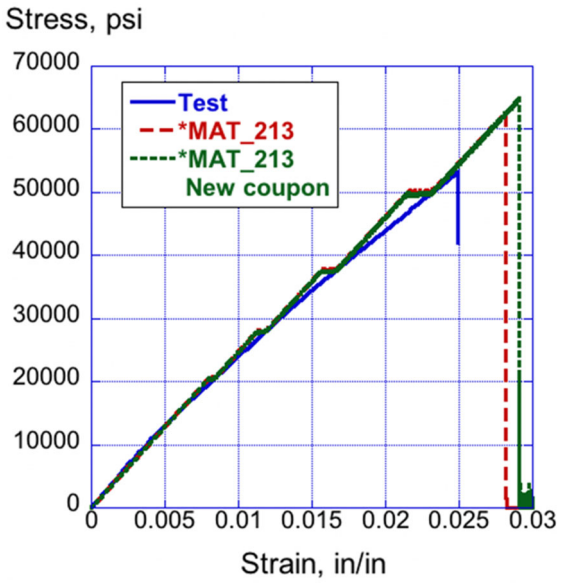


Figure C-22. Test-analysis comparison plot for transverse tension. The predicted are responses from two models: 1-in. x 1-in. coupon and the 1-in. x 6-in. coupon.

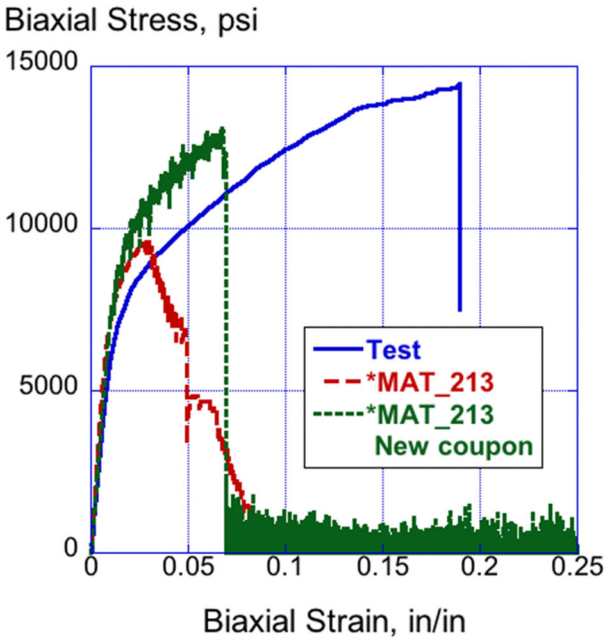


Figure C-23. Test-analysis comparison plot for biaxial tension. The predicted responses are from two models: 1-in. x 1-in. coupon and the 1-in. x 6-in. coupon.

## C-12. Influence of Varying Face Sheet Thickness and Foam Width for the Sinusoid Energy Absorber

Early on, one suggestion to improve the test-analysis correlation for the sinusoid model was to reduce the foam thickness from 1.5 in. to 1.25 and 1.0 in, as shown in Figure C-24. For these simulations, a reduced thickness was used for the face sheets. Acceleration-time-history results are shown in Figure C-25. These results are promising in that the 1.0-in.-thick foam model with a face sheet thickness of 0.1 in. does the best job of matching the test data. However, the fact remains that the test article had a foam thickness of 1.5 in. Consequently, other avenues will have to be explored to generate improved test-analysis comparisons for the sinusoid energy absorber.

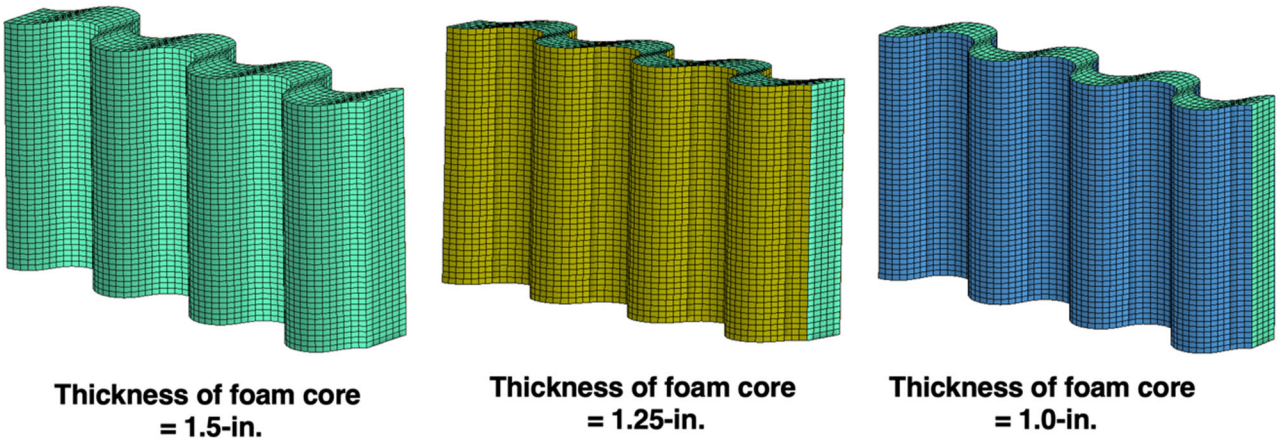


Figure C-24. Variations in foam thickness.

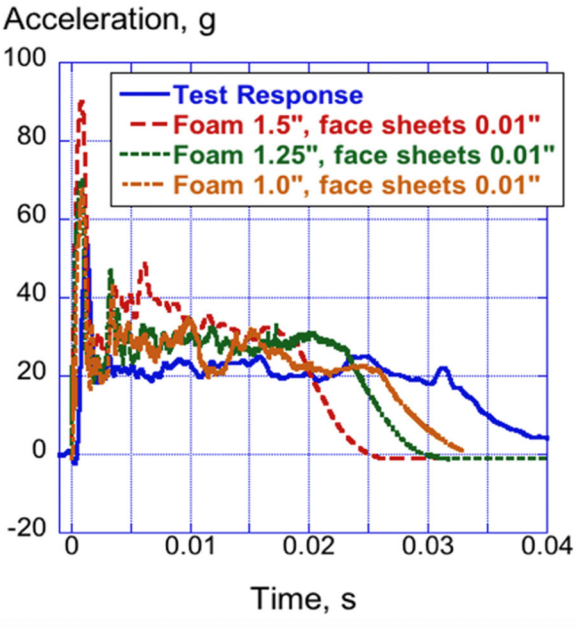


Figure C-25. Test-analysis comparisons of vertical acceleration responses for three different foam thicknesses.

### C-13. Influence of Adding Crush Trigger Mechanisms

One approach for improving the level of test-analysis correlation is to introduce a crush trigger. Two trigger mechanisms that have been used previously with good success are the steeple and chamfer triggers, shown schematically in Figure C-26. The role of the trigger is to fail initially at a lower load than if the trigger were not present, and to initiate stable crushing. Both trigger mechanisms were incorporated into the sinusoid model, as shown in Figures C-27 and C-28.

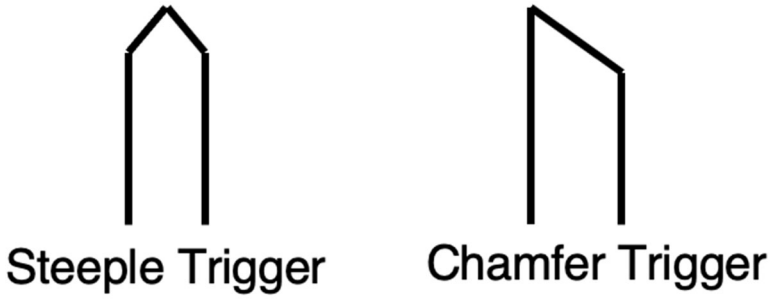


Figure C-26. Schematic drawings of two crush trigger mechanisms.

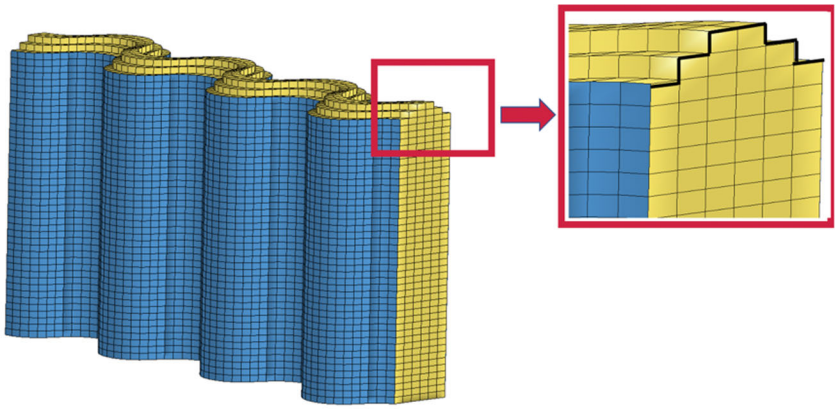

Figure C-27. Steeple trigger added to the sinusoid model.

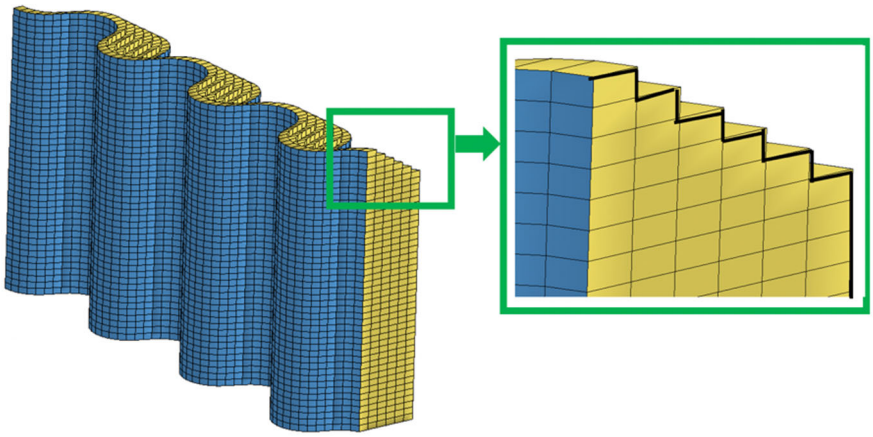

Figure C-28. Chamfer trigger added to the sinusoid model.

Acceleration and displacement time history results for the steeple trigger are shown in Figure C-29(a) and (b), respectively. The test acceleration response has an average sustained crush acceleration of 22.11 g for a pulse duration of 0.0 to 0.03 s. The model response has an average sustained crush acceleration of 25.01 g for the same pulse duration, which is a difference of 13.1%. The test displacement response exhibits a maximum crush displacement of 4.08 in. In contrast, the model response has a maximum crush displacement of 3.22 in., which is a difference of 21.08%. These results show that, while the sinusoid model remains too stiff in comparison with the test, the analytical results are improving with the trigger.

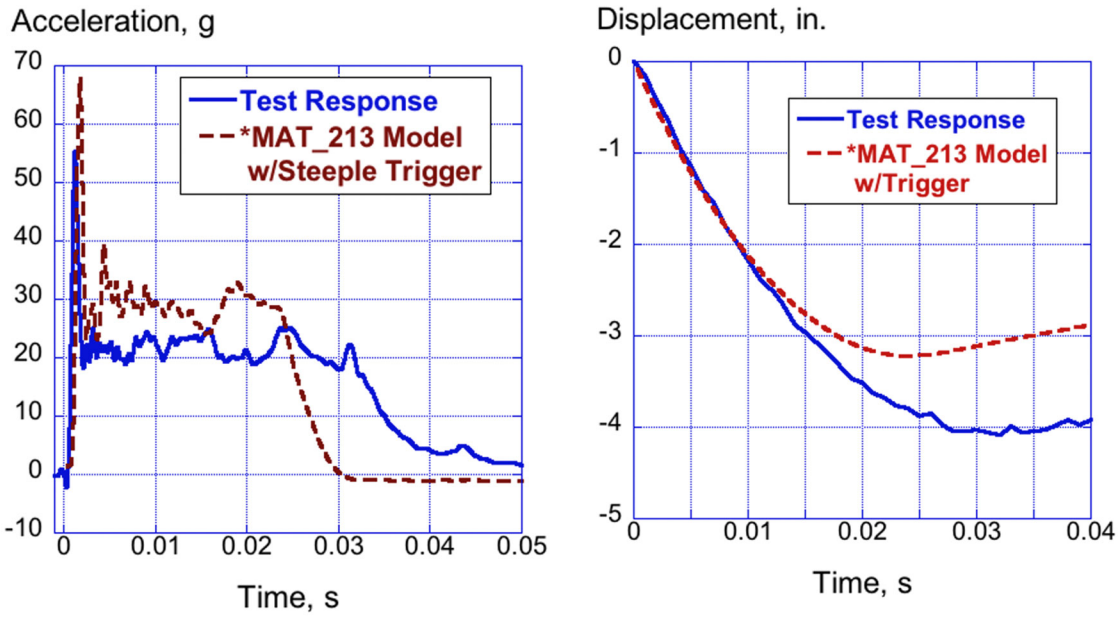


(a) Acceleration responses. (b) Displacement responses.

Figure C-29. Test-analysis comparisons for the sinusoid model with a steeple trigger.

Acceleration and displacement time history results for the chamfer trigger are shown in Figure C-30(a) and (b), respectively. The test acceleration response has an average sustained crush acceleration of 22.11 g for a pulse duration of 0.0 to 0.03 s. The model response has an average sustained crush acceleration of 24.53 g for the same pulse duration, which is a difference of 10.9%. It is also interesting to note that the chamfer trigger has lowered the initial peak load to match the test peak closely. The test displacement response exhibits a maximum crush displacement of 4.08 in. In contrast, the model response has a maximum crush displacement of 3.5 in., which is a difference of 14.2%. The results for the chamfer steeple are encouraging and demonstrate the benefit of incorporating a crush trigger.

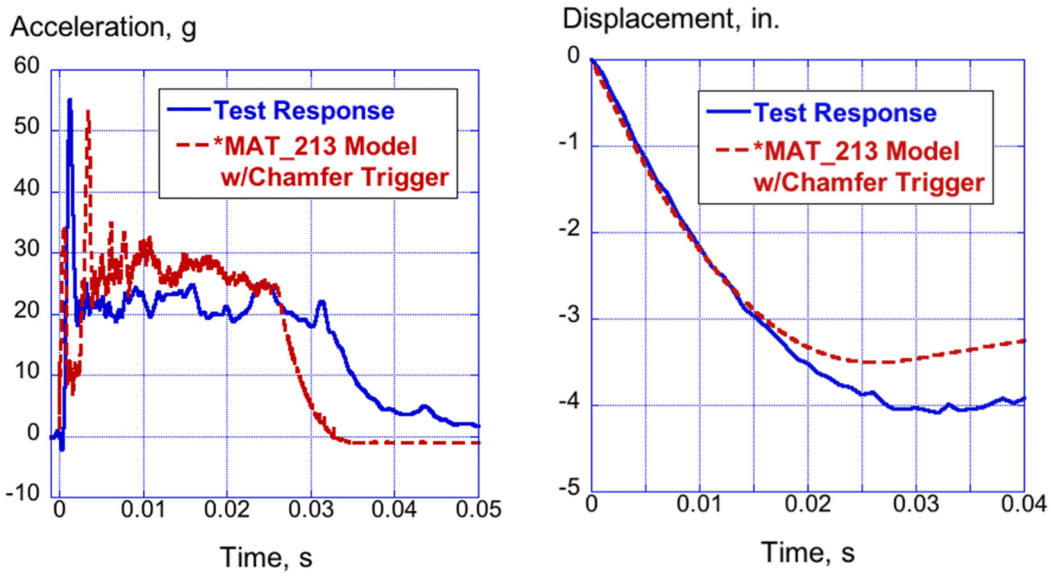


(a) Acceleration responses. (b) Displacement responses.

Figure C-30. Test-analysis comparisons for the sinusoid model with a steeple trigger.